Two Alabama Case Studies for Remote Sensing of Water Resources

by

Samriddhi Shakya

A thesis submitted to the Graduate Faculty of
Auburn University
in partial fulfillment of the
requirements for the Degree of
Master of Science

Auburn, Alabama
May 9, 2015

Keywords: Remote sensing, LiDAR, METRIC model, Evapotranspiration

Approved by

Luke Marzen, Chair, Professor of Geography, Department of Geosciences
Chandana Mitra, Assistant Professor of Geography, Department of Geosciences
Brenda Ortiz, Associate Professor, Department of Crop Soil & Environmental Science

Abstract

Managing water resources is one of the main challenges for water resource managers. This thesis uses geospatial technologies to assist in monitoring water resources through two case studies that are of concern to both state and national agencies. The first case study attempts to improve the isolated wetland classification by introducing LiDAR data. Jones (2013) applied GeOBIA methods to classify and catalog the isolated wetlands of Northern Alabama using high resolution aerial imagery where errors in rooftops, asphalt and shadows were observed. This research attempted to improve the classification methods for wetlands and tested methods to remove rooftops and asphalt mistakenly classified as wetlands using the LiDAR data and GeOBIA. The accuracy percentage achieved for the isolated wetlands classification was 90.4%, an improvement of 10% from the initial classification analysis where LiDAR data were not used.

The second case study focuses on consumption of water by agricultural land and golf courses. Calculating evapotranspiration (ET) with Landsat Thematic Mapper satellite imagery through the use of the Mapping EvapoTranspiration at high Resolution with Internalized Calibration (METRIC) model, it is shown to be an effective tool for estimating water consumption on irrigated lands. The case study developed methods to estimate ET in the irrigated agricultural lands and golf courses in twenty HUC 12 watersheds in the Wiregrass region of Alabama using remote sensing methods and METRIC model. The model was able to estimate seasonal ET for year 2005 and 2010 in the study showing there was an increase in water consumption for both agricultural land and golf courses with the latter being more substantial.

Acknowledgment

I would like to offer my sincere gratitude to my advisor, Dr. Luke Marzen, for accepting me as his research assistant and taking the challenge to guide me throughout my Master's studies. His unceasing support throughout my graduate studies has provided me the opportunity to develop both professionally and personally. I would like to express deep and sincere appreciation to Dr. Chandana Mitra for her continuous support, supervision and encouragement throughout the Office of Water Resources project. I gratefully acknowledge Dr. Brenda Ortiz for her continuous guidance and crucial contribution to my thesis work on evapotranspiration and collecting weather station data.

I would like to acknowledge Tyler Jones for the technical support in GIS and remote sensing throughout my thesis project. I would like to express my sincere appreciation to Nishan Bhattarai for his continuous support and guidance in helping me understand the concept and workflow of the METRIC model. I would like to thank Michael Barbour, an expert in GIS, for his help in the isolated wetland project. I would also like to acknowledge Environmental Protection Agency (EPA), Office of Water Resource (OWR), and Department of Geosciences for funding this research and my Research and Teaching assistantships the past two years.

My deep hearted gratitude to all the people who accompanied and supported me during this journey. Finally, very special thanks to my mother Ganga Shakya, my sister Manisha Shakya Siddhi and my Late father Madan Kaji Shakya for their love, care and encouragement.

Table of Contents

List of Figures

Chapter 1

Chapter 3

Chapter 4

Chapter 5

Appendix

List of Tables

Chapter 3

Chapter 4

Chapter 1: Introduction

Remote sensing (RS) is the art and science of acquiring information about an object or phenomenon without being in direct physical contact with the body. Using RS, researchers can quantify and observe important biological and physical characteristics of earth's surface in addition to human activities that impact the environment (Jensen, 2006). RS can also be described as a science of acquiring, processing and interpreting imagery traditionally based on the principle of electromagnetic radiation and how incident energy from the sun interacts with the surface of earth. Radiation detected by sensors are reflected and emitted energy from the earth with the reflected energy being in the form of reflected solar while the emitted energy being the thermal infrared (TIR) and microwave portion of the electromagnetic spectrum (Schmugge et al., 2002). The technology associated with RS has been used widely in many applications related with hydrology, forestry, agriculture, cartography, geology and meteorology among others.

Remote sensing has been used quite extensively in research and applications related to hydrology. Many studies have been conducted to develop different remote sensing techniques and methods to obtain quantitative and spatial measurements of important hydrologic parameters (Gregg and Casey, 2004; Karaska et al., 2004). For example, it has been used to catalog and monitor the spatial extent, organic and inorganic constituents, depths and temperature of water bodies (Jensen, 2006). Schultz (1988) suggested that a problem in hydrological studies is that there are not enough observations to accurately describe hydrological processes. Remote sensing has been more promising than the traditional way in collecting extensive field data. Importantly,

he also notes that remote sensing offers the following advantages over traditional field based methods (1) it gives area measurements instead of point measurements; (2) it can collect and store vast information about a place; (3) it provides high resolution in space with a time stamp; (4) it creates and stores data in digital form; (5) there is no interference between data acquisition and the process being observed; (6) it generates information about remote areas of the earth where taking measurements in situ is difficult; and (7) it is cost effective compared to traditional observation of hydrological quantities (Schultz, 1988). Extracting information from a remotely sensed dataset can be achieved by trained image analysts by implementing the knowledge about the fundamental elements of image interpretation which are shape, size, tone, shadow, pattern, texture, site, association, and resolution in the land cover mapping (Olson, 1960).

This research thesis focused on two case studies using remote sensing in water related applications in the state of Alabama. The case studies will employ Geographic Object Based Image Analysis (GeOBIA) in classification of water features and golf courses and remote sensing models will be developed to help estimate water usage. The first case study will focus on the classification of isolated wetlands in Lee County using National Agriculture Imagery Program (NAIP) imagery and Light Detection and Ranging (LiDAR) data. The second case study will focus on estimating evapotranspiration in the irrigated areas for agricultural lands and Golf Courses of twenty Hydrological Unit Code (HUC) 12 watersheds in the Wiregrass region of Alabama using Landsat images and employing METRIC model.

Case Study 1: Eliminating the errors of rooftops from isolated wetlands classification of Lee County using LiDAR data

1.1 Study background of case study 1

Wetlands are areas of land that satisfy one or more of the following conditions: 1) land that supports the growth of hydrophytes (aquatic vegetation); 2) most portion of the substrate have an un-drained hydric soil; and 3) areas without soil and without hydrophytes that are saturated with water (Cowardin et al., 1979). The United States Department of the Interior (USDI) Fish and Wildlife Service initiated the National Wetland Inventory (NWI) project in 1975 to catalog the nation-wide wetlands of the United States so that it can provide information to biologists and other people concerned with conservation of wetlands (USFWS, 2013).

Geographically isolated wetlands can be defined as wetlands that are surrounded by dry lands and have no direct surface-water connection with rivers, ponds, streams, estuaries or oceans (Tiner, 2003). However, they can still be connected to underground water (Winter and LaBaugh, 2003) and have as equal importance as non-isolated wetlands. NWI data for Alabama reveals that there are several areas with gaps in digital wetland data. A substantial part of Alabama's analog maps have still not been digitized, and majority of what has been done are coastal and large water bodies rather than isolated and transient waters (Jones, 2013). The need for an inventory of information on isolated wetlands is important to monitor and assess the changes in wetlands and guide the policy makers in making good decisions for conservation. Jones (2013) applied GeOBIA to classify the isolated wetlands of Northern Alabama from NAIP imagery yielding an accuracies of 83.7% and 87.7% for aerial imagery inspection and field verification respectively. The errors in classification were mostly of rooftops, asphalt and shadows (Jones, 2013). This research will test whether the errors in wetland classification can be

eliminated by classifying building rooftops from LiDAR point clouds and eliminating those misclassified wetlands from the classification.

1.1.1 Study area

The study area for the case study covers Lee County in Alabama, United States. According the United States Census Bureau of 2010, the population of the county is 140,247. The total area of the county is approximately 615 sq. miles, with 608 sq. miles of land and 76 sq. miles of water (U.S. Census Bureau, 2015). There are total of seven urban areas in the county with Auburn-Opelika being the largest. Figure 1 below shows the border of Lee County which is the study area for this case study. Lee County is chosen for the study area because LiDAR data are readily available from a partnership between Auburn University, Lee County, and the Cities of Auburn and Opelika.

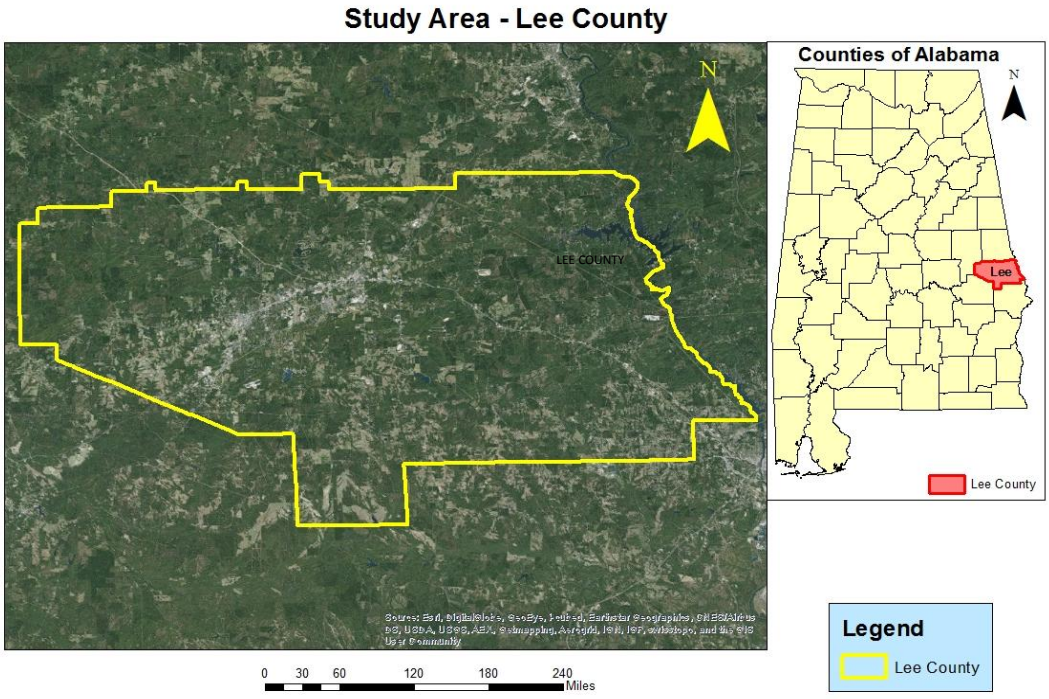

Figure 1.1: Lee County, AL

1.1.2 Objectives

The overall objective of this case study is to develop methods to classify the isolated wetlands of the Lee County using GeOBIA methods by integrating multispectral images and LiDAR data. The method developed can be further applied to classify wetlands in other parts of Alabama. This project will be accomplished with the following objectives:

- Identify and delineate isolated wetlands in the study area using high-resolution NAIP images.
- Removal of identified rooftop errors in initial wetland mapping classification.
    - Comparison between building rooftops classification results from GeOBIA and Point Cloud Task method in LP360 software to see which method can be used for the classification of building rooftops in Lee County.
    - Eliminate the errors of building rooftops in wetland classification by erasing those errors by introducing the building rooftops classified from LiDAR point cloud in GIS environment.
- Accuracy Assessment of the classified isolated wetlands by visual inspection with NAIP imagery.

1.1.3 Research questions

- What is the spatial extent of isolated wetlands in Lee County?
- Which method was better to classify building rooftops: GeOBIA or Point Cloud Task method in LP360 software?
- How has the introduction of the LiDAR improve the wetlands classification?

Case Study 2: Estimating evapotranspiration as a proxy for water usage in the irrigated areas and golf courses in the Wiregrass region of Alabama.

1.2 Study background of case study 2

Water is one of the most important elements for the existence of living organisms on Earth. Managing water resources wisely and sustainably is one of the main challenges for water resource managers. Although abundantly available, water is certainly not free. It is important to understand the natural systems and physical laws that control the hydrological cycle and how each process relates to water usage. According to a World Health Organization (WHO) (2003) report, 1.2 billion people lacked access to safe and affordable water (Rijsberman, 2006). The WHO/UNICEF Joint Monitoring Program (JMP) (2013) report found that estimated 768 million people still did not have access to improved drinking water, which included 185 million people who relied on surface water. With the increasing water scarcity in the world, it is very important that people consume water efficiently and preserve the natural sources of water. To accomplish this, it is very important to have knowledge about how much water is being consumed.

Irrigation of cropland is one of the major consumers of water throughout the world. In part, because of excessive irrigation, freshwater has become scarce in most part of Asia and Africa which might escalate in coming decades (Rijsberman, 2005). Different irrigation systems have been used to irrigate agricultural lands in this world. One of the commonly used irrigation systems is sprinklers such as Central Pivot Irrigation Systems (CPIS) that have been used in many areas to increase crop production. There are different types of CPIS but commonly used CPIS normally "consists of one single sprayer or sprinkler pipeline of relatively large diameter, composed of high tensile galvanized light steel or aluminum pipes supported above ground by towers that move on wheels, long spans, steel trusses and/or cables." The pivot is at the center to

which one end of the pipeline is connected. The pipeline moves in circular pattern about the pivot irrigating the plants with frequently spaced sprayers (Phocaides, 2007, p. 10.1).

According to United States Geological Survey (USGS) data for 2005, total irrigation withdrawals for the United States were about 128,000 million gallons per day (Mgal/d) which comprised of 37 percent of total freshwater withdrawals and 62 percent of total freshwater withdrawals for all categories, when thermoelectric power was not taken into consideration. Irrigation from surface water was accountable for 58 percent of the total irrigation withdrawals. The data also revealed that a total of 61.1 million acres were irrigated of which 30.5 million acres used sprinkler system such as CPIS.

Large volumes of water are also consumed for the irrigation of recreational golf courses. Golf is a sport that has experienced a huge growth and success in recent decades. The total number of golfers since 2003 exceeds more than 61 million around the world with United States comprising over half of that figure. According to the National Golf Foundation (2014) data, there has been remarkable increase in the number of golfers in United States from 11.2 million in 1970 to nearly 38 million in 2004: among which 13 million are regular participants. In 2003, there were a total 25,000 golf courses worldwide with United States alone having 15,827 golf courses which covered more than 1.7 million acres (Wheeler and Nauright, 2006). According to the NGF's (2012) report, there were a total of 15,619 golf courses in United States of which 25 percent are privately owned. To maintain the turf of the golf courses, a huge volume of water is required. It was estimated that an 18-hole golf course requires 3,000 to 5,000 cubic meters per day, which is equivalent to the daily consumption requirement for 2,000 families or 15,000 individual Americans (Wheeler and Nauright, 2006). According to the Worldwatch Institute data from 2001, 9.5 million cubic meters of water is used per day to irrigate all the world's golf

courses which is tantamount to the amount of water used per day to support 4.7 billion people at United Nations daily minimum requirement (Brown et al., 2001).

Since both agricultural land and golf courses consume very large amounts of water, it is important for regional water resource managers to have an accurate inventory of irrigated lands and golf course areas and to also have ways to estimate the water consumption in these areas. Part of this study is funded by the Alabama Office of Water Resources whose resource managers are seeking methods to help the monitor the water consumed by these two land uses. It is posited that golf courses and irrigated agricultural land can be accurately classified from NAIP images using GeOBIA methods. But due to the lack of NAIP images on monthly basis which is important for the classification of agricultural land, the case study will only focus on developing classification methods in GeOBIA for the golf courses. While secondary data from National Land Cover Dataset (NLCD) and National Agricultural Statistics Service (NASS) will be used to categorize agricultural areas. In addition, by estimating evapotranspiration (ET) with Landsat Thematic Mapper satellite imagery using the Mapping EvapoTranspiration at high Resolution with Internalized Calibration (METRIC) model, it is thought that water usage can be estimated (Bastiaanssen et al., 2005). The thermal bands of Landsat can be used to derive the Land-Surface Temperature (LST) to give estimates of evaporative flux patterns which serves as a proxy of the surface moisture over a range of different spatial scales (Marzen et al., 2003; Hain et al., 2009; Hain et al., 2011).

1.2.1 Study area

The study area for the identification of golf courses and agricultural lands, and estimating evapotranspiration is twenty HUC 12 watersheds in the Wiregrass region of Alabama. It is an area that encompasses the southeastern part of Alabama. The region's name is based on the

native *Aristida stricta*, known as "wiregrass" due to its texture and also because it is amply found in the regions longleaf pine forest (Byrd, 2009). This name was originated during the earliest days of European inhabitation in this region. Dothan is the region's most developed city and claims the agricultural title of "Peanut capital of the world." The Wiregrass region has many golf courses and recreation centers. The regions boundary can vary depending on who defines it. For the purpose of this thesis, the focus will be on Houston County, Alabama.

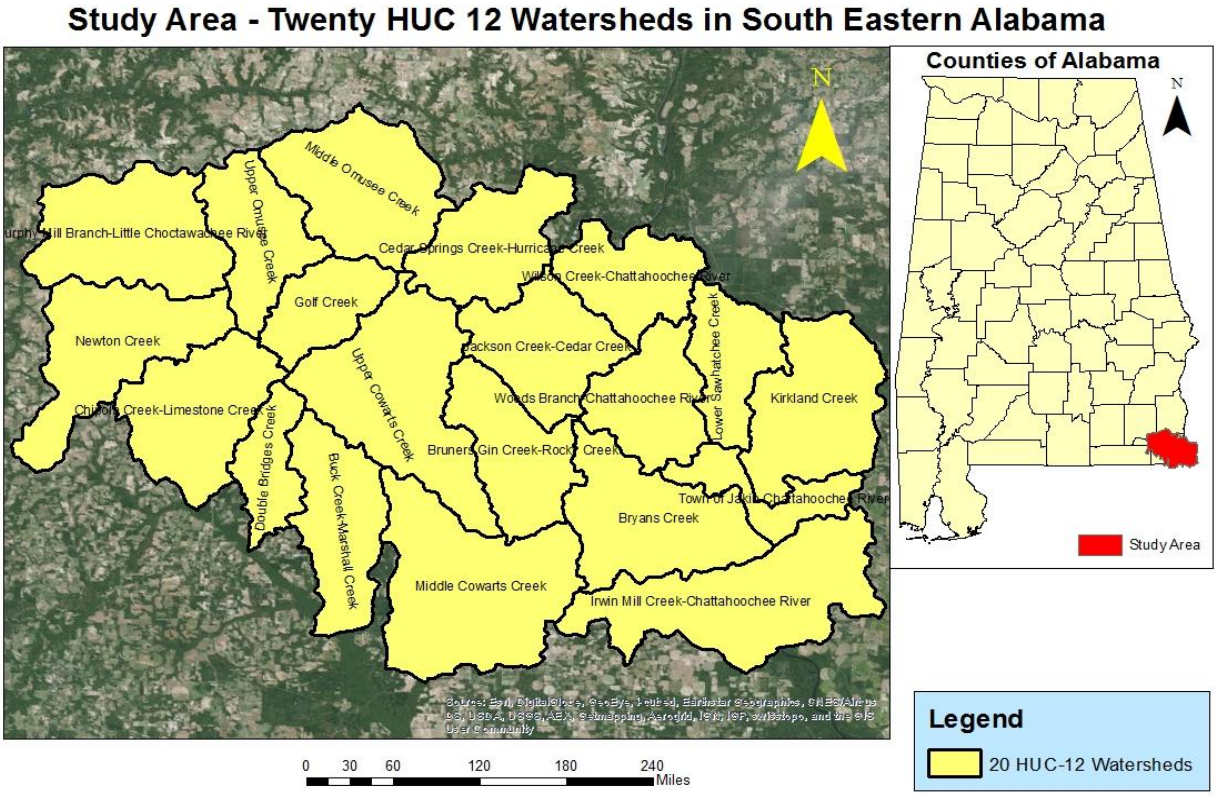

Figure 1.2: Study area delineating Twenty HUC Watersheds in SE Alabama

1.2.2 Objectives

The goal of this case study is to develop methods to estimate evapotranspiration in the irrigated agricultural areas and golf courses of the study area using remote sensing methods and

the METRIC model. The study will also focus on the classification of the golf courses using GeOBIA methods. This project will be accomplished with the following objectives:

- To classify golf courses in twenty HUC 12 watersheds in the Wiregrass region of Alabama using NAIP imagery by implementing GeOBIA methods and develop a ruleset that best classifies golf courses.
- Assess the validity of (METRIC) model for estimating evapotranspiration (ET) by comparing it with the ET data from USGS ET stations in Florida.
- Estimate evapotranspiration of irrigated agricultural lands and golf courses in twenty HUC 12 watersheds in the Wiregrass region of Alabama implementing METRIC model and using Landsat 5 –Thematic Mapper imageries for the year 2005 and 2010.

1.2.3. Research questions

- What is the spatial extent of Golf courses in the study area?
- Can the ruleset developed for the classification of golf courses be applied to other places in Alabama to identify golf courses?
- Can METRIC model be used with remotely sensed data to provide a reliable estimate of evapotranspiration?
- How has the trend in water consumption changed from 2005 to 2010 in both agricultural land and golf courses?

Chapter 2: Literature Review

The literature review reveals background information required for this thesis research and analysis. It commences with the background of geographically isolated wetlands and their functionality to the environment. It explains how isolated wetlands are different from other wetlands but serve the same purpose to the environment as other types of wetlands. The next section describes traditional pixel based classification and Geographic Object Based Image Analysis (GeOBIA). This section also covers different processes involved in GeOBIA. Next, a section describes LiDAR technology and how it has been applied to improve the classification of land cover mapping. The next section describes how remote sensing has been used to classify wetlands. It focuses on how others have used different methods to classify the wetlands and what results they achieved from the classification. The next section describes how remote sensing has been used to classify building rooftops using LiDAR and is related to this study to help remove rooftop errors in wetlands mapping. An emphasis is placed on the different methods and software that have been used to map buildings or rooftops. The next section describes LP360 software and its use to classify LiDAR point clouds using the Point Cloud Tasks (PCT) methods.

This is followed by a description of irrigation systems and how they have been used in United States for irrigation of agricultural lands and golf courses. It also focuses on how irrigation has impacted surface water and ground water and how the trend of water use has changed since 1950. The next section describes how much water golf courses consume on daily basis to maintain the turf. A section is also included on evapotranspiration (ET), why it is

an important indicator of water usage, and describes different methods that have been used to measure ET. Finally, there is a section introducing the METRIC and SEBAL models used to estimate ET.

2.1 Geographically isolated wetlands:

Geographically isolated wetlands are disconnected with other water bodies and do not have a downstream surface outlet. Formed in a depression, these wetlands are isolated from water bodies because of the higher elevation of surrounding lands (Leibowitz, 2003; Tiner, 2003; Snodgrass et al., 1996). These types of wetlands are connected to the surface water occasionally during flood stages. Twenty-eight percent of wetlands in North Dakota, for example, were connected to intermittent surface water during the flood stages (Leibowitz, 2003). Although isolated wetlands are often not connected to other water bodies, they can still be connected through ground water depending on the geological structure of a place (Winter and LaBaugh, 2003; Sutter and Kral, 1994).

In terms of functionality to the local environment, both isolated wetlands and non-isolated wetlands serve similar benefit to the environment. The role of wetlands cannot be underestimated as they play an important role by providing vital services such as recharging ground water supplies, providing habitat for wildlife, reducing floods, transforming nutrients, maintaining water quality, protecting shorelines, surface-water storage, flood water protection, aquatic productivity and shoreline stabilization (Tiner, 2003). Neely and Baker (1989) mentioned that wetland depressions act as storage and prevent run off from being connected to regional riverine systems which helps prevent flooding. Wetlands also provide habitat for many living creatures such as waterfowl and native fishes and serve as a water source for domestic livestock, and humans (Tiner, 2003).

2.2 Geographic Object Based Image Analysis. (GeOBIA)

Extracting of information from remotely sensed datasets has been achieved in different methods such as manual interpretation, automated pixel based classification and GeOBIA. While manual interpretation are very accurate and are mostly done by trained human image analysts, it is very time-consuming to produce land-cover mapping over large areas (O'Neil-Dunne et al., 2009).Before the advent of GeOBIA, the classification of remotely sensed imagery was done mostly using pixel based methods. The pixel-based classification is an automated method where each pixel is classified to a land-cover class on the basis of its spectral properties. This technique does not take into consideration other elements of image interpretation such as shape, size, tone, shadow, pattern, texture, site, association, and resolution (O'Neil-Dunne et al., 2009). Supervised and unsupervised classification methods are the two most commonly used methods in the pixel based classification which produce thematic layers most commonly related to land cover. Pixel-based classification gives satisfactory results for moderate-resolution datasets with spectral information. However this technique does not perform as well for high-resolution datasets that contains a combination of spatial, spectral and contextual information (Cleave et al., 2008).

With advancement of technology in the acquisition of aerial and satellite imagery, the spatial resolution of images increased producing higher resolution images. The traditional pixel classifier usage is limited however due to the increasing number of pixels which can often be too complex for classification (Baatz and Schape, 2000). The increasing availability of high resolution imagery and realization of the limitation of pixel based classifications, in part, led to the development of GeOBIA, which overcomes the limitation of pixel based analysis by grouping the pixels into primitive image objects (Blaschke, 2010). GeOBIA uses attributes such as the object's color (spectral information), size, meaningful statistic and texture calculation,

an increased uncorrelated feature space using shape, topological features (neighbor, super-object, etc.), close relation between real-world objects and image objects and occurrence to other image objects to interpret and analyze images in a manner that closely resembles what human analysts can see with their eyes (Lillesand et al., 2004; Benz et al., 2004). In other words, this method groups pixels into meaningful objects which can be analyzed and interpreted in a way that very closely resembles human visual experience (Blaschke, 2008; Lillesand et al., 2004) and is arguably more suitable for medium to high resolution imagery compared to the traditional pixel based methods (Benz *et al*., 2004) . Many studies have shown that GeOBIA methods are superior to pixel-based methods for land cover classification from high-resolution imagery (Blaschke, 2010) and can perform powerful automatic and semiautomatic analysis in many remote sensing applications often in a more efficient and repeatable process (Benz et al. , 2004).

The first step in GeOBIA involves segmentation. The image segmentation algorithm groups pixels into objects which are generally based on one of the two basic properties of the pixel's gray-level values: discontinuity and similarity (Gonzalez, 1987, Haralick and Shapiro, 1985). While in the first approach, segmentation of the image is based on the abrupt changes in the pixel level; the second approach adopts methods like threshholding, region growing and splitting, and merging to segment the image (Addink et al., 2012). The initial segmentation is dependent on the information of pixel values and features of the intermediate image objects and provides image objects with certain values for spectral behavior, shape and context (Benz et al., 2004). Image objects are clusters of pixels that have similar spectral and spatial (i.e., texture) information. The key distinction that can be made on objects are from topology since each image object will have contextual relationship with its neighboring objects and this information can help improve the classification process (Blaschke et al., 2008).

The objects that are segmented can be related to a classification scheme including classes such as water bodies, buildings, individual tree crowns or canopy, agricultural fields and impervious surfaces. After the segmentation of the image, the image objects formed will have properties like spectral reflectance, shape, size and neighbor relations that can be further processed and classified. Different properties have been used for different classifications, such as shape and size of water bodies, to classify streams, lakes, reservoirs and seas (Navulur, 2007). Similarly, shape properties like compactness, roundness and convexity have been used to classify rivers and lakes (Van der Werff and Van der Meer, 2008). The image analyst must employ an "iterative approach that mimics the human analytical process" which involves repetition of segmentation, classification and refine until the desired output is achieved (O'Neil-Dunne et al., 2009, p.2). In addition, the image analyst should also have a very good knowledge of the place that is being classified which is imperative in image interpretation. Moreover the analyst should try to integrate the ancillary dataset such as LiDAR data, vector GIS datasets with multispectral imagery so as to gather more information about the study area which will help improve the efficiency of the classification process.

GeOBIA is used here to create meaningful objects that relate to geographically isolated wetlands including a contextual rule. Trimble's (initially produced by Definiens, Inc.) eCognition is the first object oriented image analysis software and also the most commonly used for GeOBIA software (User-Guide eCognition, 2014).

2.3 LiDAR and its importance for land use/land cover mapping

Light Detection and Ranging (LiDAR) is an optical remote sensing technology that produces highly accurate x, y and z coordinates by measuring difference in time between the emission of laser pulses and reception of reflected signal from the ground to the aircraft (Porwal and Udeechya, 2013). It is an active remote sensing technology which "operates in the visible or near-infrared region of the electromagnetic spectrum" (Zhou, 2013, p.928) and gives information about elevation at the xyz locations. The sensor in the LiDAR measure the time it takes for the emitted laser pulse of the electromagnetic spectrum to be reflected back after hitting the surface it strikes from which distance can be calculated and subsequently the height of the feature. The sensor and a Global Positioning System (GPS) receiver are mounted together in the aircraft which records the location of the pulses. Moreover, the aircraft is also equipped with an inertial measurement unit (IMU) which records the orientation of the aircraft during the flight. The LiDAR sensor can give very accurate geographic position of the objects the laser pulse is striking (Hippenstiel and Brownson, 2012). The advantage of LiDAR data is that it can be captured at both day and night. However it is usually flown in combination with optical imagery so the missions are mostly flown during the daylight hours during periods when there are minimal shadows.

With the introduction of airborne LiDAR technology in remote sensing, there has increasing interest in implementing LiDAR data in the land-use/land cover mapping. LiDAR point clouds have been used to extract features in the urban settings (Zhang et al., 2006). The point clouds have been used to identify buildings, tree canopy, water bodies and ground surfaces. Most of the times the LiDAR point clouds are interpolated into raster layers such as Digital Elevation Model (DEM) and Digital Surface Model (DSM) and are fused with the high

resolution satellite images for detailed land use/land cover classification (Zhou, 2013). DEM and DSM raster images are produced from the last return and first return of LiDAR point clouds. It is often used either as primary data (MacFaden et al., 2012; O'Neil-Dunne et al., 2012) or as ancillary data (Zhou and Troy, 2008) to aid land use/land cover classification. LiDAR data are also used to provide the intensity information of the land cover features which can help differentiate different features on the ground (O'Neil-Dunne et al., 2012; Im et al., 2008). The intensity maps are produced by triangulating intensity from the LiDAR point's first return (Berger et al., 2013) and have been used in forest- type classifications (Antonarakis, 2008) and also in urban-land cover mapping data (MacFaden et al., 2012; O'Neil-Dunne et al., 2012). There have been many studies where both height and intensity data from LiDAR have been used for land cover classification especially in developed urban settings (Shaker and El-Ashmawy, 2012; Im et al., 2008). The surface model such as nDSM is not affected by shadows, which can introduce many errors during the classification in urban areas (Zhou et al., 2009). To summarize, LiDAR point clouds can be used to generate raster surfaces such as a DEM and a DSM, and from these surfaces, trees and building features can be extracted.

In addition, LiDAR data also been used in different hydrology related applications such as mapping of wetlands and shallow water (Irish and Lillycrop, 1999) and determining depths of water (Lillesand and Kiefer, 2000; Lee, 2003). The accuracy of LiDAR generated DEMs can be high enough to detect subtle topographic patterns in relatively flat wetland regions with a Root Mean Square Error (RMSE) of 0.24m (Töyrä and Pietroniro, 2005). The DEM and DSM data obtained from LiDAR data can be used in image based wetland mapping as it can outline local depressions and hydrological patterns. LiDAR points can give elevation data with high resolution and accuracy (Toyra and Pietroniro, 2005). The problem of separating similarities

between upland and lowland vegetation while classifying wetlands from satellite imagery can be overcome by introducing elevation data from LiDAR (Ozesmi and Bauer,2002; McCauley and Jenkins, 2005; Li and Chen, 2005; Baker et al., 2006). With the use of airborne LiDAR, the classification of land cover improved to greater extent as it was observed in Lee and Shan (2003) classification of six land classes over coastal area, using airborne LiDAR elevation data and multispectral IKONOS images, where the overall classification error were reduced by up to 50 percent (Lee and Shan, 2003).

Although LiDAR incorporated with multispectral image gives good classification, it does bring errors in the classification. While processing the LiDAR point clouds in raster layer such as nDSM through interpolation, it introduces some inherent errors and uncertainty which does affect the land cover classification (Jawak et al., 2014). It is highly likely that a feature may be wrongly classified into another class. For example buildings being classified as trees since both are above ground.

2.4 Use of remote sensing in classification and mapping of wetlands

As wetlands play an important role in nature, it was necessary to conserve and wisely use them, which led to the signing of the Ramsar Convention on Wetlands in 1971 (Matthews, 1993). It is an intergovernmental treaty which aims to conserve and use wetlands sustainably by providing foundations for national actions and international cooperation (The Ramsar Convention on Wetlands, 2014). It is necessary to know the locations of wetlands to protect and sustain it which is why the mapping of wetlands plays an important role. Wetland mapping over a large area can be very costly and time consuming.

The use of remote sensing and a Geographic Information Systems (GIS) in wetland mapping dates back to the 1970's, since the launch of first Landsat satellite series ERST-1 (Wickware, 1978). Aerial photographs and manual visual inspection were commonly used for decades to map wetlands (Blaschke et.al, 2008; Lyon, 1993; Tiner, 1999). Raster images that are taken from satellites and airplanes are analyzed and classified based on the pixel's digital number (DN) value in multiple bands of electromagnetic spectrum. The introduction of Geographic Object Based Image Analysis (GeOBIA) in remote sensing methods has made identification and classification of wetlands more efficient compared to the traditional pixel based methods. GeOBIA being a relatively new method has not been used widely for the mapping of isolated wetlands but has produced good results when employed. Isolated wetlands were mapped using Landsat 7 imagery in the study of St. Johns River Water Management District of Alachua County, Florida which produced and accuracy of 88 percent (Frohn et al., 2009).

Classification of wetlands using remote sensing introduces errors of commission and errors of omission. Errors of commission are those errors that are erroneously included for consideration as wetlands when it should have been excluded. For instance, the image might have classified rooftops and shadows as wetlands, which are errors of commission. Similarly, errors of omission are those errors where the classification method fails to include the wetlands that exist in reality. Tiner (1999) suggest that errors of omission are common in wetland mapping. The IKONOS/LiDAR based classification of wetlands at Chequamegon National Forest in northern Wisconsin had an overall accuracy of 75% when using the Wisconsin Wetland Inventory (WWI) types, with omission error of 10% and commission error of 30% (Maxa and Bolstad, 2009).

Jones (2013) applied GeOBIA to classify the isolated wetlands of the Northern Alabama from NAIP imagery which yielded an accuracy of 83.7% and 87.7% for aerial imagery inspection and field verification with errors mostly of rooftops, asphalt and shadows. This research study will attempt to eliminate the errors of rooftop in isolated wetland classification by classifying building rooftops of Lee County using LiDAR data and try to mask out the classified rooftops from the wrongly classified wetlands which are shown as rooftops in aerial imagery.

2.5 Use of remote sensing in classification of building rooftops

The importance for accurate and detailed information about land-use/land cover has been felt more than ever with the growing demand of knowledge about our surrounding environment in urban land management, city planning, disaster management, environmental planning and landscape pattern analysis (Zhou, 2013), urban tree canopy goals (Maryland Department of Natural Resources, 2015) and to establish a storm water utility based on impervious surface area (City of Durham Public Works Department, 2015). Since information on land use/land cover plays a vital role in many aspects of environmental planning and policy-making, it is important to have accurate maps which give the best realistic representation of the landscape. GeOBIA methods have been commonly used for producing accurate and meaningful land-cover datasets in an effective manner. Land use/land cover mapping has been done extensively for decades to locate different heterogeneous areas in different environmental settings. To classify the urban environment, which are highly complex and heterogeneous, requires remotely sensed images with high resolution and the process can be aided by the addition of LiDAR data to adequately distinguish the different heterogeneous features of the landscape. The manual digitization for building rooftops using raw imagery is labor-intensive, time consuming and expensive and is not preferred if the study area is considerably large (Jawak et al., 2014).

With the advent of LiDAR technology and powerful computers which aids in performing analysis, different surface models (DSMs) derived from LiDAR have been increasingly incorporated with high-resolution multispectral satellite/aerial imagery for land-use/land cover classifications in urban settings. Zhou (2013) performed object-based image classification to examine if a combination of the LiDAR height and intensity data with multispectral imagery can accurately map urban land cover. The point cloud data were processed to produce three separate raster layers of normalized digital surface model (nDSM), and two intensity image layers. Zhou (2013) used two methods to do land cover classification which both used GeOBIA methods in eCognition software. A normalized digital surface model (nDSM), also known in vegetated areas as a canopy height model (CHM), is calculated from the LiDAR data by subtracting the Digital Elevation Model (DEM) from the Digital Surface Model (DSM).It represents the absolute height of all above ground features relative to the ground and can be used to extract trees and buildings (Jawak et al., 2014. In the first method Zhou (2013) used only LiDAR data, without the multispectral imagery, to classify the land cover such as buildings, pavement, trees and shrubs, and grass. A ruleset was made in the eCognition software which segmented the image and classified them into land cover classes. The second method integrated an nDSM generated from LiDAR with aerial imagery. Comparing both the methods, Zhou (2013) found that the overall accuracy of the classification based on Method two was slightly higher than that from the first method. However, both methods that used LiDAR produced much better results than of those using multispectral imagery alone.

Jawak et al. (2014) used a LiDAR point cloud for 3D feature extraction trees and buildings. LiDAR Analyst 4.2 for ArcGIS workflow for building extraction was employed to identify buildings from non-buildings (mainly vegetation). Jawak et al. (2014) was able to

extract 6,370 buildings where 6,117 buildings were correctly classified. Overestimation of trees and buildings were observed in the research and was identified as a limiting factor in the 3D feature extraction process.

Similarly many studies have been done by different approaches in GeOBIA in the classification of the buildings, however, there were no papers found comparing methods. Hofmann et al. (2002) implemented OBIA in eCognition by segmenting Airborne Laser Scanning (ALS), another term used for LiDAR, height data instead of multispectral imagery which were later exported into GIS for further analysis towards the creation of objects and to obtain the final building classification. The ALS data were also implemented by Tòvàri and Vögtle (2004) in eCognition for classification of bare earth, vegetation and buildings. Automated buildings detection in recent research has been divided into three groups depending on the input data type which are 1) gridded ALS data and derivatives, 2) point cloud segmentation and 3) combined dataset of GIS layers and aerial imagery (Rutzinger et al., 2006). Similarly by analyzing invariant moments in the ALS raw data point clouds, Maas and Vosselman (1999) used two methods to detect buildings and derive planar faces by triangulation. Moreover, Rottensteiner et al. (2005) classified buildings by implementing "probabilistic classification approach of Dempster-Shafer depending on various combinations of first pulse and last pulse DSM (Digital Surface Model), DTM (Digital Terrain Model) derived from raw ALS points and NDVI (Normalised Difference Vegetation Index) derived from ortho-photos". Vozikis (2004) used nDSM derived from ALS points and higher resolution ortho-photos to classify buildings.

Since LiDAR is a relatively new technology, there are only few software that are tailored to meet only specific purposes and can handle millions of point clouds (Hippenstiel and Brownson, 2012). The past three decades have witnessed many studies in photogrammetry,

remote sensing and computer science focusing on the study and development of automatic and semi-automatic approaches for the extraction and reconstruction of building (Mayer, 1999). Software packages such as Overwatch system's LIDAR Analyst for ArcGIS, LAStools© software, and Qcoherent software LP360 for ArcGIS have been in the market which are used to resample LiDAR point clouds into 2-D grids and advanced processing of the point clouds (Jawak et al., 2014). There are many products that function within ESRI's ArcGIS or are built as Extensions for the software such as LP360 by QCoherent, LiDAR Analyst, Feature Analyst and LiDAR Explorer which can be used for LiDAR visualization and classification (Hippenstiel and Brownson, 2012; Kovač and Žalik, 2010 ; Mumtaz and Mooney, 2008).

2.6 QCoherent LP360 software for LiDAR

LP360 is an extension plug-in for the ArcGIS software from which the users can manipulate LiDAR data like any other layers in GIS format. It is specifically designed for ArcMap data layers and has the functionality to visualize points directly from LAS files in ArcMap. The LiDAR layer generated has "a one-to-many relationship with LAS files and the relationship is very similar to that of an image or raster catalog" (QCoherent, 2012, p.3). The LiDAR layers generated from the extension can be displayed on the basis of the attributes such as elevation, classification, intensity and return. The LiDAR layer properties provide the functionality to control the color display of the points for each attribute. The vendor who produces LP360 argues that the extension makes the ArcMap Basic edition "the world's most powerful GIS environment for LIDAR point cloud processing" (QCoherent, 2012).

The LAS files of the LiDAR data are imported into the ArcGIS using the LP360 toolbar and displays the point clouds much faster and efficiently than the tools in 3D Analyst toolbar extension. The advantage of the LP360 toolbar is that the LAS files do not have to be converted

into multi-points before working with the point clouds as is the case for 3D Analyst. It is noted that the most recent version of ArcGIS 10.x has LAS tools that can work directly with LAS datasets. There are different options in LP360 toolbar from which viewing of point clouds can be done according to the elevation, classification, number of returns, point density and color bands. Moreover, the points clouds could be viewed in TIN and profile view with just a click of a button. These functionalities and others make the LP360 extension more flexible and dynamic in terms of analyzing and deriving new information from the LiDAR point clouds (QCoherent, 2012).

2.7 Irrigation systems

Irrigation of agricultural crops follows drinking water, as the second most important use of water (USGS, 2005). It is estimated that irrigation uses nearly 60 percent of all worlds' fresh water, and in United States, irrigation use accounts for more than 70 percent of freshwater (Weibe and Gollehon, 2006). About 90 percent of the water consumed by households and industry is returned to environments that replenishes the water sources. However, the reusable water rate for agriculture is only half of what is consumed, since it is lost by evapotranspiration (USGS, 2005).

A central pivot irrigation system (CPIS) is the most common irrigation system in United States first introduced in the late 1950's in Nebraska (T.L. Irrigation, 2015). Although it was not commercially feasible until 1960's, this system is now very widely used with more than 20 million acres of land worldwide of which 75 percent of that land lies in United States. Half of all sprinkle irrigation and one fourth of all irrigation in United States employ central pivot systems. This irrigation system gained popularity, as it required less labor and fixed cost, in addition to its simplicity, flexibility and reliability (Bleisner and Spare, 2001). The crops that are watered with

CPIS often can be distinguished in aerial imagery due to its circular patterns when viewed from above.

CPIS has been instrumental in helping achieve substantial yield in crop production. According to the Ground Water Foundation (2014), the center pivot fitted with low pressure, dropped nozzles and pressure regulator is around 85-95 percent efficient and have been used to irrigate corn, sorghum, cotton, onions, wheat, coffee, fruits, flowers, and many more. In order to achieve cost advantage of CPIS, relatively large acreage must be irrigated. However, this system has some disadvantage as it can irrigate only the circular area inside which is about 80 percent of the square area and it depends on irrigation coverage beyond the end of the machine (Bleisner and Spare, 2001).

Humans dominantly use surface water for the irrigation but there has been increasing trend in the use of groundwater. In 1950, the surface water withdrawals accounted for 77 percent of all irrigation and this has decreased to 59 percent in 2005. The trend in groundwater use is increasing and is three times more than what it was in 1950's (USGS, 2005). Groundwater provides more than 50 billion gallons of water per day for agricultural needs in United States (USGS, 2014a). Excessive pumping before the ground water is replenished has led to decrease in the volume of groundwater in most parts of the United States. Pumping groundwater at a faster rate before it is recharged can lead to environmental problems such as 1) lowering of water table, 2) reduction of water in streams and lakes, 3) land subsidence, and 4) deterioration of water quality.

2.8 Irrigation for agriculture in Alabama

The state of Alabama is water rich with plenty of precipitation averaging 55 inches (1,400 mm) of rainfall per year (Marcus and Kiebzak, 2008; Srivastava et al., 2010). The average

annual precipitation can vary from a minimum 50 inches in the southeast Alabama to a maximum 68 inches in the southwest (Dougherty et al., 2007). In addition, the state also consists of 77,000 miles (124,000 km) of perennial and intermittent streams and rivers, and has more than 560,000 acres(226,600 ha) of ponds, lakes, and reservoirs (Marcus and Kiebzak, 2008). The state is also blessed with 13 major river basins such as Coosa, Mobile, Chattahoochee, Tallapoosa, Tombigbee and Tennessee. Although the state is blessed with copious amount of water resources and precipitation, the U.S. Geological Survey (USGS) reported that in year 2000 the consumption of water for irrigation was only 28.7million gallons (0.11 mcm) of surface water per day (mgd). This amount equivalents roughly 2% of the 1,530 million gallons (5.79 mcm) of surface water withdrawn per day in the state which ignores the 8,020 mgd (30.36 mcm) used in once-through cooling for thermoelectric power generation, most of which is returned (Hutson, 2004). The data reveals that Alabama has been using smaller percentage of its surface withdrawals, ignoring thermoelectric power, in contrast to California where agriculture uses approximately 82% of their surface waters (Marcus and Kiebzak, 2008). The rainfall in this state is very vital as it serves irrigation for ninety-six percent of farms which uses rain-fed systems (Marcus and Kiebzak, 2008; Srivastava et al., 2010). The water withdrawn for agricultural use is less than 2 percent. The southeastern part of Alabama has been more affected in terms of agricultural production due to inter-annual and intra-annual variability in rainfall. However, the situation is very contrasting in comparison to the western part of United States where 70% of farms are irrigated even if only 30% of their agricultural lands are rain-fed. For example, California uses 97% of its water withdrawal for agriculture (Marcus and Kiebzak, 2008).

Although being considered one of the wettest states in the country, Alabama is suffering from inefficiencies in the agricultural practices. Wounded by lack of irrigation infrastructure,

investment, governance, constraints on water access, and lack of knowledge of irrigation techniques, the farmers of Alabama are not able to compete well with Western United States where irrigated farms are often subsidized. This limitation has resulted in the decline of approximately three million acres to approximately ten million acres of row crops in the past fifty years which has cost the state a loss of minimum US$2 billion per year which occurs mostly within the poorest parts of Alabama (Marcus and Kiebzak, 2008). For example feed corn yields are only 119 bushels per acre (7.47 mt⁄ha, in comparison with a national average of 148 bushels per acre and an average in California of 172 bushels per acre (9.29 mt⁄ha). Similarly, Cotton yields are 1.56 bales per acre (137.63 kg⁄ha) compared with 1.73 nationally (152.63 kg⁄ha) and 2.48(218.80 kg⁄ha) in California (Marcus and Kiebzak, 2008). Over the past few decades, there has also been significant decrease in row crop production because most of it are rain-fed (Srivastava et al., 2010).

Another reason for low productivity in agriculture is because most of the precipitation happens during the winter months, which is off season for growing crops. Dougherty et al. (2007) cites an example of Belle Mina in Northern Alabama that received only 560 mm (22 in) of rain during the growing season (May–October) of the annual 1,350 mm (53 inch) of rain. In addition, Alabama is also plagued by drought resulting in significant crop production loss. Although being very rich in water resources, the annual farm crop receipts in Alabama is only US$484 million which is very similar to that of New Mexico's US$468 million annually but has western dry land agriculture. However, McNider et al. (2005) states that the productivity in cotton can be increased from 60-80 to 200-250 bushels per acre (616.76-822.35 kg⁄ha to 2055-2569.84 kg⁄ha) through irrigation: moreover productions in pecans and fulfillment of vegetable contracts can also be assured.

According to the law in Alabama, the right to use surface waters flowing in the property are afforded only to the riparian owners (Marcus and Kiebzak, 2008). This ruling has led to the increase in consumption of groundwater by the non-riparian farmers predominantly in the southern part of Alabama which is tantamount to approximately 14.5 mgd (0.06 mcm) (Hutson, 2004). However, most of the farmers were not able to obtain the ground water because of the exceeding cost for the drilling wells and pumping water and low interest loans. Only wealthy farmers and those who received lower interest loans were able to afford and enjoy the benefits of ground water. In total, only 3.8% of Alabama croplands were irrigated and the reason behind the low percentage being irrigated were due to riparian legal restrictions, cost restrictions, lack of ground-water development and geographic limitations (Marcus and Kiebzak, 2008). ACES (1994) points that most of the groundwater sources in Alabama are either insufficient or unfeasible for irrigation. In contrast, California has 94% of its cropland irrigated and the whole of United States has 17% of its agricultural crops irrigated (Marcus and Kiebzak, 2008). Moreover, irrigation determines the size of the farm in this state. Although there are some small farms that are irrigated, if the farm is larger than the probability of it being irrigated is higher. This situation is illustrated by recognizing that large farms over 1,000 acres (405 ha) constitute only 3% of farms in Alabama, but they account for 58% of irrigation (Marcus and Kiebzak, 2008).

Most of the farm sizes in Alabama are small with an average area of 197 acres (80 ha) (Marcus and Kiebzak, 2008). However, the cause for agricultural inefficiency in Alabama is not attributed to the farm size but rather due to mitigation of rainfall variability. There are two ways to mitigate rainfall deficit. The first approach can be by utilizing and having information about the climate, seasonal weather forecasts and climate products. This information can help farmers

plant favorable crops, alter planting schedules or tiling practices to that they can evade crop losses during unfavorable years. While the second approach is confronting environmental, economic, and political challenges that can hinder the irrigation practices in the state (Marcus and Kiebzak, 2008). The riparian model in Alabama states that in order to have a sustainable increases in investment of agricultural water, the water management must by trumped by individual rights: however Marcus and Kiebzak (2008) concluded that the state of Alabama would benefit if it had a regulated riparianism which is consistent with American Society of Civil Engineers (ASCE) Regulated Riparian Water Code (2004) in a variable water supply condition. Srivastava et al. (2010) asserts that a practical way of dealing with water supply is "water harvesting." During the winter months when the precipitation and stream flows are high, withdrawal and storage of surface water can be done in off-stream reservoirs and that water can be utilized during the crop growing season when that water is scarce. The average amount of water required for irrigation of the crops, even though water consumption for different crops varies, is around 457 mm (about18 in.) for 0.4 ha (1 ac) irrigated area. This amount of water would be sufficient for most crop irrigation except during droughts suggesting that water harvesting might be a good alternative to irrigate plants during crop growing season (Srivastava et al., 2010).

2.9 Golf courses

A golf course constitutes of series of holes that normally consists of five different areas namely teeing ground, fairways, green (with a flagstick and hole) and rough. A typical golf course consists of 18 holes but can also be any multiple of nine (Diaz et al., 2007). It is very important to irrigate the golf course to control the growth and quality of turf in order to maximize playability and to increase the aesthetic condition that is suitable for golf players

(Weatherhead et al., 2006). The rising demand of irrigation for golf courses can be a problem to a place where there is limited water resources.

The turf grasses of the golf courses are different from the normal vegetation. Kenna (1995) describes that the management practice, surface mats, plant canopy and dense root system of turf of the golf courses are different from the agricultural crops which makes it inappropriate to extrapolate agricultural monitoring studies to golf courses. Compared to the row crop agriculture, golf courses have low volume of run-off water and reduced eroded sediments in the turf (Welterlen et al., 1989). Moreover, golf courses have high evapotranspiration and good drainage compared to other crops (Ward and Elliot, 1995). As it is different from the native vegetation and needs to be maintained properly for playability, golf courses are irrigated often which consumes lot of water. Because of potential environmental impacts since the late 1980's, most of the golf courses in United States are required to monitor groundwater and surface water in order to fulfill the permit condition.

During the 1990's and 2000's people became aware of the environmental impact of golf courses due to excess use of chemicals on turfs, deforestation, health risk to humans and wildlife, and high water consumption (Wheeler and Nauright, 2006). For example, there are more than 100 golf courses in the Greater Palm Springs, California which consumes more than 3780 m^3/day: most of the golf courses draw water from Colorado River basin (Wheeler and Nauright, 2006). Platt (1994) stated that there were three municipal golf courses in Tampa in the 1990s that consumed approximately 2120 m^3/day, which is tantamount to the daily water needs of 5,000 citizens. There have not been much research and studies done for the golf courses in Alabama. However, it is very important for the concerned authority to estimate how much water is being consumed by both agricultural land and golf courses. By estimating evapotranspiration (ET)

from remotely sensed images, a rough estimate of how much water is being consumed by agricultural land and golf courses can produced.

2.10 Evapotranspiration as an indicator of water usage

ET is a combined process of evaporation and transpiration. Evaporation is the process of liquid converting into water vapor resulting in water vapor being removed from a surface on rivers, lakes, healthy vegetation and moist soils. Transpiration is the process where moisture is transported to the plant leaf stomata from the roots where it evaporates into vapor and is released in the atmosphere. Therefore, evapotranspiration is the combined process where water is lost by evaporation from soil surface and transpiration from the plants (Allen et al., 1998). It is the consumption of water by agricultural plants that consists of water that is transpired and evaporated from plant and soil surfaces, plus water retained within plant tissues, which amounts to less than 1% of the total evaporated during a normal growing season (Jensen, 1969). In the process of evapotranspiration, large quantities of water are transferred to the atmosphere as a result of soil evaporation and vegetation transpiration.

It is very important to have a good understanding in the spatial and temporal distribution of evaporative depletion because it can be used to help manage river basins and water supply systems where evapotranspiration takes place. Policymaker's decisions concerning inefficient consumption of water are often made based upon limited available information related to the evaporative depletion of water resources and the land use/land cover digital maps (Bastiaanssen et al., 2005). People involved with agriculture, water resources, and national security are interested in the difference between actual and potential ET at high spatial resolution as it serves as an indicator of crop water deficits (Allen et al., 2005). In addition, spatial estimates of ET have been used in a hydrology-vegetation models implemented to represent important "processes

in hydrology-vegetation systems in a physically realistic manner, consistent with the types of data likely to be available for model input and testing" (Wigmosta et al., 1994, p.1666). Allen et al. (2005) also used ET estimation to calculate soil moisture as an important parameter for weather and flood forecast models.

2.11 Remote sensing methods for estimating ET

Remote sensing methods using satellite and airborne images is becoming more common to estimate spatial-temporal distribution of evapotranspiration (Courault, 2005; Bastiaanssen et al., 2005; Bhattarai, 2010). The data measured from satellites in association with surface energy balance models can provide information about spatial distribution of ET and help better comprehend evaporative depletion. It also describes how to establish a link between land use, water allocation and water use. It is an indirect method of estimating ET that is composed of "set of equations in a strict hierarchical sequence to convert the spectral radiances measured by satellites or airplanes into estimates of actual ET" which does not require "prior knowledge on soil, crop, and management conditions" (Bastiaanssen et al., 2005,p. 86). Satellite-based ET maps can be used to derive spatial information about daily or seasonal ET at pixel scale that can aid in many water resource management applications. This indirect method of measuring ET has given us more possibilities to do studies in the area of water resources management (Bastiaanssen and Bos, 1999; Bastiaanssen et al., 2000; Menenti, 2000). Currently there are different satellite-based approaches of different spatial coverage and temporal resolution for routine monitoring of ET.

Thermal infrared (TIR) bands from the satellites have been used to derive Land-Surface Temperature (LST or T_s) to give estimates of evaporative flux patterns and serves as a proxy of the surface moisture over a range of different spatial scales (Hain et al., 2009; Hain et al., 2011).

TIR data can be obtained from different satellite sensors. However at present, the only satellite that gives routine, global thermal imagery at scales to analyze water usage patterns over heterogeneous agricultural areas are the Landsat satellites (Anderson et al., 2012a). These moderate resolution Landsat sensors with thermal bands are useful to map the ET at local scales and can identify and quantify individual agricultural crops (Kramber et al., 2008). The temporal resolution of recent Landsat satellites is 16-18 days. This is not optimal for ET estimation; because moisture conditions on the ground can be dynamic depending on the rainfall, irrigation and heterogeneous drying varying with soil, vegetation, topography, and local climate. To overcome this limited temporal resolution robust methods have been developed to interpolate between infrequent satellite overpasses to give us daily or seasonal information on the ET (Anderson et al., 2012b). Therefore, remote sensing can be an effective tool to estimate ET to assist in monitoring water usage from agricultural land and golf courses.

2.12 SEBAL and METRIC model to calculate ET

The Surface Energy Balance Algorithm for Land (SEBAL) is an energy balance model that was developed by Bastiaanssen and his associates (Bastiaanssen et al., 1998a; Bastiaanssen et al., 1998b; Bastiaanssen 2000; Bastiaanssen et al., 2002, 2005) and modified by Allen et al. (2002). It is an operational tool that can be used to target, monitor, and evaluate irrigation and drainage systems. Spatial variation of ET at local and regional scales across different land use/land cover can be mapped using the SEBAL model which uses red, green, blue, near infra-red and thermal data of Landsat images (Bhattarai, 2010). The SEBAL model is advantageous compared to other methods because it can accurately quantify seasonal or annual ET with minimal ground data. The accuracies obtained from previous studies were found to be 85% on a daily basis and 95% on a seasonal basis (Bastiaanssen, et al., 2005). Because of the good

accuracy results associated with SEBAL, this model has been commonly used to estimate ET in many countries such as China, Niger, Sri Lanka, Spain, US, Kenya, Morocco, the Netherlands and Turkey (Bhattarai, 2010). The SEBAL model also eliminates the need to correct complex and time consuming atmospheric errors.

Mapping EvapoTranspiration at high Resolution and with Internalized Calibration (METRIC) is the modified version of SEBAL and both have similar foundation, techniques and principles (Allen et al., 2007). METRIC is an "image-processing model which is used for measuring evapotranspiration as a residual of the surface energy balance" (Allen et al., 2005, p 251). Both METRIC and SEBAL models use data from thermal infrared radiation in addition to near infrared and visible bands of the remotely sensed image of Landsat images or other remote sensing satellites like MODIS. Allen et al. (2005) suggests that ET is measured based on pixel-by pixel for the instantaneous time of the satellite image and it depends on complete energy balance for each pixel. ET can be described as:

$$ET = \text{net radiation} - \text{heat to the soil} - \text{heat to the air}$$

Being an energy balance model, SEBAL and METRIC use near surface temperature gradient (dT) that is indexed to radiometric surface temperature. Use of dT has excluded the need to use absolute surface temperature calibration which was a major hurdle in operation satellite ET. METRIC also uses the same technique applied by SEBAL to estimate ET eliminating the need to measure accurate aerodynamic surface temperature and air temperature which are required to compute sensible heat flux at the surface (Allen et al., 2007).

The implementation of weather-based reference ET to formulate energy balance ET separates METRIC from SEBAL model. This is achieved by establishing energy balance at "cold" pixels which makes maximum utilization of the existing technology (details of the

workflow are provided in Appendix). It also creates ground reference for satellite based actual ET estimates and effectively serves the purpose of "reality check" on actual estimates of ET. The METRIC model has satellite-based energy balance model internally calibrated at dry and wet conditions which are two extreme points. The calibration is done using local weather data. Similarly by using an alfalfa based reference ET (ET_{ref}) which is computed from hourly weather data, each image can be auto-calibrated (Allen et al., 2007). The reason alfalfa (ET_{ref}) is favored over the clipped grass (ET_{ref}) is that it gives good representation of the "upper limit of ET from well-watered vegetation" (Waters et al., 2002, p.13). The accuracy and reliability of the ET_{ref} are established on the basis of lysimetric measurements and other studies having high confidence (ASCE-EWRI, 2005). The need for refined atmospheric correction of the surface temperature (T_s) and reflectance albedo measurements using radiative transfer models are eliminated with the use of internal calibration of the sensible heat computation in SEBAL and METRIC, and the indexed temperature gradient (Tasumi et al., 2005). Similarly, the impacts of biases in the estimation of aerodynamics stability correction and surface roughness are reduced with the use of internal calibration (Allen et al., 2007).

High quality accurate maps of ET can be obtained from METRIC with emphasis on regions that have high resolution and are less than few a hundred kilometers in scale. METRIC focuses only on narrow regions at relatively high resolution of 30m to provide detailed and accurate estimates of ET. The model also takes into consideration the impacts of regional advection. However, trained experts who have experience in energy balance, radiation physics and acceptable familiarity with vegetation characteristics and short period weather data are required to deal with this narrowed focus (Allen et al., 2007). Compared to other traditional applications of satellite based energy balance, METRIC has substantial advantages over them as

reference ET is used for calibration instead of evaporative fraction (Bastiaanssen et al., 1998a; Bastiaanssen, 2000). By using reference ET to extrapolate the instantaneous ET for periods of 24 hours and longer, regional advection effects can be compensated by not tying the evaporative fraction to the net radiation as ET can exceed daily net radiation in many arid or semi-arid areas (Allen et al., 2007). The model is also advantageous in the sense that it is not necessary to know information about the development stage and specific type of crop while computing ET from crop coefficient curves. Moreover, reduced ET caused by shortage of water can also be detected from energy balance (Allen et al., 2007).

2.13 Theoretical basis of METRIC

Bastiaanssen et al. (1998a, 2005) and Bastiaanssen (2000) have explained the theoretical and computational basis of SEBAL and METRIC. While satellites regularly collect data of surface reflectance and surface temperature, the sensors don't measure the near surface vapor content. Satellite imagery is used to determine ET by employing energy balance at the surface (Allen et al., 2007). SEBAL and METRIC systems are "operational energy-balance based remote sensing models" that have been commonly used to estimate ET from remotely sensed data from satellite. The energy consumption of ET from energy balance at the surface is "calculated as residual of the surface energy equation" (Allen et al., 2005, p. 254).

$$LE = R_n - G - H \quad (1)$$

where LE = latent energy consumed by ET; R_n = net radiation which is the sum of all incoming and outgoing short-wave and long-wave radiation at the surface; G = sensible heat flux conducted into the ground; and H = sensible heat flux convected to the air. The parameters in equation (1) are generally expressed in Wm^{-2}. Potential ET is the measure of the ability of the atmosphere to remove water from the surfaces by evapotranspiration assuming that there is no

control on water supply whereas actual ET is water removal from surface due to the ET process (Pidwirny and Jones, 2009).Using the energy balance model is effective as actual ET is estimated instead of potential ET (based on amount of vegetation) so as to capture the reduction of ET caused by a lack of soil moisture (Allen et al., 2005). A limitation in the energy balance approach is that the computation of LE is dependent on the accuracy of summed estimates of R_n, G and H. However, METRIC overcomes this drawback by emphasizing internal calibration of H instead of LE, to absorb all the intermediary errors and biases. In the METRIC model, R_n is calculated from narrow-band reflectance measured from the satellite and surface temperature; G is calculated from R_n, Normalized Difference Vegetation Index (NDVI) and surface temperature; and H is computed from surface temperature ranges, surface roughness, and wind speed using buoyancy corrections (Allen et al., 2007). The algorithms applied in METRIC to determine parameters R_n and G has its roots from algorithms used in early SEBAL applications by Bastiaanssen et al. (1998a). To improve the accuracy in a large area of surface of surface condition, albedo in METRIC was updated (Allen et al., 2007).

The algorithm used for both METRIC and SEBAL are similar however they differ in terms of how the "H function" is calibrated for each specific satellite image. H is calculated from an aerodynamic function for both METRIC and SEBAL,

$$H=\rho C_p * DT/r_{ah} \quad (2)$$

where ρ is density of air, C_p is specific heat of air at constant pressure, and r_{ah} is "aerodynamic resistance between two near surface heights (generally 0.1 and 2 m) which is computed as a function of estimated aerodynamic roughness of the particular pixel and using wind speed extrapolated to some blending height above the ground surface (typically 100 to 200 m), with an iterative stability correction scheme based on the Monin-Obhukov functions" (Allen et al., 2005,

p.255). The near surface temperature difference between the two near surface heights are represented by dT parameter. As it is challenging to estimate surface temperature (T_s) precisely from a satellite because of uncertainties in atmospheric attenuation and contamination and radiometric calibration of the sensor, dT is estimated as a relatively simple linear function of T_s (Allen et al., 2007).

$$dT = a + bT_s \quad (3)$$

The validation and empirical substantiation for using the linear relation between dT and T_s have been provided by Bastiaanssen (1995) and Bastiaanssen et al. (2005). By assuming theoretically that constant temperature at height well above the surface to be independent of H and with the incorporation of all instability effects in $r_{ah,}$ T_s is proportional to H for fixed aerodynamic condition in equation (2). A segment of temperature profile, which is represented by dT, is proportional to both H and T_s. The equation (3) depends on the range of surface roughness. With the increase in roughness and reduction in $r_{ah,}$ with the same given H, dT reduces as a result of more efficient transfer of H and Ts also reduces because of the same reason (Allen et al., 2005).

In the SEBAL model of Bastiaanssen (1998), the parameters a and b in equation (3) are calculated by setting dT = 0 when T_s is at the surface temperature of a local water body and where H is expected to be zero. Similarly, $dT= (Hr_{ah}) / (\rho C_p)$ at T_s for a "hot" pixel that is dry where an LE=0 assumption is made. From (1), $dT= ((R_n-G) r_{ah})/ (\rho C_p)$ is computed at the "hot" calibration pixel. METRIC model employs the same method and assumptions made in SEBAL for the hot pixel. However, for the lower calibration point of dT, a well-vegetated pixel having relatively cool temperature is selected (Allen et al., 2005).Here dT is calculated as:

$$dT=((R_n-G-k\,ET_r)\,r_{ah}) / \rho C_p \quad (4)$$

For equation (3), a and b coefficients are calculated using two values of dT matched with related values of T_s. The Landsat images can be implemented to identify the fields of alfalfa or other high leaf area. The value of ET from these fields is estimated to be very similar to the value of "reference ET (ET_{ref})" computed for an alfalfa reference (Allen et al., 2005). The METRIC model implements standardized ASCE Penman–Monteith equation for alfalfa reference (ASCE-EWRI, 2004). This value is normally greater than grass reference ET (ET_o) by 20 to 30 percent. The k factor in equation (4) is set to 1.05 with the assumption that "viewed field having high vegetation and colder than average temperature, as compared to other high vegetation fields, will have ET that is about 5% greater than ET_{ref} due to higher surface wetness or merely due to its rank within the population of alfalfa fields (or other highly vegetated areas)." The k factor is reduced in proportion to a vegetation index during the winter and early season periods. Similarly, LE is assigned to hot pixel on the basis of daily soil evaporation model (Allen et al., 2005, p. 256).

The stability corrected r_{ah} is used to compute new dT values for "hot" and "cold" pixels, and new values for correlation coefficients, "a" and "b". These values are used to compute a new corrected H at each pixel level. A new stability correction is done using the corrected H image. Until successive values for dT_{hot} and r_{ah} at "hot" pixel (r_{ah_hot}) are stabilized, these processes are repeated. When the change in r_{ah} at the "hot" pixel is less than 5%, the process is stopped and the corrected value of H is determined (Allen et al., 2002a). The corrected value of H at each pixel is derived by using the corrected final dT and stability corrected r_{ah} image. Latent heat flux (λET) can be defined as "the rate of latent heat loss from the surface due to evapotranspiration" (Waters

et al., 2002, p.34). Latent heat flux for the instantaneous time of the satellite overpass is computed at each pixel using equation 5 below:

$$\lambda ET = R_n - G - H \quad (5)$$

where; λET is an instantaneous value of ET for the time when satellite passes (W/m2) (Waters et al., 2002).

The instantaneous ET (ET_{inst}) is defined as the ET at the "time of the satellite overpass time" (Waters et al., 2002, p.34) and is computed as:

$$ET_{inst} = 3600 \times \lambda ET/\lambda \quad (6)$$

where; "ET_{inst} is the instantaneous ET (mm/hr) ,λ is the latent heat of vaporization or the heat absorbed when a kilogram of water evaporates (J/kg)" (Waters et al., 2002, p.35).. It is calculated from the surface temperature image by

$$\lambda = [[2.501 - (0.002361 \times T_o)] \times 10^6] \quad (7)$$

where; T_o is surface temperature in degree Celsius (Waters et al., 2002).

Reference ET Fraction (ET_rF) or Evaporative fraction is defined as "the ratio of the computed instantaneous ET (ET_{inst}) for each pixel to the reference ET (ET_r) computed from weather data" (Waters et al., 2002, p.35). ET_rF at each pixel level is computed using reference ET at the image time as:

$$ET_rF = ET_{inst} / ET_{ref} \quad (8)$$

where; ET_{ref} is the ASCE Penman-Monteith standardized form of reference ET (mm hr^{-1}) at the image time derived from REF-ET software (Allen et al., 2000b; Waters et al., 2002).

A Daily ET (ET_{24}) map is derived using the evaporative fraction (ET_rF) and cumulative 24-hour ET for the day of the image. It is more important and useful than the instantaneous ET.

It is calculated assuming that the ET_rF computed in equation (8) is constant for 24 hour average. It can be expressed as:

$$ET_{24} = ET_rF \times ET_{ref\_24} \quad (9)$$

ET for a period (monthly or two-month) is calculated by computing cumulative reference ET for the period represented by the image processed as:

$$ET_{period} = ET_rF \times \sum_{i=1}^{n} ET_{ref\_24i} \quad (10)$$

where; ET_{ref_24i} is the cumulative reference ET for the time period from REF-ET software, and n is the number of days used for ET extrapolation (Waters et al., 2002).

2.14 Validation of the METRIC model

Bhattarai (2010) did the validation for the METRIC model by comparing ET values from model with ET values from the USGS ET stations in in Florida. The daily, monthly and two-month ET validation was done using regression analysis by plotting estimated model ET versus observed ET values at USGS stations. It performed well in terms of estimating daily, monthly and two-month ET at USGS. The study reflected that the error in daily METRIC ET differed from -1.64 mm to 0.72 mm and had a mean bias error (MBE) of 0.05 mm. It had a root mean square error (RMSE) of 0.48 mm/day (% RMSE =10%). The study found that there was a strong linear relationship between estimated and measured daily ET with R^2 =0.83 and Nash-Sutcliffe Coefficient (ENS) of 0.82. Similarly in terms of monthly ET, it varied from -39 mm to 28 mm with MBE of -2 mm and RMSE of 16 mm (% RMSE = 16%). Furthermore, the study was also conducted to estimate two month ET and varied from -68 mm to 43 mm with a MBE of -5 mm, RMSE of 30 mm (% RMSE = 16%). The study found good linear relationship between estimated and measured monthly and two-month ET. The R^2 and ENS for monthly ET was 0.77 and

0.7745 respectively and for two months it was 0.73 and 0.71 respectively (Bhattarai, 2010). The study supported that model performed well in estimating the daily, monthly, and two-month ET.

Chapter 3: Improving isolated wetlands classification using LiDAR data in Lee County, Alabama

3.1 Introduction

Isolated wetlands are wetlands that are surrounded by dry lands and have no direct surface-water connection with rivers, ponds, streams, estuaries or oceans (Tiner, 2003). Formed in depressions, isolated wetlands are cut off from traditional waters due to higher elevation of the surrounding land (Leibowitz, 2003; Tiner, 2003). As illustrated by the existing National Wetland Inventory (NWI), there are many areas in Alabama that do not have the digital inventory for the wetland data. A substantial part of Alabama's analog wetlands maps have still not been digitized, and majority of what has been done are coastal and large water bodies rather than isolated and transient waters (Jones, 2013). The need for an inventory of information on isolated wetlands is important to monitor and assess the changes in wetlands and guide the policy makers in making good decisions for its conservation. Jones (2013) applied GeOBIA to classify the isolated wetlands of Northern Alabama from NAIP imagery which yielded an accuracy of 83.7% for aerial imagery inspection with classification errors mostly comprising of building rooftops, asphalt and shadows (Jones, 2013). This research attempts to improve the classification methods for wetlands and will test methods to remove rooftops mistakenly classified as wetlands.

3.1.1 Study area

The study area for the case study covers Lee County in Alabama, United States. According the United States Census Bureau of 2010, the population of the county is 140,247.

The total area of the county is approximately 615 sq. miles, with 608 sq. miles of land and 76 sq. miles of water (U.S. Census Bureau, 2015). There are total of seven urban areas in the county with Auburn-Opelika being the largest. Figure 3.1 below shows the boundary of Lee County, which is the study area for this case study. Lee County is chosen for the study area because LiDAR data are readily available from a partnership between Auburn University, Lee County, and the Cities of Auburn and Opelika.

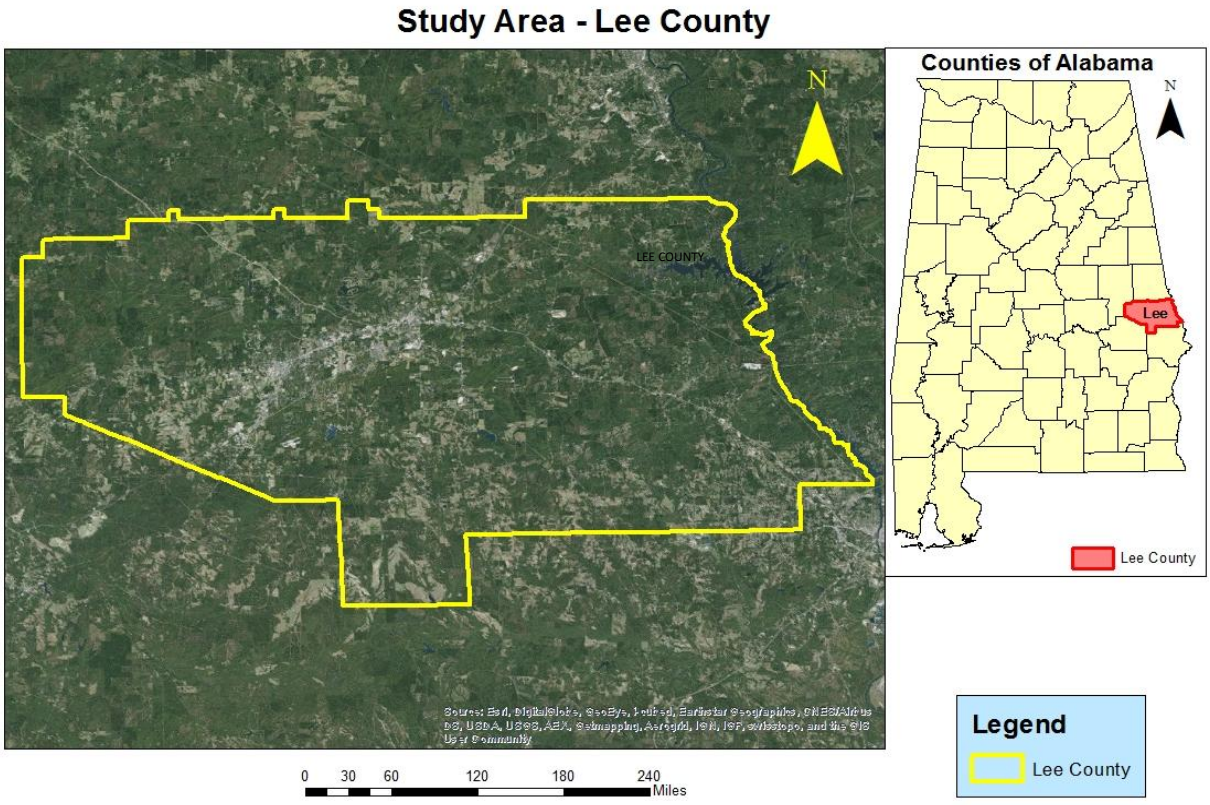

Figure 3.1: Lee County, AL

3.1.2 Objectives

The goal of this study is to improve classification methods to identify isolated wetlands by integrating multispectral images and LiDAR data. The method developed can be further

applied to classify wetlands in other parts of Alabama. This project will be accomplished with the following objectives:

- Identify and delineate isolated wetlands in the study area using high-resolution NAIP images.
- Removal of identified rooftop errors in initial wetland mapping classification.
    - Comparison between building rooftop classification results from GeOBIA and Point Cloud Task method in LP360 software to see which method performs better.
    - Eliminate the errors of building rooftops in wetland classification by erasing those errors by introducing the rooftops classified from LiDAR point cloud in GIS environment.
- Accuracy Assessment of the classified isolated wetlands by visual inspection with NAIP imagery.

3.1.3 Research questions

- What is the spatial extent of isolated wetlands in Lee County?
- Which method was better to classify building rooftops: GeOBIA or Point Cloud Task method in LP360 software?
- How has the introduction of the LiDAR improve the wetlands classification?

3.2 Data used

The data used for the classification of wetlands are as follows:

3.2.1 NAIP imagery

The National Agriculture Imagery program (NAIP) acquires digital aerial imagery of the United States during the agricultural growing season (USDA, 2013). It is funded by the United States Department of Agriculture's (USDA) Farm Service Agency (FSA) through the Aerial

Photography Field Office (APFO) in Salt Lake City. The program was initiated in 2003 and initially had a goal to acquire imagery on a 5 year cycle but now attempts to collect imagery on a 3 year cycle beginning from 2009 (USDA, 2013). The spatial resolution of the imagery is one meter and has three to four bands including red, green, blue and more recently many states have begun to collect near-infrared as the fourth band. The distribution and organization of the NAIP imagery is in accordance to the existing United States Geological Survey (USGS) 7.5 minute topographic quadrangles grid system with each NAIP image conforming to one quarter quadrangle or 3.75x3.75 minute having a buffer of 300m on all four sides. The standard projection of the tiled images is in the Universal Transverse Mercator (UTM) coordinate system using the North American Datum (NAD) of 1983 (USDA, 2013; Jones, 2013).

3.2.2 Airborne LiDAR

Airborne Light Detection and Ranging (LiDAR) is an optical remote sensing technology that produces highly accurate x, y and z coordinates by measuring the difference in time between the emission of laser pulses and reception of reflected signal from the ground from the aircraft (Porwal and Udeechya, 2013). The LiDAR dataset used in the study was a part of the Lee County LiDAR survey acquired during winter 2011. The data consists of mass point cloud datasets in LASer (LAS) format that can be managed, visualized, and analyzed in a Geographic Information System (GIS). The average point spacing of the LiDAR for Lee County is 3.54 feet. The projection of the LiDAR data is in the State Plane Coordinate System (SPCS) Alabama east zone with horizontal datum of North American Datum of 1983 (NAD83(HARN)) and vertical datum - North American Vertical Datum of 1988 (NAVD88(GOEOID03) for converting ellipsoidal heights to ortho-metric heights.

3.2.3 National Hydrography Dataset (NHD)

The National Hydrography Dataset which is provided by USGS consists of digital vector datasets of the surface water components such as streams, lakes, ponds, rivers, canals, dams and stream gages which are used for general purpose mapping and in the analysis of surface-water systems. The NHD along with Watershed Boundary Dataset (WBD) employs an "addressing system based on reach codes and linear referencing" that gives information such as water quality, water discharge rate and fish population about the water (USGS, 2013). The NHD data are used to help determine which classified wetlands are considered to be isolated.

3.2.4 FEMA DFIRM

To determine the isolation of the wetland from floodwater, a floodplain dataset from Federal Emergency Management Agency's (FEMA) Digital Flood Insurance Rate Map (DFIRM) was used. The DFIRM dataset provides the spatial extent of Special Flood Hazard Areas (SFHA), which are areas that have a one percent chance of flooding on any given year. The SFHA gives the national standard for floodplain data and are used in this project to define geographic isolation by having 40 meter buffers on these floodplains (Jones, 2013).

3.3 Classification of isolated wetlands using NAIP imagery

3.3.1 Methods used

3.3.1.1 Data preparation of NAIP imagery

The NAIP imageries for the Lee County are organized and distributed with the existing USGS 7.5 minute topographic quadrangles grid system. Each NAIP image corresponds to one quarter quadrangle or 3.75x3.75 minute with an overlap of 300 meter buffer on all sides (Jones, 2013). The study area of Lee County consists of 54 Digital ortho-photo quarter quadrangles (DOQQ), which is a very large dataset. Although there are many studies in the literature about

GeOBIA processes, most of these deal only with small datasets (Chan et al., 2009). Since image segmentation is a complex and resource intensive operation, it is advisable to have powerful personal computers with higher capabilities in terms of speed and storage performances (O'Neil-Dunne et al., 2009). Since the study area might contain billions of pixels even in an area of 1000 km^2, the best approach to deal with this limitation is to tile the images. While doing this, the input datasets are partitioned into separate tiles and are individually analyzed. After analyzing each tile the resulting products are recombined in the final dataset (O'Neil-Dunne et al., 2009).

3.3.1.2 GeOBIA methods

3.3.1.2.1 Segmentation

Image segmentation is the most essential step in object-based image analysis where digital images are subdivided into less complex partitioned regions known as image object primitives. This process of GeOBIA is defined by the shift from spectral information of individual pixel to more meaningful objects that enables the user to implement rule-oriented image analysis based on spatial and spectral attributes, and image object relationships (Hay and Castilla, 2006). The image object primitives gives us meaningful information on spectral values, shape, extent, statistics, texture calculation, topological features (neighbor, super-object etc.) and helps better understand the relationship between real world objects and image objects (Benz et al., 2004). Based on this meaningful information, image objects can be classified into land use/land cover classification. Figure 3.2 shows a NAIP image before and after multiresolution segmentation is executed.

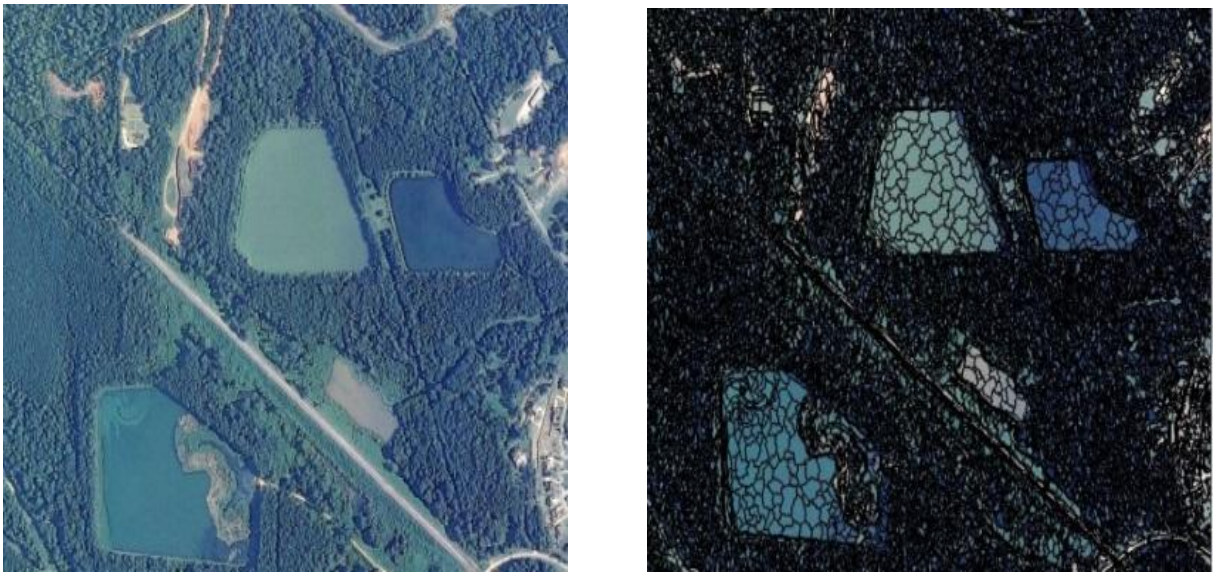

(i) (ii)

Figure 3.2: Images before (i) and after (ii) Multi-Resolution Segmentation.

Segmentation of pixels into objects make it possible for decision-tree based image analysis where ruleset can be developed based on the information about object relationships as well as spatial and spectral attributes. There are different segmentation methods but the most commonly used algorithm is multi-resolution segmentation (MRS) (Benz et al., 2004). MRS is a bottom up region-merging technique which starts with a small one-pixel object and merges into a bigger one in several subsequent steps, MRS segments the image pixels based on the scale, weight of the spectral reflectance, shape and compactness. Pixels having similar spectral reflectance are grouped into a single object while also considering shape and compactness of the polygon. The scale parameter determines the scale or size of the image object primitive and the value for it depends on what the analyst is trying to classify which is mostly based on trial and error approach. This parameter plays an important role in the occurrence or absence of certain object classes and the same object in different scales can appear differently (Benz et al., 2004). There can be hierarchical dependency between different scales. As scale is very important for

reshaping objects into meaningful features such as wetlands or building rooftops, the analyst can perform segmentation at different scales.

The parameters for MRS were chosen based on trial and error process. The scale parameter for this project was 35 with shape and compactness value as 0.2 and 0.7 respectively. The weights values for the red, green, and blue (RGB) bands were set to one while NIR is given the value of 2. The NIR band was given the value of 2, which is a double weight to account for water having a relatively low reflectance in the NIR portion of the electromagnetic radiation spectrum. Figure 3.3 shows the parameters for multi-resolution segmentation.

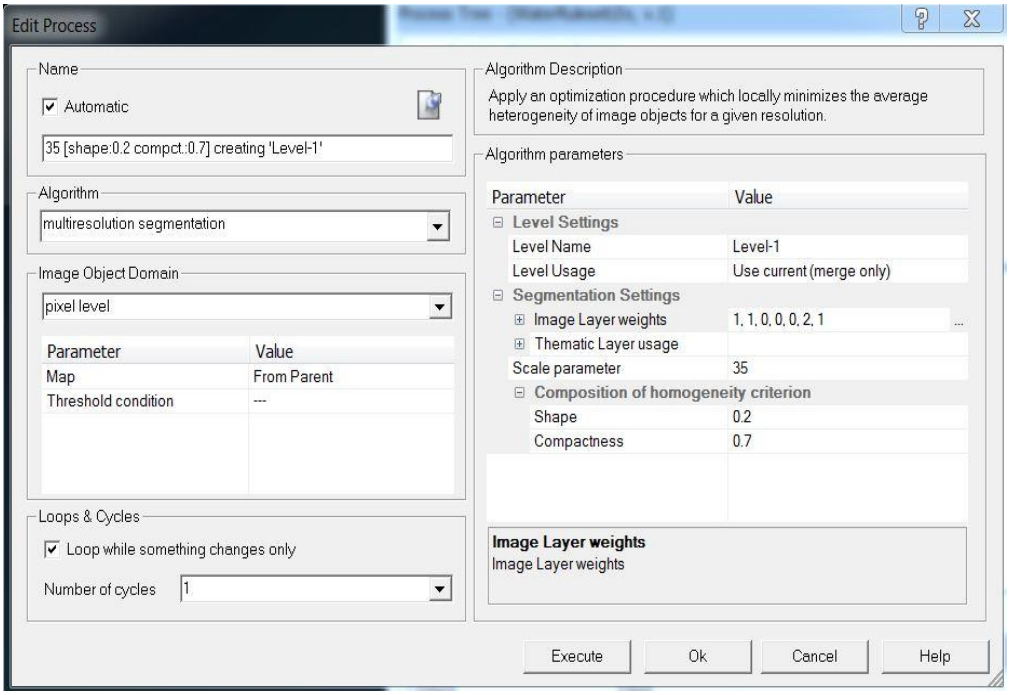

Figure 3.3: Parameters for Multi-Resolution Segmentation.

3.3.1.2.2 Classification

The classification method is the process of assigning a class category to object primitives (polygon formed from a group of pixels) based on spectral attributes and hierarchical relationships. Different features have different spectral responses and this information can be

used classify the image into different land use/land cover classes. A ruleset, consisting of a sequence of processing algorithms, was developed to classify water bodies and exported into GIS layers in eCognition software. It is mostly based on using the trial and error approach, which has become common in this sort of analysis (Myint et al., 2011). The ruleset for this project used information such as mean spectral reflectance of near infra-red (NIR), open water spectral signature, homogeneity, ratio green, standard deviation of NIR, ZABUD, and texture to classify the water bodies.

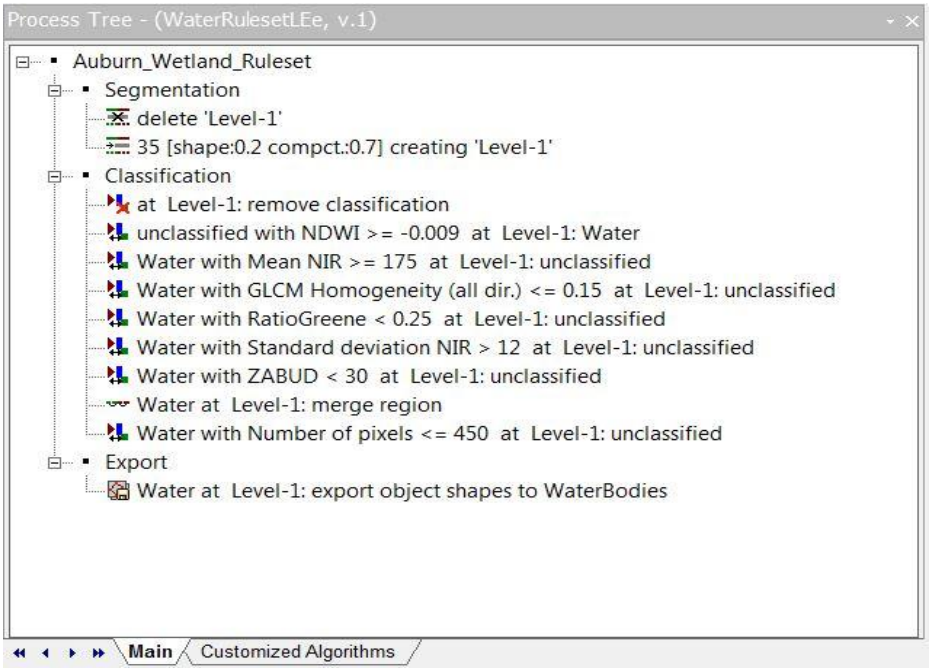

Figure 3.4: Ruleset used for the classification of wetlands

Open water spectral signature is analyzed by

([Mean Green]-[Mean NIR])/ ([Mean Green] + [Mean NIR])

which defined open water bodies while excluding vegetation. Ratio Greene is the defined by

[Mean Green]/ ([Mean Blue] + [Mean Green] + [Mean Red] + [Mean NIR])

Ratio green helps to eliminate some of the shadows that are wrongly classified as wetlands. However it does not completely eliminate all the errors of shadow. ZABUD is the rule developed to identify discontinuous built up area (Lewinsky, 2007) and it helped to eliminate the impervious surfaces that were wrongly classified as wetlands. The formula for ZABUD can be defined as

((([Mean Blue]-[Mean Green]) ^2) + (([Mean Green]-[Mean Red]) ^2) + (([Mean Red]-[Mean NIR]) ^2))^0.5

It is an index used to identify built up area from the LandSAT-ETM+ in the original ZABUD derived by Lewinsky (2007) but has been modified for four band spectral images such as the NAIP images in this study. This index is efficient in extracting asphalt features such as roads (Kokje and Gao, 2013). Figure 3.5 shows the classification of water bodies in blue color from the ruleset developed in Figure 3.4.

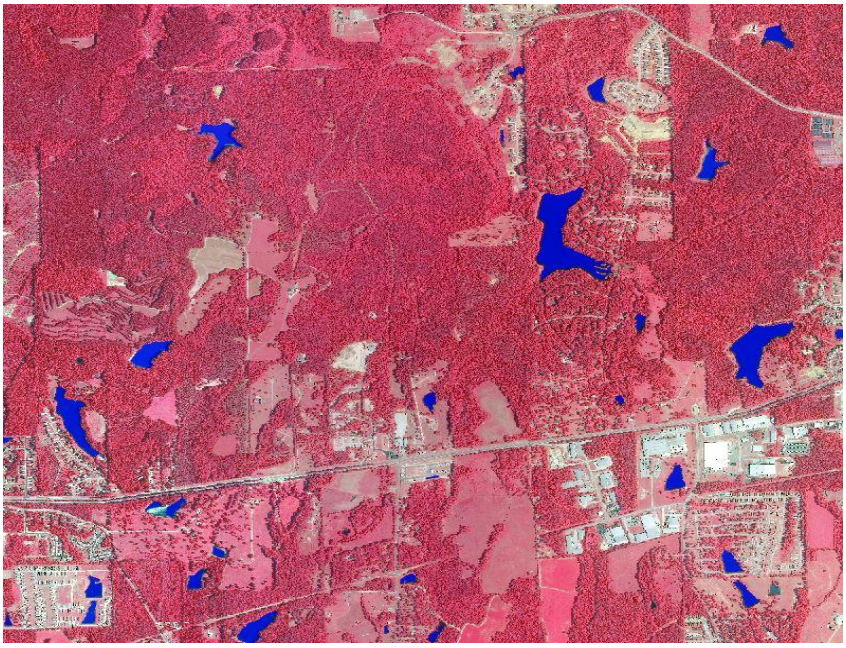

Figure 3.5: Classification of water bodies delineated in blue color

3.3.1.2.3 Export to vector layer

After the classifying the water bodies, they were exported into a geo-referenced vector polygon layer using appropriate naming schemes. The eCognition software allows the user to add attributes to the exported water body GIS layers based on their object attributes. After the ruleset was developed, it was applied to individual project tiles as a batch process using the Analyze tool in eCognition resulting in the output layers with appropriate naming schemes. The GIS layers of all the individual project tiles were merged in the GIS producing a single water body layer.

3.3.2 Results and discussion

Classification of wetlands using GeOBIA methods resulted in 2,195 water bodies being initially classified that included rivers, lakes, wetlands, streams etc. The water bodies classified are shown in the Figure 3.6 in light blue color.

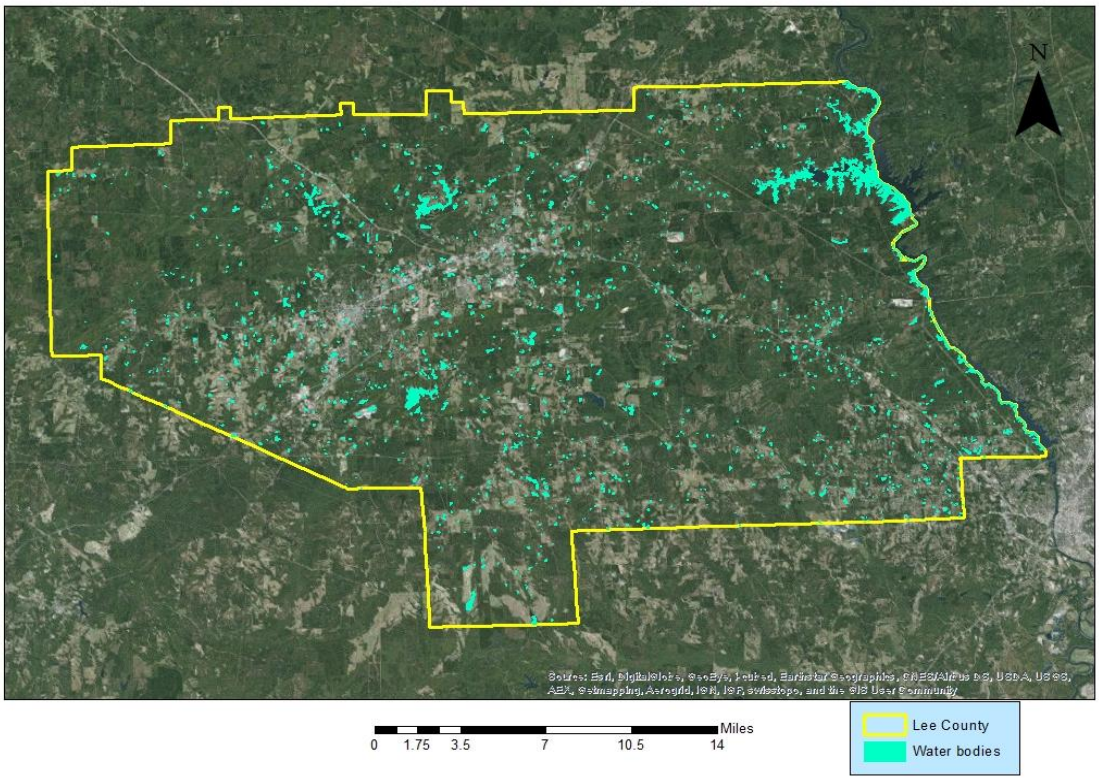

Figure 3.6: Classified water bodies from the ruleset developed in GeOBIA

To validate the geographic isolation, the resulting water body layer was buffered with NHD dataset and existing 100-year floodplain data in accordance with the Tiner Methodology (Tiner, 2003). Although, hydric soils were used as a data source for mapping wetland in Jones (2013), these data for Lee County do not exist and were not used. Isolation was defined by selecting only those water bodies that did not overlap with the 40 meter buffer with NHD dataset and FEMA DFIRM floodplain data. A buffer of 40 meter NHD dataset was done in GIS producing the output as shown in the Figure 3.7 and Figure 3.8.

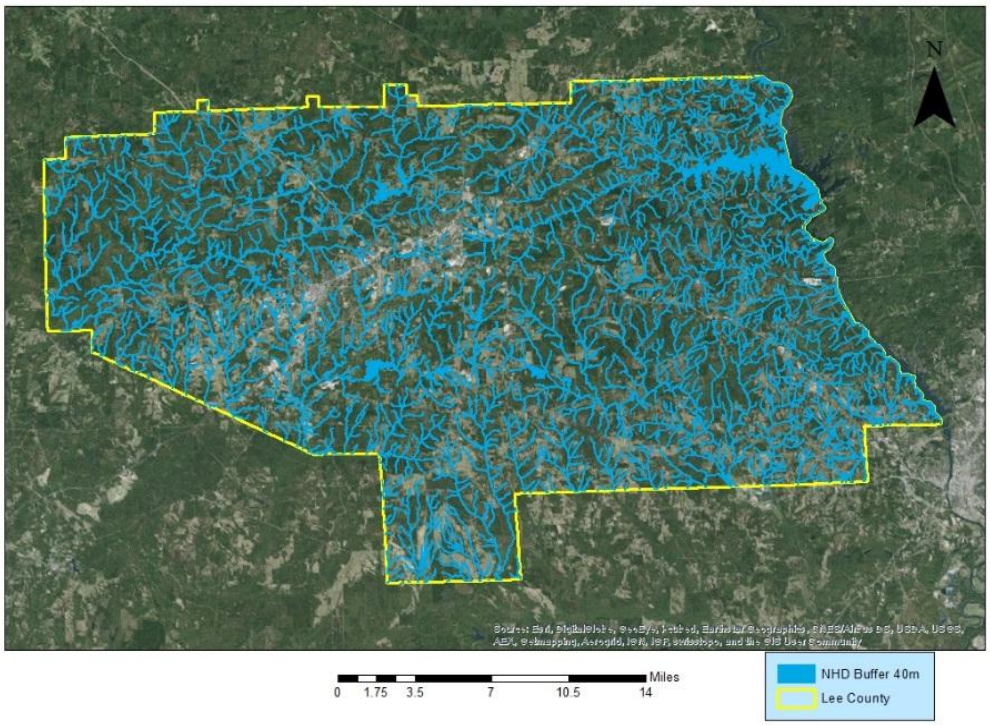

Figure 3.7: 40 meter buffer of NHD dataset represented in blue color

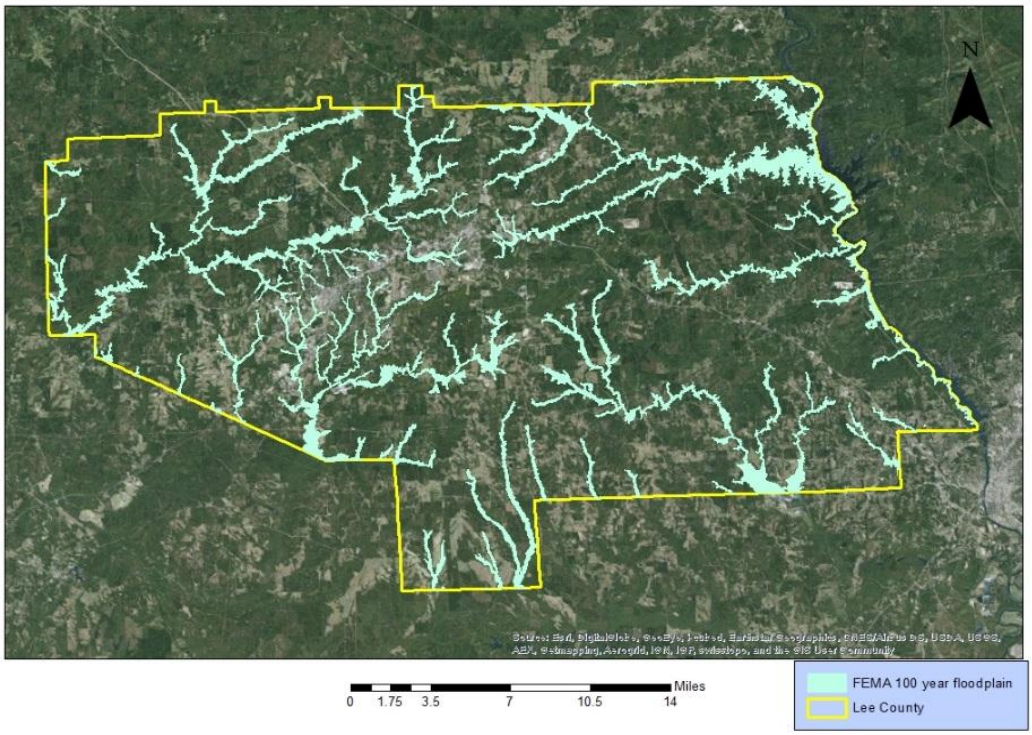

Figure 3.8: FEMA DFIRM 100 year floodplain data represented in light blue color

A “Select by Location” query function was performed in GIS, where only water bodies that did not intersect the 40m buffer NHD layer and floodplain were selected and exported into a new layer for isolated wetlands. A total of 976 isolated wetlands were classified in Lee County as shown in the Figure 3.9.

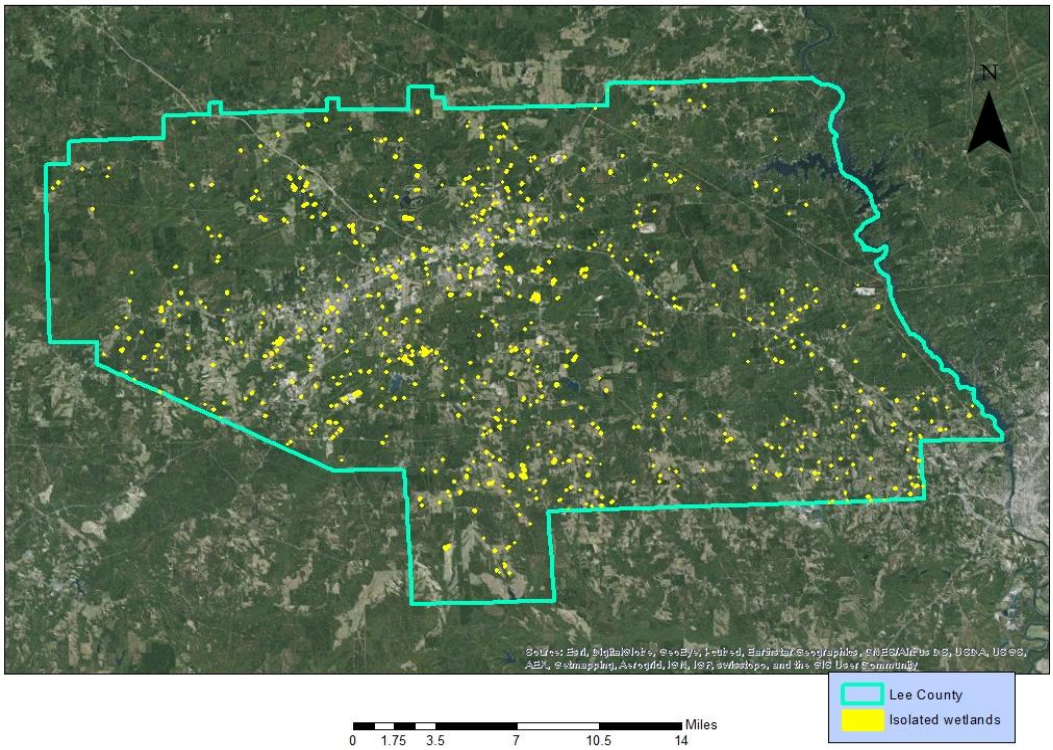

Figure 3.9: Wetlands classified after defining isolation before eliminating rooftops errors

3.3.3 Accuracy assessment

The classification of isolated wetlands using GeOBIA resulted in total of 976 polygons. The accuracy assessment was done for the isolated wetlands for the whole Lee County to see if there were errors of building rooftops, asphalts and shadows as it was detected in Jones (2013) results. The Alaska Pak v3.0 for ArcGIS 10.x was used to randomly select 250 polygons from the isolated wetland classification and exported into new layer as shown in Figure 3.10. The

accuracy was assessed on these 250 points by visually inspecting the polygon with the NAIP imagery.

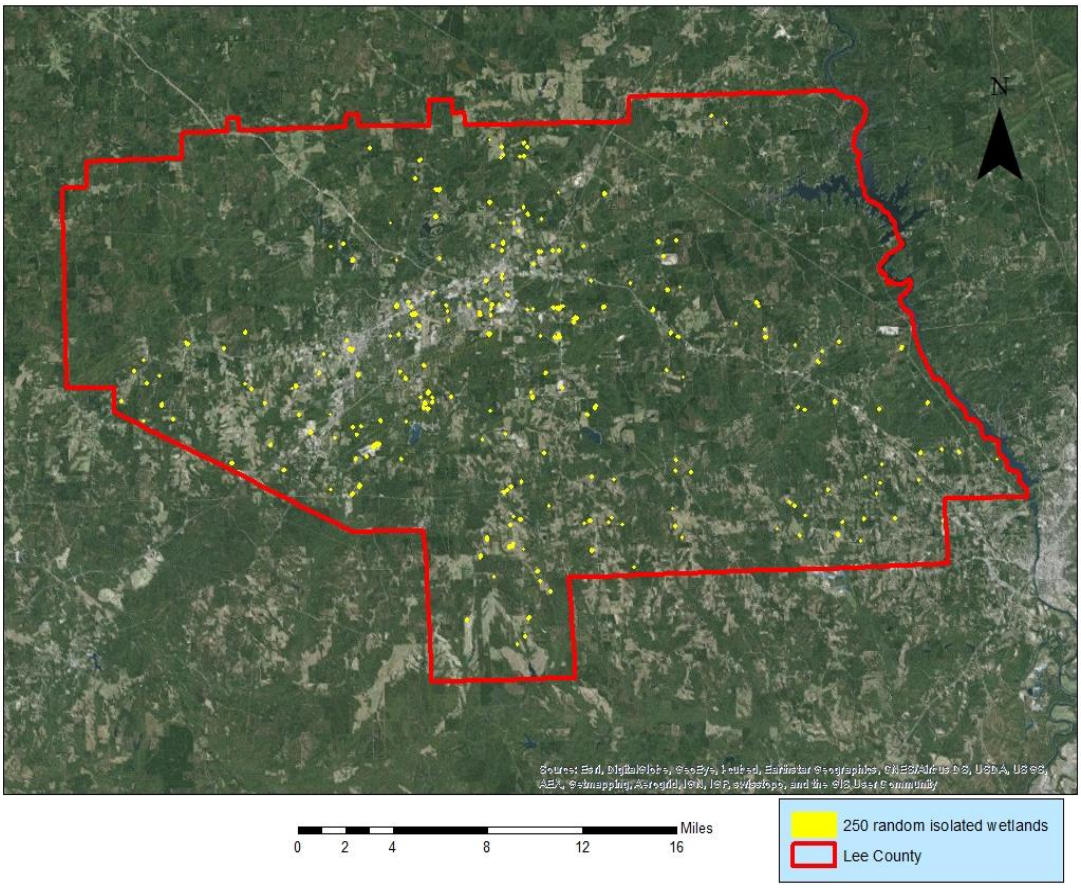

Figure 3.10: 250 randomly selected isolated wetlands for accuracy assessment in Lee County

The errors considered for this project were of commission rather than omission which means it was assessed for only those isolated wetlands that were classified. The accuracy assessment of isolated wetlands from the GeOBIA method is shown in the Table 3.1.

S.N		Number of polygon
1	Correctly classified isolated wetlands	201
2	Errors of building rooftops	19
3	Errors of shadows, asphalt	30
4	Total	250

Table 3.1: Accuracy assessment results of isolated wetlands classification

Accuracy percent was measured as the percentage ratio of correctly classified isolated wetlands by total wetland polygons selected. The accuracy percent for the initial GeOBIA approach is 80.4% which is shown in the Table 3.2.

Method	Accuracy Percent
Correctly classified isolated wetlands	(201/250)*100% = 80.4%

Table 3.2: Accuracy percent of isolated wetland classification

Figure 3.11: Classification errors where building rooftops were classified as wetlands

The accuracy assessment of the 250 isolated wetlands showed that there were errors of building rooftops, asphalts and shadows. Out of the 250 selected for the accuracy assessment, there were 19 errors of building rooftops as shown in Figure 3.11 and 30 errors of asphalt and shadows. Similarly, some of the correctly classified wetland polygons were incomplete in shape and did not cover the whole area of wetland as in NAIP images.

3.4 Improving the isolated wetlands classification through the removal of rooftops

3.4.1 Comparison of two methods for classification of building rooftops in pilot study

Jones (2013) applied GeOBIA to classify the isolated wetlands of Northern Alabama from NAIP imagery resulting in an accuracy of 83.7% for aerial imagery inspection. The classification of the wetlands in the previous study had errors most commonly where wetlands were wrongly classified as building rooftops. Similarly, the classification of isolated wetlands done above in Section 3.3 had errors of rooftops, shadows and asphalt. This research study attempts to classify the building rooftops in Lee County and use that rooftop layer to eliminate the rooftop errors in initial isolated wetland classification. This research study first determines the best methods to classify building rooftops by testing on a small section of Lee County in Figure 3.12 using LiDAR data with two different methods described in the literature. For the first case, building rooftops were classified using GeOBIA methods in eCognition software through a combination of imagery and LiDAR. For the second method building rooftops were classified using the Point Cloud Tasks (PCT) method in LP360 software, which is an extension for ArcGIS and relies only on the LiDAR data. The results of the rooftop classification from both methods were compared to see which gives better classification results by visually comparing the results with the high resolution NAIP imagery. The method that produces better results in terms of accuracy in presence and shape was used to classify the rooftops for the whole of Lee County.

After delineating the rooftop polygons for the whole Lee County, the data was used to mask out the wetlands that were wrongly classified.

3.4.1.1 Study area

The study area for the project covers the southeastern part of Lee County in Alabama, United States. The total area of the study area is 37.4 sq. miles, which consists of both urban and rural areas. Figure 3.12 below shows the border of the study area inside the border of Lee County. The southeastern part of Auburn was chosen because this area has both buildings and vegetation to compare the results for the two methods.

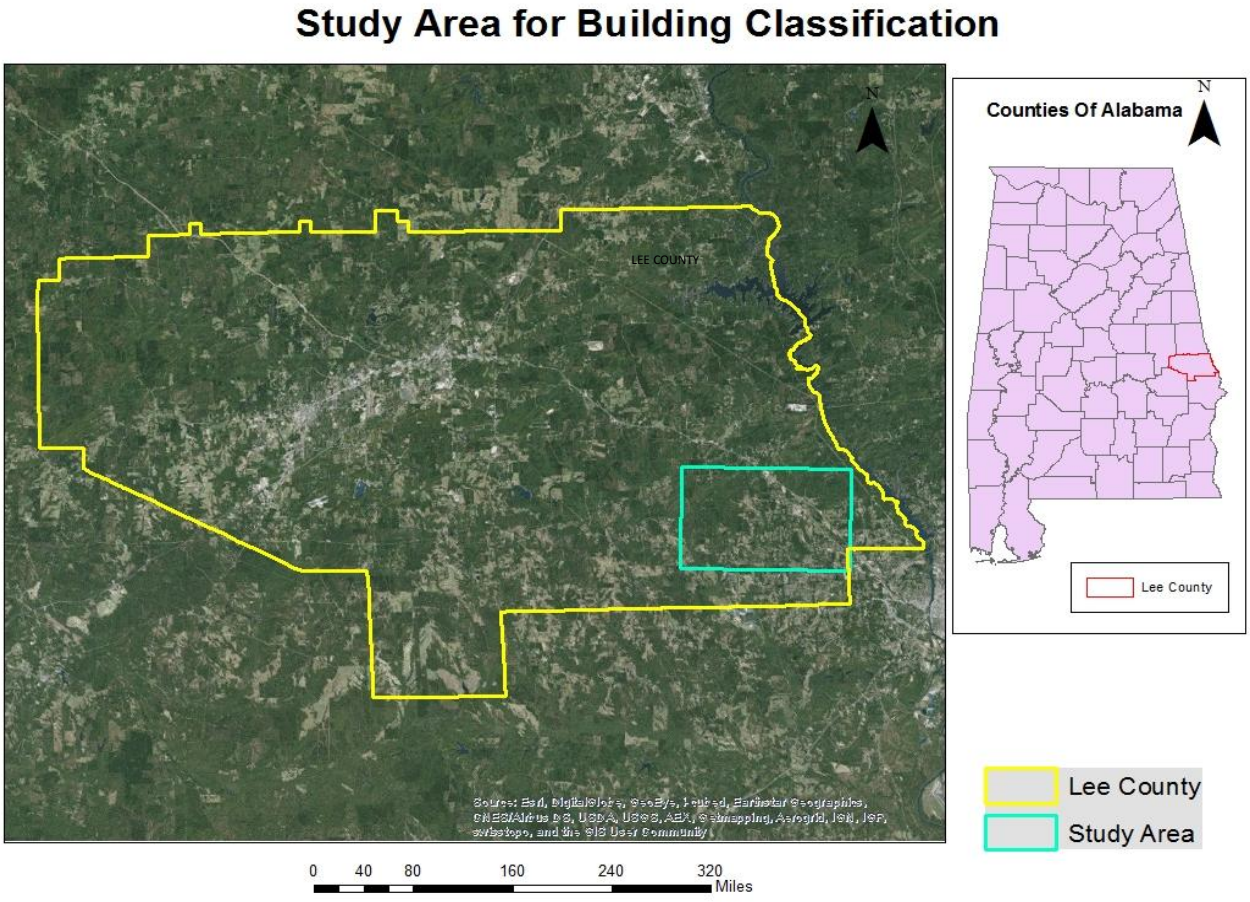

Figure 3.12: Study area which is within the blue boundary of Lee County, AL

3.4.2 Methods used

3.4.2.1 Data preparation of National Agriculture Imagery Program *(*NAIP*)* imagery for rooftop removal

The NAIP imagery for the Lee County are organized and distributed with the existing USGS 7.5 minute topographic quadrangles grid system incorporated. Each NAIP image corresponds to one quarter quadrangle or 3.75x3.75 minute with an overlap of 300 meter buffer on all sides (Jones, 2013).The study area for this project consists of 2 Digital Ortho-photo Quarter Quadrangle (DOQQ) NAIP images which were mosaicked into a single image. The mosaicked image was then tiled into 5000 feet x 5000 feet with an overlap of 500 feet (10 percent) between those tiles using the dice image command in ERDAS Imagine 2013.

3.4.2.2 Data preparation of LiDAR

The LiDAR data of the study area, which are in LAS format, were prepared differently for the two methods tested. For classifying rooftops with eCognition and GeOBIA methods the LAS data were converted into multipoint feature classes for both bare earth and non-ground features in ESRI's ArcMap. Bare earth multipoint was created from the last return of LiDAR data while non-ground multipoint was created from first return. The multipoint features produced from the LAS files were used to create a terrain dataset using the New Terrain wizard tool in the Arc Catalog window. The terrain dataset can be used to produce raster-based digital elevation models for modeling and analysis. A Digital Elevation Model (DEM) and a Digital Surface Model (DSM) raster images were produced from the bare earth and non-ground terrain dataset respectively using 3D Analyst tools in ArcGIS. Figure 3.13 shows the images of DEM and DSM of one section of the study area. Figure 3.13 (i.) only shows ground whereas (ii.) shows where there are non-ground discrete features.

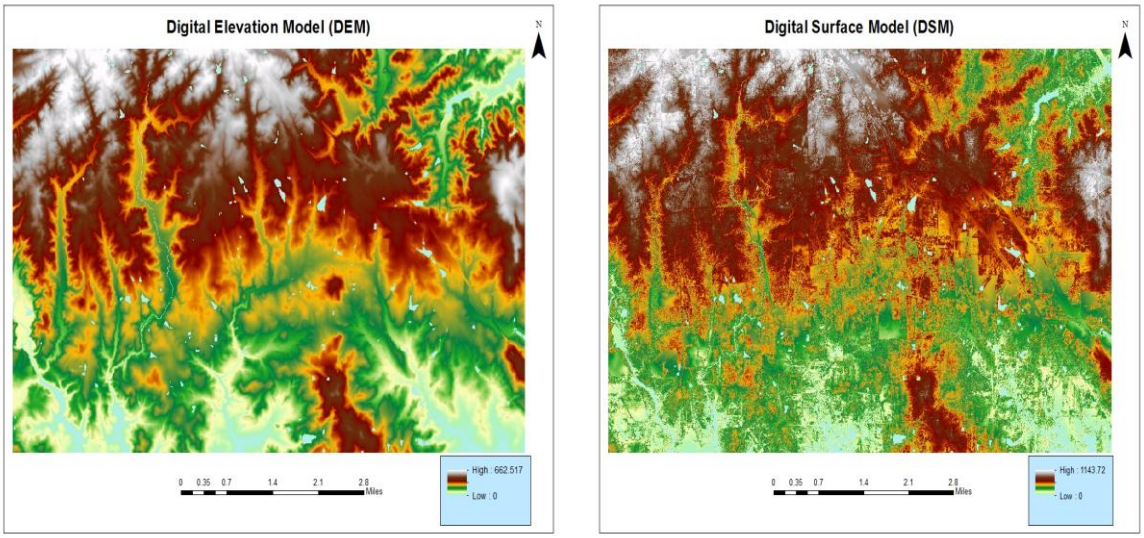

(i) (ii)

Figure 3.13: (i) DEM (ii) DSM of study area

A new raster image, called the Normalized Digital Surface Model (nDSM), represents the height of the features above ground level and was derived by subtracting the DEM from the DSM using the raster calculator. Similarly, an intensity map was created from the LiDAR point cloud using the intensity attribute of the point clouds. The nDSM and intensity raster were then tiled into 5000 feet x 5000 feet with an overlap of 500 feet (10 percent) between those tiles using the dice image command in ERDAS Imagine 2013. Figure 3.14 below shows the images of nDSM and intensity.

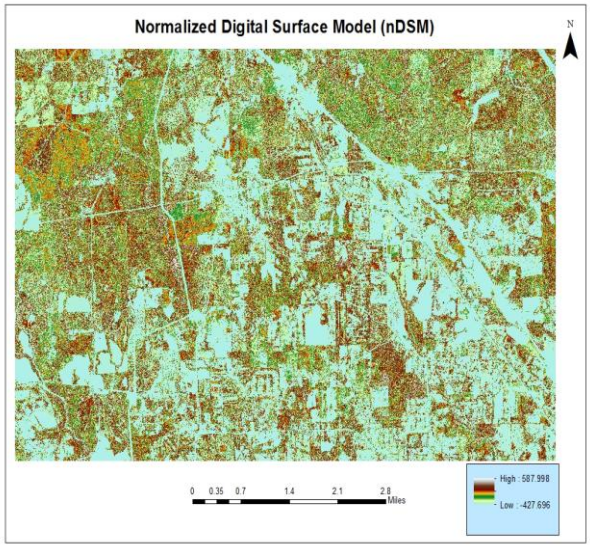

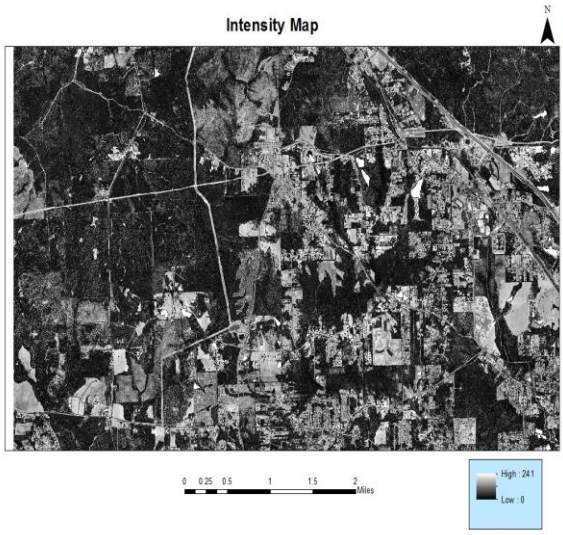

(i) (ii)

Figure 3.14: (i) nDSM (ii) Intensity Raster of study area

After the project based tiling of NAIP imagery, intensity and nDSM raster, the customized import routine was executed within eCognition environment which creates a series of individual project files. The four band layers of NAIP images were integrated with the intensity and nDSM layer resulting in a six band layer with the same spatial extent.

3.4.2.3 GeOBIA methods

3.4.2.3.1 Segmentation

Multi-Resolution Segmentation (MRS), as explained in section (3.3.1.2.1) was used in this task which is a bottom up region-merging technique which starts with small one-pixel objects and merge into a bigger one in several subsequent steps (Benz et al., 2004). Through a trial and error process, the scale parameter value MRS for this project was set to 20 with shape and compactness value set to 0.5 and 0.7 respectively. The weight of all spectral bands was set to 0 except for NIR which was set to 2 since building rooftops have low reflectance in the NIR

portion of the electromagnetic radiation. Figure 3.15 shows an example of multi-resolution segmentation of an area that shows building rooftops as multiple object primitives.

Figure 3.15: Images after Multi-Resolution Segmentation.

3.4.2.3.2 Classification

A ruleset was developed to classify rooftops and to export them as GIS layers in eCognition software. The ruleset for this project used information such as mean spectral reflectance of NIR, Normalized Difference Vegetation Index (NDVI), Normalized Digital Surface Model (nDSM), standard deviation of nDSM, relative boarder to building rooftops, and ratio of Length to Width and texture to classify the building areas. Figure 3.16 shows the ruleset developed for the classification of rooftops.

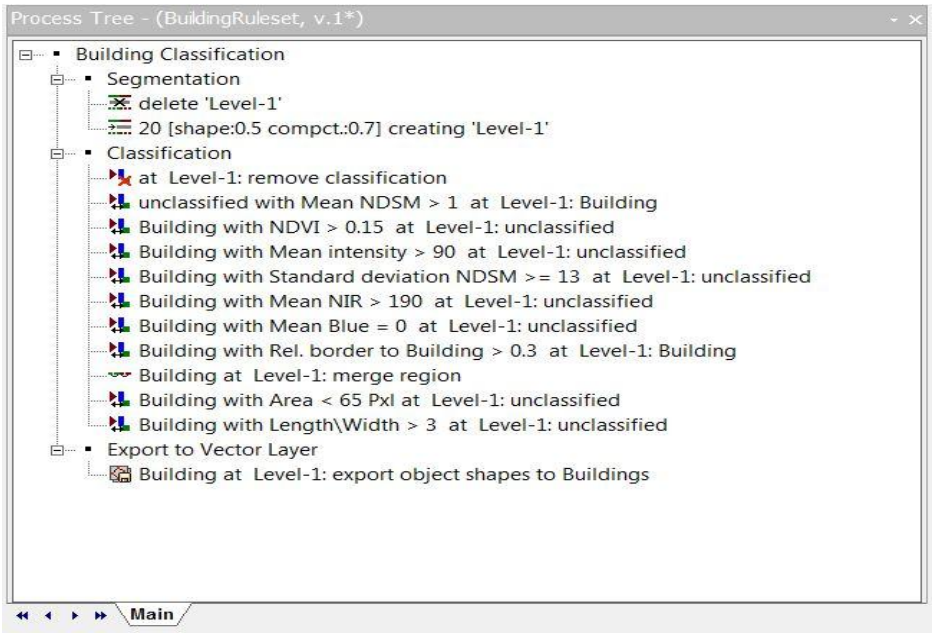

Figure 3.16: Ruleset developed for classification of rooftops

Figure 3.17 below shows the classification of rooftops in green color of two separate areas using the ruleset.

Figure 3.17: Classification of building rooftops in the study area

3.4.2.3.3 Export to vector layer

After the classification of the rooftops, they were exported into geo-referenced vector polygon layer using appropriate naming schemes. The eCognition software allows the user to add attributes to the exported building rooftops layer based on the object attributes. As with the wetlands classification, the ruleset was applied to individual project tiles as a batch process using the Analyze tool in eCognition resulting in the building rooftops output layer with appropriate naming schemes.

3.4.2.4 LP360 methods

A second method was used to test an approach that relied only on the LiDAR data to classify rooftops. One advantage of using LP360 is that the software extension works directly with the LAS datasets and has the capability to work very rapidly with very large datasets at a regional or county-wide scale (QCoherent, 2012). Advanced point cloud tasks (PCT) in the LP360 extension were used to filter and extract rooftops of the study area. The filter was used to classify or change the classification values for LiDAR point clouds. After the classification was implemented, the extractor was used to pull information from the point cloud data into GIS layers. The LiDAR data provided by vendor was only classified for the ground and non-ground features. Therefore to refine the classification, the non-ground features such as vegetation, buildings and water bodies were classified using PCT.

3.4.2.4.1 Height Filter

First, a height filter was made which classified all the features above the ground (non-ground points) into Low, Medium and High Vegetation. The height filter uses the terms Low, Medium and High Vegetation but this is misleading as all features are classified including man-made features such as buildings. Implementing the height filter uses the minimum and maximum

object height parameters to classify and eliminate points above a ground surface according to the classification requirement. Different ranges of height were used to classify point clouds into the features as shown in the Figure 3.18.

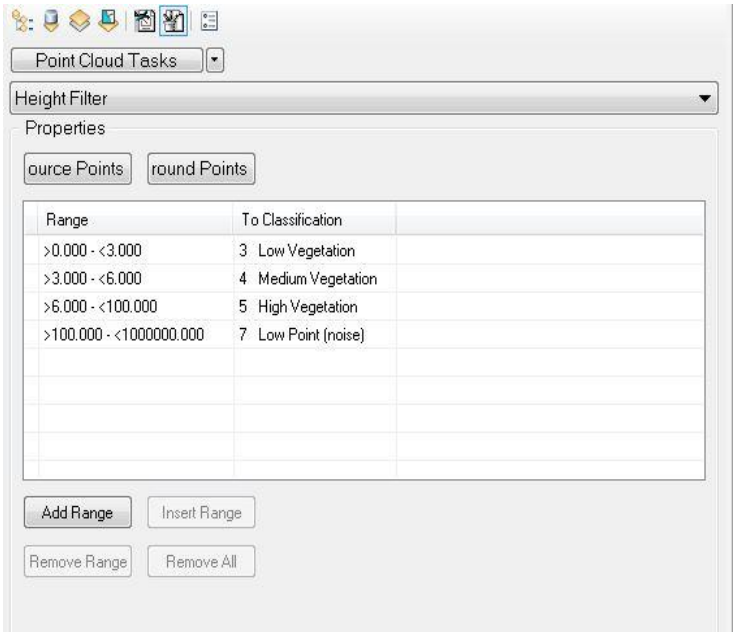

Figure 3.18: Height filter defining classes for different height range including both vegetated and non-vegetated features.

The ranges of height values were followed according to the tutorial exercise of LP360 software from QCoherent (QCoherent, 2014). Figure 3.19 shows the points clouds being classified as ground in a brown color and Low, Medium, High features in different shades of green colors. There are strips of tile overlap where more points were collected.

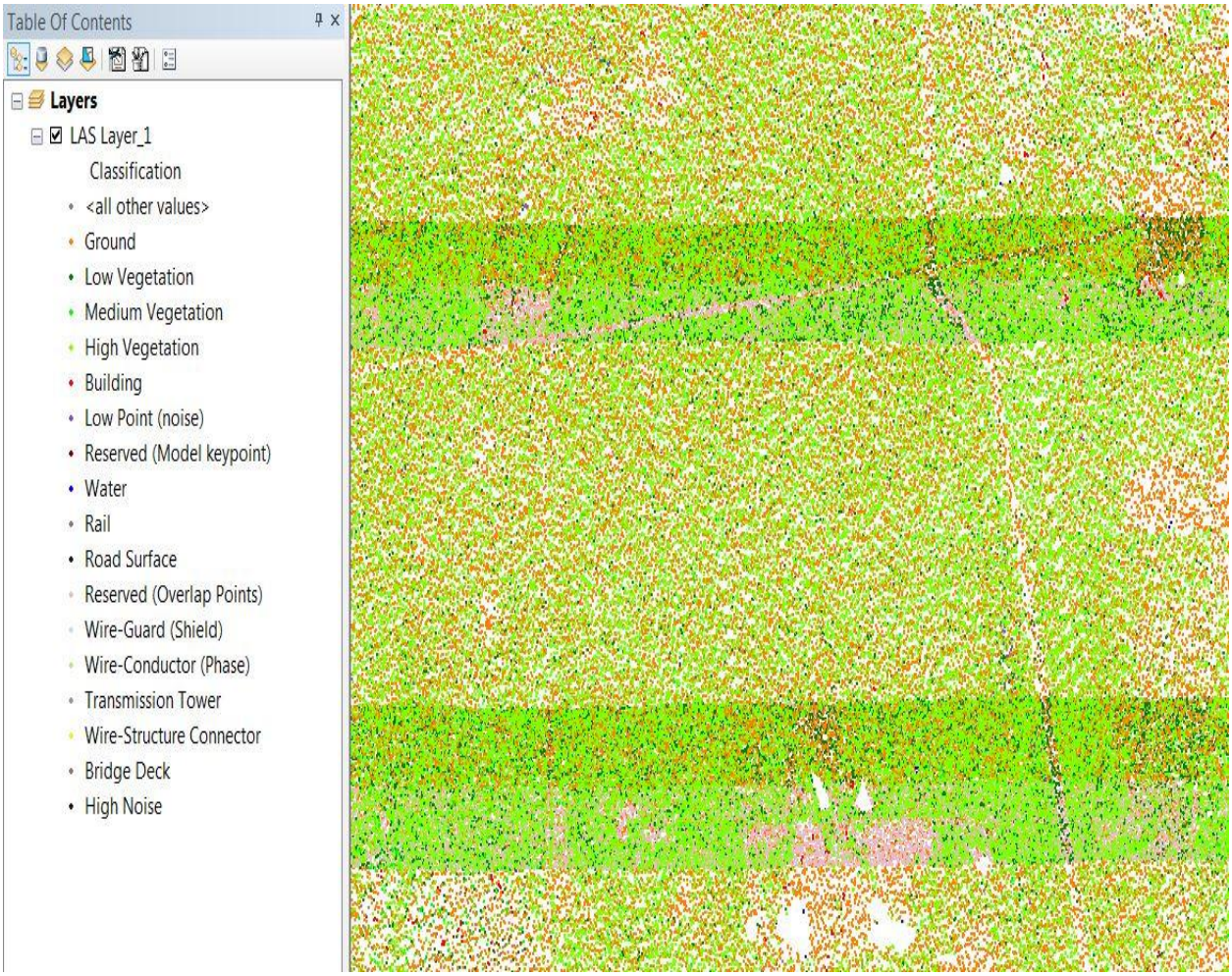

Figure 3.19: Point clouds being classified after running height filter

3.4.2.4.2 Planar Point Filter

After the implementation of the height filter, a new task was created called Planar Point Filter that differentiates points into user-defined planes and classifies those points to classes as specified by the user. This filter is commonly used for the classification of building footprints and in this case rooftops as the surfaces are planar. Minimum and maximum heights of the buildings must be defined so that features are correctly classified by satisfying local conditions. Minimum and maximum height changes from place to place. Since Lee County does not have very tall buildings, a maximum height of 600 feet above ground was used. In addition to this, the

parameters for the Minimum Plane Edges, Maximum Grow Window Area, N-Threshold, Plane Fit, Minimum Slope and Maximum Slope as followed in the LP360 tutorial were entered based on trial and error method to see which values gave better results.

Minimum Plane Edge is an important setting in which the algorithm moves the window around the data and extracts a "planar patch that has minimum square area of Min. Plane Edge X Min. Plane Edge" (QCoherent, 2012). The parameters must be chosen in such a way that it should be large enough that at least 8 points are included in the planar patches. Moreover, it should also be small enough to find multiple patches in the planes that are being extracted from the point cloud. The best approach to the Planar Point Filter is to experiment with different values in the parameters mentioned above and see which values gives a better result of the building rooftops classification. The values set for the parameters to classify building rooftops are shown in the Figure 3.20.

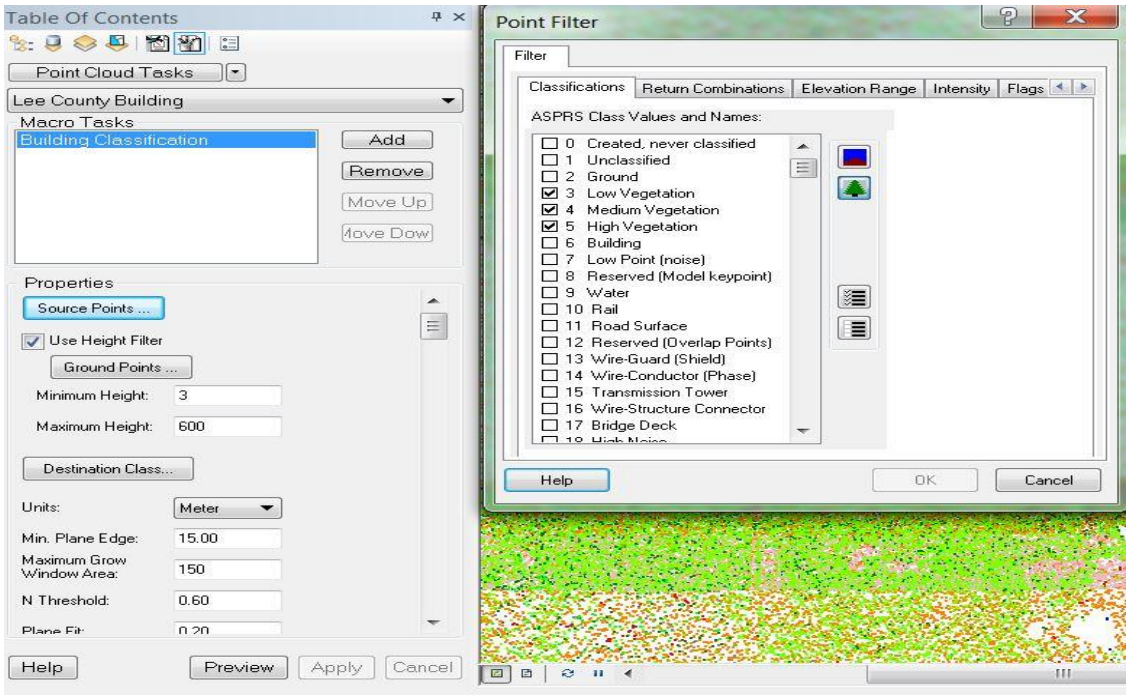

Figure 3.20: Parameter used for Planar Point Filter

After running the Planar Point Filter algorithm, the point clouds were classified into building rooftop class. Figure 3.21 below shows the classification of the point clouds into building class in point and Triangular Irregular Network (TIN). TIN is an efficient way to represent the terrain by forming dense raster grids and is made up of set of non-overlapping contiguous triangular facets, of irregular size and shape. TIN structure has been used in many applications such as shading, cataloging and visibility as it overcomes the problems caused by non-stationary property of the terrain surface (Chen and Guevara, 1987).

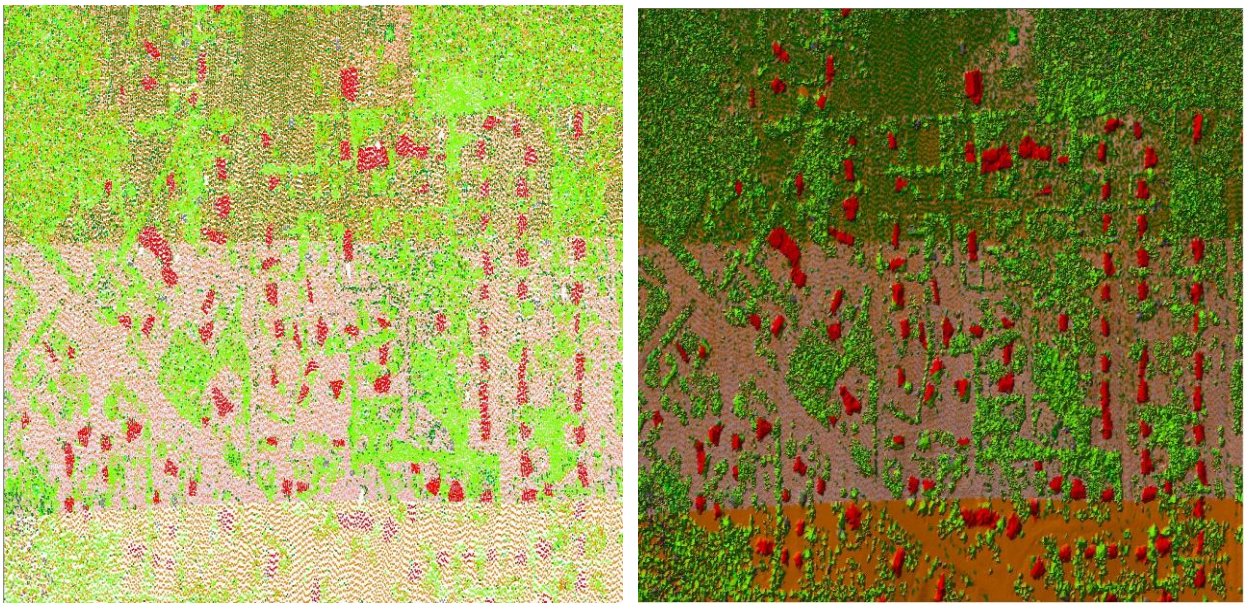

(i) (ii)

Figure 3.21: (i) Point clouds classified as point (ii) Classified rooftops displayed in TIN in red color

3.4.2.4.3 Point Group Tracing and Squaring

The Point Group Tracing and Squaring Point Cloud Task tool was used to extract traced outlines around points of a particular classification category such as buildings. In addition, the traced outlines can be squared producing an approximation of objects such as the roof outlines of buildings and exported into GIS. If squaring is performed, two layers will be generated; one for

the traced outlines, and other containing a "_sqr" suffix representing the squared outlines. The value for Boundary Trace Class to building was set in order to define outlines for the building rooftops.

In addition, the values for other parameters such as Grow Window, Trace Window, Minimum Area and Squaring Angle were also entered which were all based on trial and error method. The values should be experimented with to see which gives better results of building outlines. The Perform Squaring option should be checked if the building outlines polygons are to have corners in 90 degrees, as is the case with many buildings. Figure 3.22 below shows the parameters entered for the Point Group Tracing and Squaring algorithm.

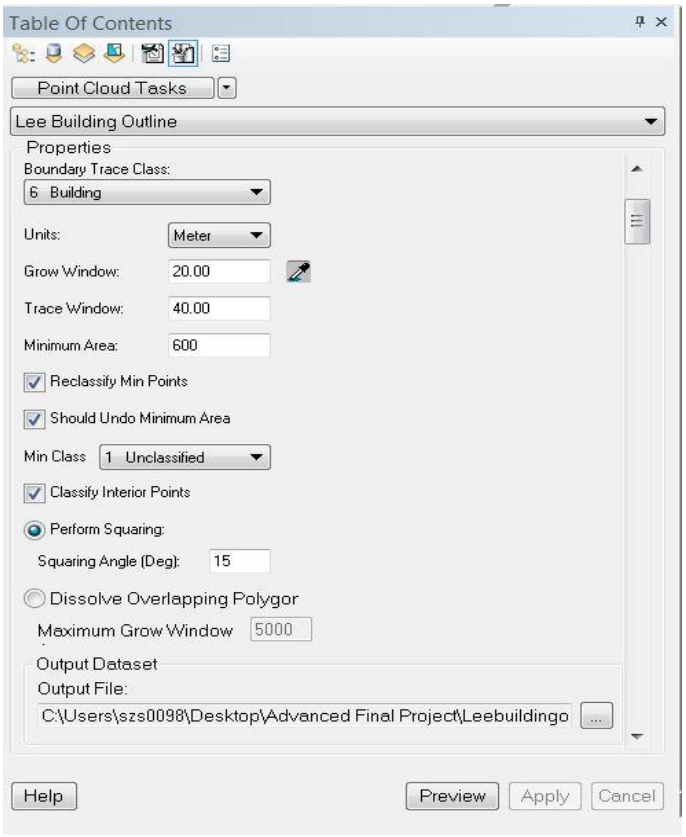

Figure 3.22: Parameter used for Point Group Tracing and Squaring Point Cloud Task

After implementing the algorithm, polygon outlines were traced on the classified building rooftops point clouds automatically as shown in the Figure 3.23 below.

(i) (ii)

Figure 3.23: (i) Classified rooftops in TIN (ii) traced polygons showing the rooftops outlines

3.4.2.4 Accuracy assessment

The classification of building rooftops using both GeOBIA and PCT method resulted in total of 3,125 and 5,540 polygons in the pilot study area. The PCT method was able to extract more rooftops compared to the GeOBIA method. However, there were also some errors where building rooftops polygons appeared in the forest and grassland. This might be one of the reasons for very high difference in building rooftop classification between two methods. The errors were mostly in forest and in open space where there were rooftop polygons as shown in Figure 3.24.

Figure 3.24: Errors of wrongly classified building rooftops in forest

The AlaskaPak v3.0 for ArcGIS 10.x was used to randomly select 250 polygons from the 5,540 and 3,125 classified polygons and the accuracy was assessed on those 250 points by visually inspecting the polygon with the NAIP image. The errors considered for this project were of commission rather than omission meaning it was assessed for only those building rooftops that were classified. The accuracy assessment for both methods is shown in the Table 3.3.

S.N	Type	PCT	GeOBIA
1	Correctly classified building rooftops polygons	223	154
2	Correctly classified but incomplete polygon	4	49
3	Incorrectly classified polygons	23	47
4	Total polygon	**250**	**250**

Table 3.3: Accuracy sssessment result for PCT and GeOBIA

Accuracy percentage for both the methods was measured as the percentage ratio of correctly classified polygons (which includes incomplete polygons) by total polygon. The accuracy percentage for both methods is shown in the Table 3.4.

Methods	Accuracy Percent
PCT	(227/250 * 100)% = **90.8%**
GeOBIA	(203/250 * 100)% = **81.2%**

Table 3.4: Accuracy percent for PCT and GeOBIA

While comparing the shape of the building rooftops polygons classified from both methods, the shapes of polygons from GeOBIA were less accurate than the rooftops generated in LP360. The Figure 3.25 shows an example of the building rooftop classification results from both methods for the same area. In addition to the less accurate shape, it also shows that GeOBIA method missed classifying many of the building rooftop that PCT was able to map.

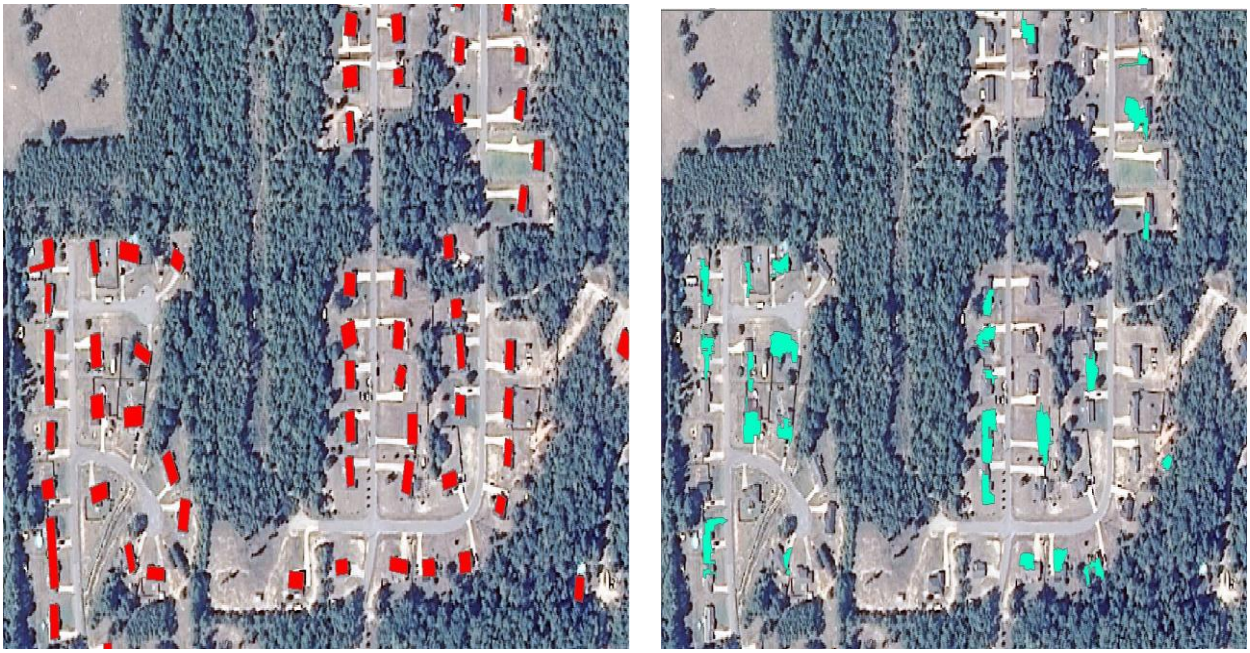

(i) (ii)

Figure 3.25: Classified rooftops from (i) PCT method (ii) GeOBIA method

Overall PCT was better at classifying building rooftops in both number and shape than GeOBIA. However, PCT also had a problem with classifying parts of the forest and grasslands

as building rooftops so in general the number of building rooftops classified by PCT is an overestimate while GeOBIA underestimates the number of building rooftops.

3.4.3 Applying PCT method to classify building rooftops of the Lee County

Assessing both the PCT method and the GeOBIA method for rooftop classification in a small section of Lee County, it was found that the PCT method performed better for the application of removing building rooftops wrongly classified as wetlands. Therefore, the PCT method was implemented to extract building rooftops of the Lee County. In total, there were 49,341 building rooftops extracted for the whole of Lee County as shown in Figure 3.26 in red color.

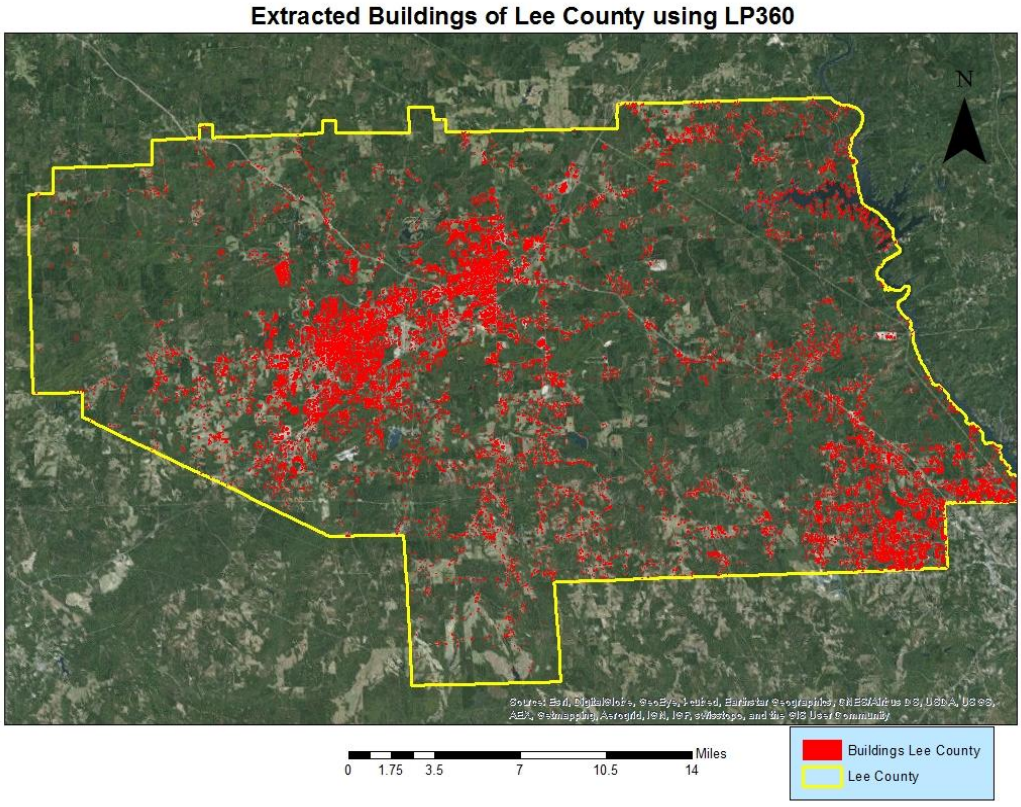

Figure 3.26: Classified rooftops from PCT method

There were a minimal amount of errors encountered during the extraction of building rooftops. The errors were mostly in forest and in open space where there were polygons of rooftops classified, however these errors were ignored because they did not overlap with any of the wetland errors. Overall, this method was able to classify most of the building rooftops of Lee County to help improve the overall isolated wetlands classification.

3.4.4 Removal of rooftops from isolated wetland classification

The classified isolated wetlands had errors of rooftops and shadows in the classification. Therefore to correct the error of rooftops, the isolated wetlands layer and building rooftops layer extracted from LP360 software were overlaid on top of each other and "Select by Location" query function was performed . Only those isolated wetlands were selected which did not intersect with the building layer and were exported into a new layer which is the corrected isolated wetlands of Lee County. There were a total of 871 isolated wetlands shown in the Figure 3.27 in yellow color.

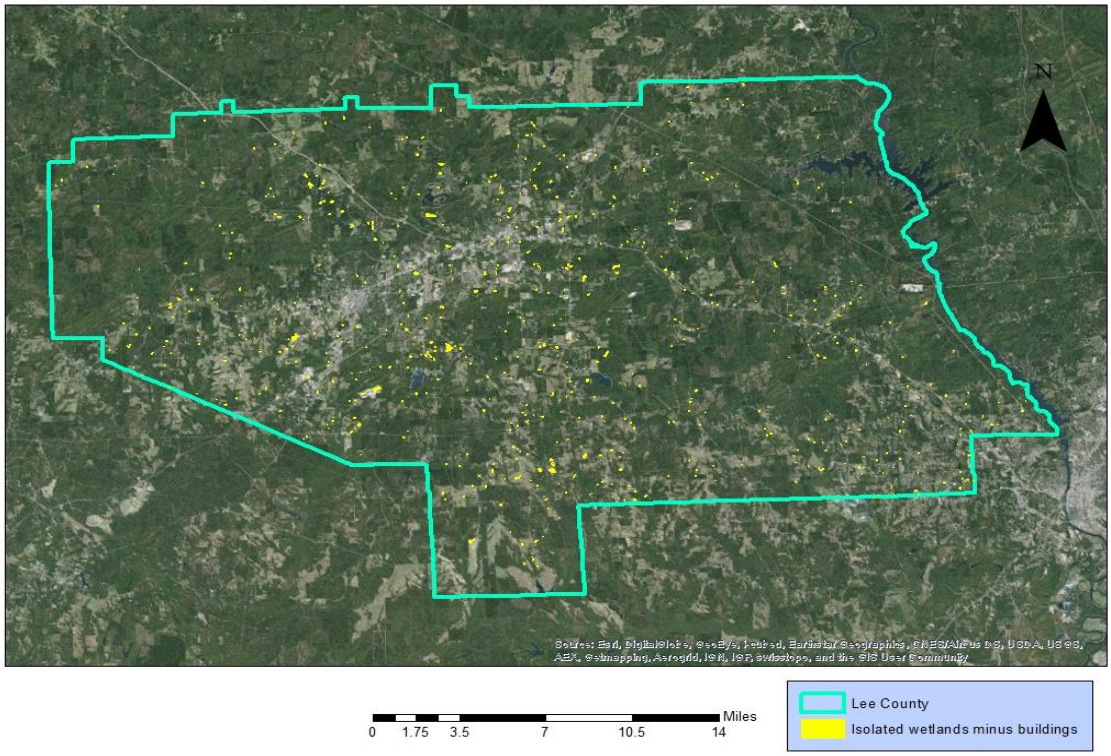

Figure 3.27: Isolated Wetlands classified after eliminating building rooftop errors

3.4.5 Accuracy Assessment of classified isolated wetlands

The classification of isolated wetlands after removing the rooftop errors in GIS environment resulted in total of 871 polygons. The Alaska Pak v3.0 for ArcGIS 10.x was used to randomly select 250 polygons from the 871 classified polygons and the accuracy was assessed on those 250 points by visually inspecting the polygon with the NAIP image. The errors considered for this project were of commission rather than omission which means it was assessed for only those isolated wetlands that were classified. The accuracy assessment of isolated wetlands from the GeOBIA method after removing the errors of rooftop is shown in the Table 3.5.

S.N	Type	Number of polygon
1	Correctly classified isolated wetlands	226
2	Errors of building rooftops	0
3	Errors of shadows, asphalt	24
4	**Total**	**250**

Table 3.5: Classification results for isolated wetlands

There were no errors in the isolated wetlands dataset due to building rooftops because of the LiDAR removal process. The errors were due to asphalt and shadows that were not detectable with the LiDAR analysis. Accuracy percent was measured as the percentage ratio of correctly classified isolated wetlands by total wetland polygons selected. The accuracy percent for the classified wetlands is 90.4% as shown in the Table 3.6.

Method	Accuracy Percent
Correctly classified isolated wetlands	(226/250)*100% = **90.4%**

Table 3.6: Accuracy percent for isolated wetlands

3.5 Results and discussion

The isolated wetlands of Lee County were first classified using the GeOBIA methods. Multi-resolution segmentation was performed and classification of the images was based on the ruleset developed to classify water bodies. The ruleset developed used information such as mean spectral reflectance of NIR, open water spectral signature, homogeneity, ratio green, standard deviation of NIR, ZABUD, and texture to classify the water bodies. After classification, the water body polygons were exported into GIS layers and isolation for the wetlands was defined using the 40 m buffer of NHD dataset and FEMA DFIRM floodplain data in accordance with the Tiner Methodology (Tiner, 2003). In total 976 isolated wetlands were classified in the Lee

County. The accuracy of the classification was assessed to see the errors of building rooftops. Accuracy assessment for the wetlands was done by randomly selecting 250 polygons of isolated wetlands in Lee County using the Alaska Pak v3.0 for ArcGIS 10.x and was assessed by inspecting the selected polygons with NAIP images. The accuracy percent of the classification was 80.4 % in which there were 19 errors of rooftops.

To deal with the errors of building rooftops in wetland classification, two methods were adopted to classify the building rooftops in a small section of Lee County as a pilot project. The two methods were compared to see which one performed better. The Point Cloud Tasks (PCT) method was determined to perform better and was used to classify all the building rooftops of Lee County. In total, 49,341 building rooftops were extracted for the Lee County and although that is an overestimation, the errors were not due to any water bodies. The dataset was used to mask the errors in the isolated wetlands product.

After producing the rooftops GIS layer, it was overlaid with the isolated wetlands layer and "Select by Location" query function was performed. Only those isolated wetlands were selected which did not intersect with the building rooftops layer and were exported into a new layer representing the corrected isolated wetlands in Lee County. In total there were 871 isolated wetlands. The accuracy of the isolated wetland classification was assessed in the study area. Accuracy assessment for the isolated wetlands was done by randomly selecting 250 polygons in the study area using the Alaska Pak v3.0 for ArcGIS 10.x and was assessed by inspecting the selected polygons with NAIP images. The accuracy percent of the classification was 90.4% in which there were no errors of rooftops. However, there were still some errors mostly associated with shadow and asphalt. The percentage accuracy for the isolated wetlands classification improved to 90.4% from 80.4% after using LiDAR to remove rooftop errors. This study shows

that integrating LiDAR data into wetlands classification can improve the overall accuracy of the classification using an efficient automated process.

.

Chapter 4: Estimating evapotranspiration as a proxy for water usage in the irrigated areas and golf courses in twenty (HUC) 12 watersheds in the Wiregrass region of Alabama.

4.1 Introduction

Managing water resources wisely and sustainably is one of the main challenges for water resource managers. Although abundantly available, water is certainly not free. It is important to understand the natural systems and physical laws that control the hydrological cycle and how each process relates to water usage. Information about water usage supplements the study of surface water and ground water availability, which can be vital in understanding water usage demand and in managing water consumption for the future. Moreover, it can also be important in maintaining an adequate water quality and quantity that is desired by humans and needed to sustain ecosystems. There are different factors that affect the water supply and its usage such as "demographics, economic trends, legal decisions, and climatic fluctuations" (Kenny et al., 2009, p. 2). In many cases, agricultural lands should be irrigated to strengthen plant growth and water is applied for "pre-irrigation, frost protection, application of chemicals, weed control, field preparation, crop cooling, harvesting, dust suppression, leaching salts from the root zone, and water lost in conveyance" (Kenny et al., 2009, p. 2).

The common irrigation methods are sprinklers, micro-irrigation and surface flood systems which all withdraw fresh water. One of the commonly used sprinkler systems is a Central Pivot Irrigation Systems (CPIS). CPIS have been used in many areas to increase crop production. According to United States Geological Survey (USGS) data for 2005, total irrigation

withdrawals for the United States were about 128,000 million gallons per day (Mgal/d) which comprised of 37 percent of total freshwater withdrawals and 62 percent of total freshwater withdrawals for all categories, when thermoelectric power was not taken into consideration. Irrigation from surface water was accountable for 58 percent of the total irrigation withdrawals. The data also revealed that a total of 61.1 million acres were irrigated of which 30.5 million acres used sprinkler system such as CPIS. There was an increase in irrigated acreage from 25 million acres in 1950 to 58 million acres in 1980. After that it was static for a while and again increased in 2000 to 2005 to more than 60 million acres. Similarly, there has been increase in the acreage that uses sprinkler and micro-irrigation systems accounting for 56 percent of total irrigated acreage in 2005 (Kenny et al., 2009).

Large volumes of water are also consumed for the irrigation of recreational golf courses. Golf is a sport that has experienced a huge growth and success in recent decades. The total number of golfers since 2003 exceeds more than 61 million around the world with United States comprising over half of that figure. In 2003, there were a total 25,000 golf courses worldwide with United States alone having 15,827 golf courses covering more than 1.7 million acres (Wheeler and Nauright, 2006). According to the NGF's (2012) report, there were a total of 15,619 golf courses in United States with 25 percent being privately owned. To maintain the turf of the golf courses, a huge volume of water is required. It was estimated that an 18-hole golf course requires 3,000 to 5,000 cubic meters per day, nearly equivalent to the daily consumption requirement for 2,000 families or 15,000 individual Americans (Wheeler and Nauright, 2006). According to the Worldwatch Institute data from 2001, 9.5 million cubic meters of water is used per day to irrigate all the world's golf courses which is tantamount to the amount of water used

per day to support 4.7 billion people at United Nations daily minimum requirement (Brown et al., 2001).

Since both agricultural land and golf courses consume very large amounts of water, it is important for regional water resource managers to have an accurate inventory of irrigated lands and golf course areas and to also have ways to estimate the water consumption in these areas. Part of this study was funded by the Alabama Office of Water Resources whose resource managers are seeking methods to help the monitor the water consumed by these two land uses. Estimating evapotranspiration (ET) with satellite imagery using the Mapping EvapoTranspiration at high Resolution with Internalized Calibration (METRIC) model can be an effective tool for water resource managers to gain knowledge about the water consumption in irrigation practices and make better policies to sustain and manage water distribution.

4.2 Study area

The study area for the identification of golf courses and agricultural lands, and estimation of ET includes the twenty HUC 12 watersheds in the Wiregrass region of Alabama shown in Figure 4.1. It is an area that encompasses the southeastern part of Alabama. The region's name is based on the native *Aristida stricta*, also known as "wiregrass" due to its texture and because it is amply found in the regions longleaf pine forest (Byrd, 2009). This name was originated during the earliest days of European inhabitation in this region. Dothan is the region's most developed city and claims the agricultural title of "Peanut capital of the world." The Wiregrass region has many golf courses and recreation centers. The region's boundary can vary depending on who defines it. For the purpose of this thesis, the focus will be mostly on Houston County, Alabama.

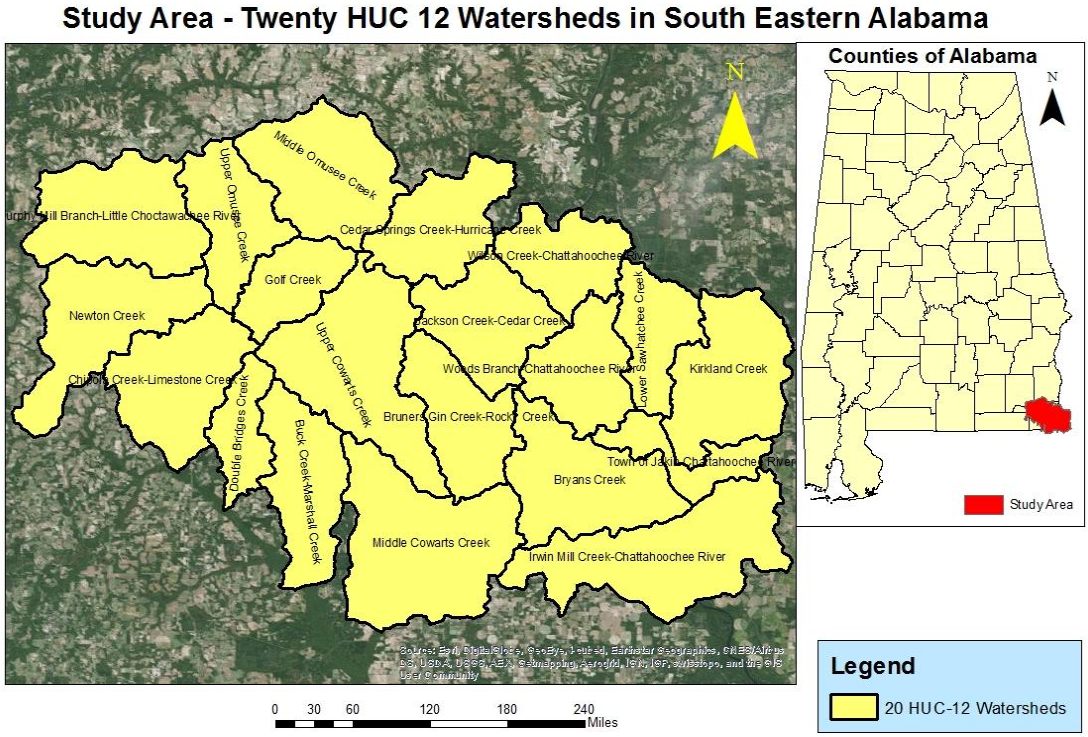

Figure 4.1: Study area delineating Twenty HUC Watersheds in SE Alabama

4.3 Objectives

One goal of this study is to develop methods to estimate evapotranspiration in the irrigated agricultural areas and golf courses of the study area using remote sensing methods and METRIC model. The study also focuses on the classification of the golf courses using GeOBIA methods since golf courses are not a separate class in any of the secondary land use/land cover datasets used to identify agricultural areas. This project was accomplished with the following objectives:

- To classify golf courses in twenty HUC 12 watersheds in the Wiregrass region of Alabama using NAIP imagery by implementing GeOBIA methods and develop a ruleset that best classifies golf courses.
- Assess the validity of (METRIC) model for estimating evapotranspiration (ET) by comparing it with the ET data from USGS ET stations in Florida.

- Estimate evapotranspiration of irrigated agricultural lands and golf courses in twenty HUC 12 watersheds in the Wiregrass region of Alabama implementing METRIC model and using Landsat 5 –Thematic Mapper imageries for the year 2005 and 2010.

4.4 Research questions

- What is the spatial extent of golf courses in the study area?
- Can the ruleset developed for the classification of golf courses be applied to other places in Alabama to identify golf courses?
- Can METRIC model be used with remotely sensed data to provide a reliable estimate of evapotranspiration?
- How has the trend in water consumption changed from 2005 to 2010 in both agricultural land and golf courses?

4.5 Data used

The data required for the estimation of evapotranspiration (ET) and classification of golf courses are as follows:

4.5.1 Imagery

Landsat 5 Thematic mapper (TM) satellite images were used to determine the evapotranspiration of the agricultural land and golf courses in the study area. Landsat 5 Thematic mapper (TM) was launched in 1984 by NASA and collected data nearly twice per month consistently until November of 2011 (USGS, 2015). The Landsat TM satellite has seven bands consisting of three visible bands (RGB), two near infra-red bands, a thermal band and mid infra-red band. The repeat cycle for the satellite is 16 days. The temporal resolution of recent Landsat satellites is 16-18 days which is not optimal for ET estimation; because moisture conditions on the ground can be dynamic depending on the rainfall, irrigation and heterogeneous drying varies

with soil, vegetation, topography, and local climate. To overcome this temporal limitation, robust methods have been implemented to interpolate between infrequent satellite overpasses to give us daily or seasonal information on the ET (Anderson et al., 2012b). The Landsat images for Houston County covering the study area for the year 2005 and 2010 were downloaded from the USGS Glovis website. The year 2005 and 2010 was chosen at the request by the lead investigators of the Office of Water Resources funded project. The downloaded images were cloud free or had less than 10 percent of cloud cover. Table 4.1 and 4.2 provide information about the downloaded Landsat images, cloud cover percent and ET mapping period for year 2005 and 2010.

S.N	Landsat image date	Cloud cover percent	ET mapping period
1	04/27/2005	0 percent	April 2005
2	05/13/2005	4 percent	May –June 2005
3	08/17/2005	0 percent	July-August 2005
4	09/02/2005	0 percent	September 2005

Table 4.1: Landsat 5 images used for METRIC analysis for the year 2005 (Source: USGS)

S.N	Landsat image date	Cloud cover percent	ET mapping period
1	04/09/2010	0 percent	April 2010
2	05/27/2010	0 percent	May 2010
3	06/12/2010	1 percent	June 2010
4	07/30/2010	8 percent	July-August 2010
5	09/16/2010	2 percent	September 2010

Table 4.2: Landsat 5 images used for METRIC analysis for the year 2010 (Source: USGS)

National Agriculture Imagery Program (NAIP) images from 2011 were used to classify the golf courses using Geographic Object Based Image Analysis (GeOBIA) methods. The NAIP captures digital aerial imagery of the United States during the agricultural growing season (USDA, 2013). The program is funded by the United States Department of Agriculture's (USDA) Farm Service Agency (FSA) through the Aerial Photography Field Office (APFO) in Salt Lake City. The program was initiated in 2003 and initially attempted to collect imagery on a 5 year cycle but now aims for a 3 year cycle beginning from 2009(USDA, 2013). The spatial resolution of the imagery is one meter and has three to four bands including red, green, blue and more recently many states have begun to collect near-infrared (NIR) as the fourth band. The distribution and organization of the NAIP imagery is in accordance to the existing United States Geological Survey (USGS) 7.5 minute topographic quadrangles grid system with each NAIP image conforming to one quarter quadrangle or 3.75x3.75 minute having a buffer of 300m on all four sides. The projection of the tiled images is in the Universal Transverse Mercator (UTM) coordinate system using the North American Datum (NAD) of 1983 (USDA, 2013; Jones, 2013).

4.5.2 Secondary data for land use/land cover

Secondary data for land use/land cover and crop data layer were used to identify irrigated areas so that ET can be estimated only for the irrigated agricultural areas only. The source of secondary data of agricultural areas were provided by a combination of the National Land Cover Dataset (NLCD) for 2006 and National Agricultural Statistics Service (NASS) data for 2010. NLCD consists of 16- class land cover classification scheme that encompasses the whole of United States. It is produced under a cooperative project directed by the Multi-Resolution Land Characteristics (MRLC) Consortium. It is made on the basis of a decision tree classification of circa 2006 Landsat satellite data and is produced from analyzing the spectral characteristics of

Landsat images from 2001 to 2006. The main purpose NLCD project is to produce a consistent land use/land cover data layer of the country from the 30m resolution Landsat Thematic Mapper satellite data. The NLCD map has a 30m spatial resolution.

The NASS data collected by the United States Department of Agriculture is from a program which prepares reports covering almost every aspect of US agriculture by conducting surveys every year (USDA, 2014). The NASS Crop Data Layer (CDL) is the classification of different crops and land use/land cover which has a spatial resolution of 30 m. It is produced from Landsat 5TM sensor and the Indian Remote Sensing RESOURCESAT-1 (IRS-P6) Advanced Wide Field Sensor (AWiFS) which is collected during the current crop growing season (USDA, 2014). The NASS provides timely, accurate, and useful statistics in service to U.S. agriculture and National CDL provides classification maps based on different crops. Crops that are grown from April to the end of September were taken into consideration for calculation of seasonal ET in this thesis.

4.5.3 Weather data from weather stations

Weather data from reference weather stations were required for the processing of the METRIC model. The weather parameters for the Houston County are available in the weather and climate websites such as Agricultural Weather Information Service (AWIS) Weather Services and the Center for Hurricane Intensity and Landfall Investigation (CHILI) where weather data can be obtained for the present and past years. Hourly and daily data for solar radiation, precipitation, temperature, relative humidity and wind speed were required to compute reference ET (ET_{ref}) in the Ref-ET software.

4.6 Methods

4.6.1 Extraction of golf courses and agricultural land in Wiregrass Region

4.6.1.1 Segmentation of NAIP image for golf courses

The Multispectral Resolution Segmentation (MRS) algorithm was used to segment NAIP images. The setting of rule parameters was done in a repetitive trial and error process. The scale parameter value was set to 40 with shape and compactness value set to 0.2 and 0.7 respectively. The weight of spectral band for near infra-red (NIR) was set to 2 while all other bands (red, green, blue) was set to 1 because the NIR band plays a significant role in separating vegetated areas from non-vegetated areas. The segmented image objects obtained were subjected to the spectral difference segmentation algorithm, which combines smaller image objects into bigger image objects that have similar spectral values. This segmentation helped create large objects and separate golf courses from other land use/land cover classes. The value of spectral difference segmentation was set to 8. The weights of the bands were set similar to that of multispectral resolution algorithm. Figure 4.2 shows an example where the NAIP imagery was used to classify a golf course before and after segmentation.

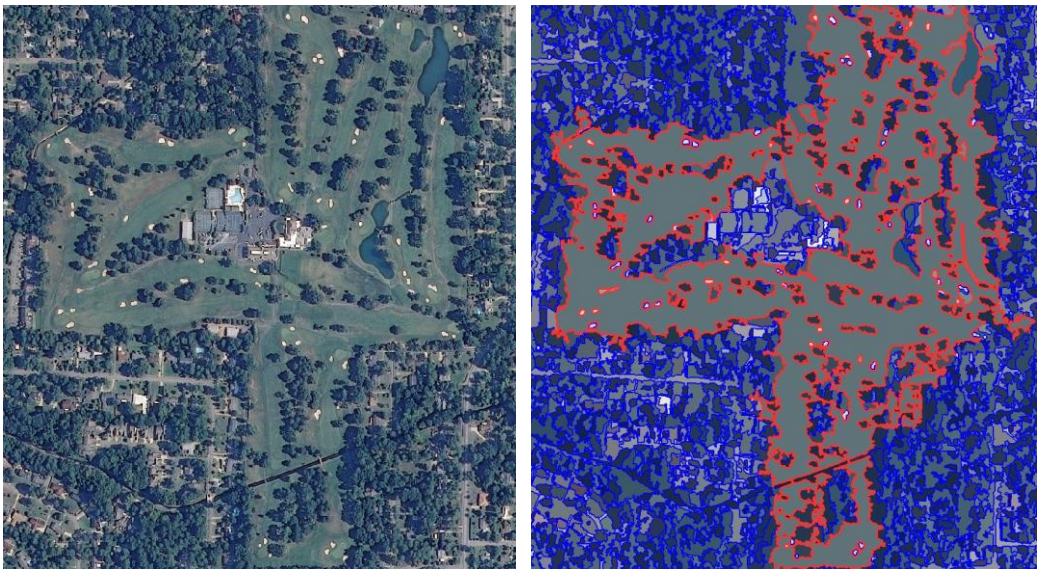

(i) (ii)

Figure 4.2(i) NAIP image of golf course before segmentation (ii) after segmentation

4.6.1.2 Classification of golf courses

A ruleset was developed to classify golf courses based on different attributes such as the Normalized Difference Vegetation Index (NDVI), spectral value of NIR, texture homogeneity, shape and size, contextual information and compactness. First, the sand traps of the golf courses were classified based on the spectral value of the NIR band, shape, size, brightness value and texture of the objects. Similarly the ponds in the golf courses were classified using spectral value of NIR, area, texture and contextual information such as distance from and traps. Finally the greens of the golf courses were classified using NDVI, texture, area and distance to sand trap and ponds. Figure 4.3 shows the ruleset developed and a classified image of golf course from the ruleset.

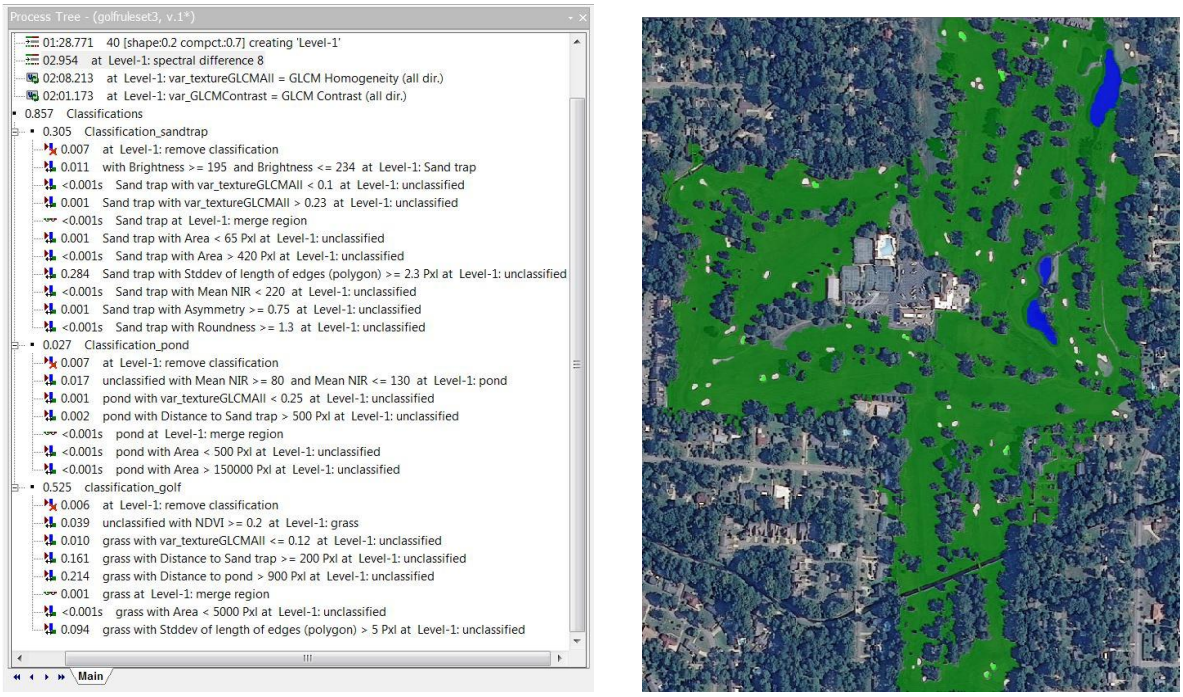

(i) (ii)

Figure 4.3: (i) Ruleset for golf course (ii) Classification of golf course

4.6.1.3 Export to vector layer

After the classification of golf courses, they were exported into a geo-referenced vector polygon layer using appropriate naming schemes. The eCognition software allows the user to add attributes to the classified polygons of golf course layer based on their object attributes. The Figure 4.4 shows the exported GIS layer of a golf course in Dothan Country Club.

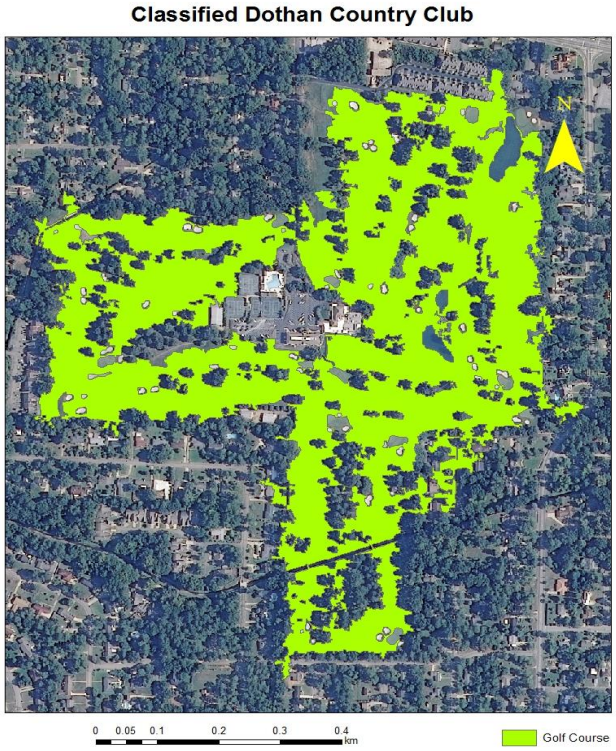

Figure 4.4: Exported GIS layers of a golf course

4.6.1.4 Extraction of agricultural lands from NLCD and NASS data

NLCD maps are classified into different land cover such as forests, wetlands, water, developed and agriculture. Since ET is estimated only for agricultural lands, a selection of agricultural land was done and exported into a separate layer in GIS. Similarly, a Cropland Data Layer (CDL) map of NASS consists of classification of different crops grown in an area. Only

the crops grown during summer (April to September) were chosen for the study area and exported into a separate layer. Therefore, two separate layers were extracted for the agricultural lands from NLCD and NASS data.

4.6.2 Estimation of evapotranspiration in Wiregrass Region

4.6.2.1 Reference evapotranspiration (ET_{ref}) estimation

The weather parameters such as solar radiation, temperature, precipitation, relative humidity and wind speed are required to calculate the reference ET (ET_{ref}) for alfalfa. The reason alfalfa (ET_{ref}) is preferred over the clipped grass (ET_{ref}) is that it gives good representation of the upper limit of ET from well-watered vegetation (Waters et al., 2002). The weather data were input in the Ref- ET software along with the coordinates and height of the weather station which gives ET_{ref} values that are required for the calculation of ET in the METRIC model. REF-ET software developed by Allen et al. (2000a) was used to compute the ASCE Penman-Monteith standardized (Allen et al., 2000b) form of reference ET (ET_{ref}) for alfalfa using actual weather data. The software was also used to calculate ASCE Penman-Monteith standardized daily form of reference ET (ET_{ref24}) and monthly reference ET (ET_{ref_month}).

4.6.2.2 Estimating and validating ET from METRIC model with ET from USGS ET station data of Florida

Landsat 5 Thematic mapper images were used to measure ET from a set of equations that are in strict hierarchical sequence and use the spectral radiance measures from the satellite (Bastiaanssen et al., 2005). The input data required to measure ET in the METRIC model are visible, NIR and thermal bands of Landsat images and hourly ET_{ref} values calculated from the Ref-ET Software. The METRIC model consists of total of fifteen models which is built step by step in Erdas Imagine Model Maker to produce different image outputs such as radiance,

reflectance, surface albedo, vegetation indices, emissivity, land surface temperature (T_s), surface roughness, aerodynamic resistance, sensible heat flux and ET from the Landsat images. Figure 4.5 below shows the workflow of METRIC model and is explained in detail in Appendix.

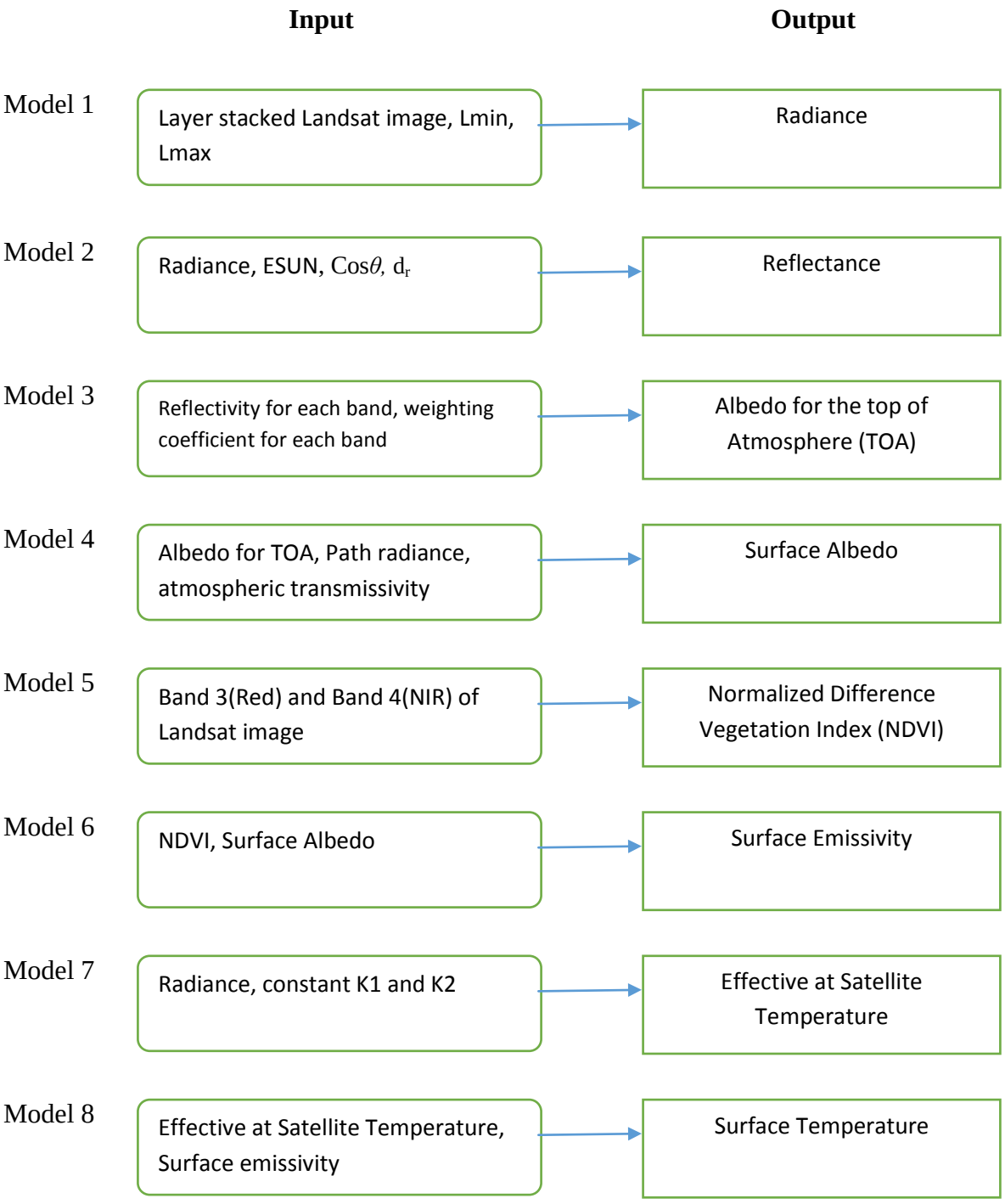

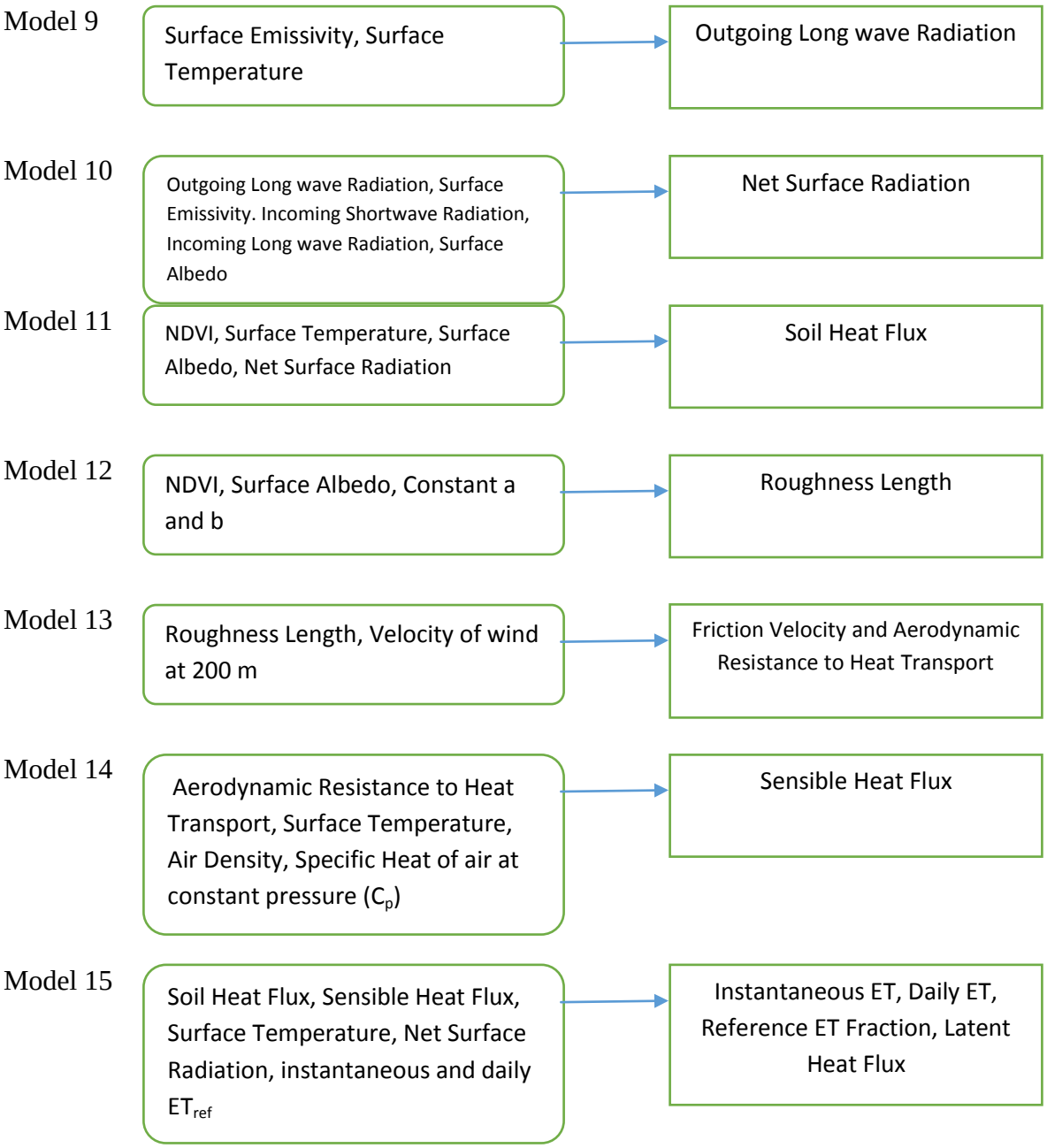

Figure 4.5: Workflow of METRIC model

Since the State of Alabama does not have any USGS evapotranspiration (ET) stations that measure ET data, validation of the ET from the METRIC model with field data in the study area was not possible. To validate the accuracy and reliability of the model, the model was tested in the areas that cover USGS ET stations in Florida (as in Bhattarai, 2010). The model was compared with ET data from the three USGS ET stations of Florida.

Landsat 5 TM images from path/row 15/41, 16/41, and 17/40 covering the three USGS sites were used in this study. The images were downloaded for the areas having USGS ET stations in Florida. Similarly Florida Automated Weather Network (FAWN) weather station data were used as inputs to the Ref ET software to derive ET_{ref} for the METRIC model. The ET derived from the Landsat 5 TM images were compared with ET data from the USGS station for the same day the images were captured. The measured ET data from the USGS stations are available online in the USGS Florida Evapotranspiration Station website. Table 4.3 shows the date, path/row, cloud cover and USGS ET locations of the downloaded Landsat images.

S.N	Date	Path/Row	Cloud cover	USGS ET station location
1	4/1/2003	16/41	0%	Kenansville, FL
2	4/3/2004	16/41	0%	Kenansville, FL
3	7/8/2004	16/41	2%	Kenansville, FL
4	4/28/2004	15/41	6%	Fort Pierce, FL
5	4/18/2001	17/40	0%	Brooksville, FL

Table 4.3: Date, Path/Row, cloud cover and USGS ET locations of the downloaded Landsat TM images

Validation of the METRIC model was done by comparing the ET from model with measured ET from USGS ET Stations by conducting Two Sample Paired T-Test to check if there was significant difference between METRIC ET versus ET at USGS stations. Two Sample Paired t-test can be used with extremely small sample sizes as small as n=2 (de Winter, 2013). In addition to this Root Mean Square Error (RMSE) was used to determine performance indicators of the model. Figure 4.6 below shows the study area locations of the Florida Automated Weather

Network (FAWN) weather stations and USGS ET weather stations that were used for the validation of the model.

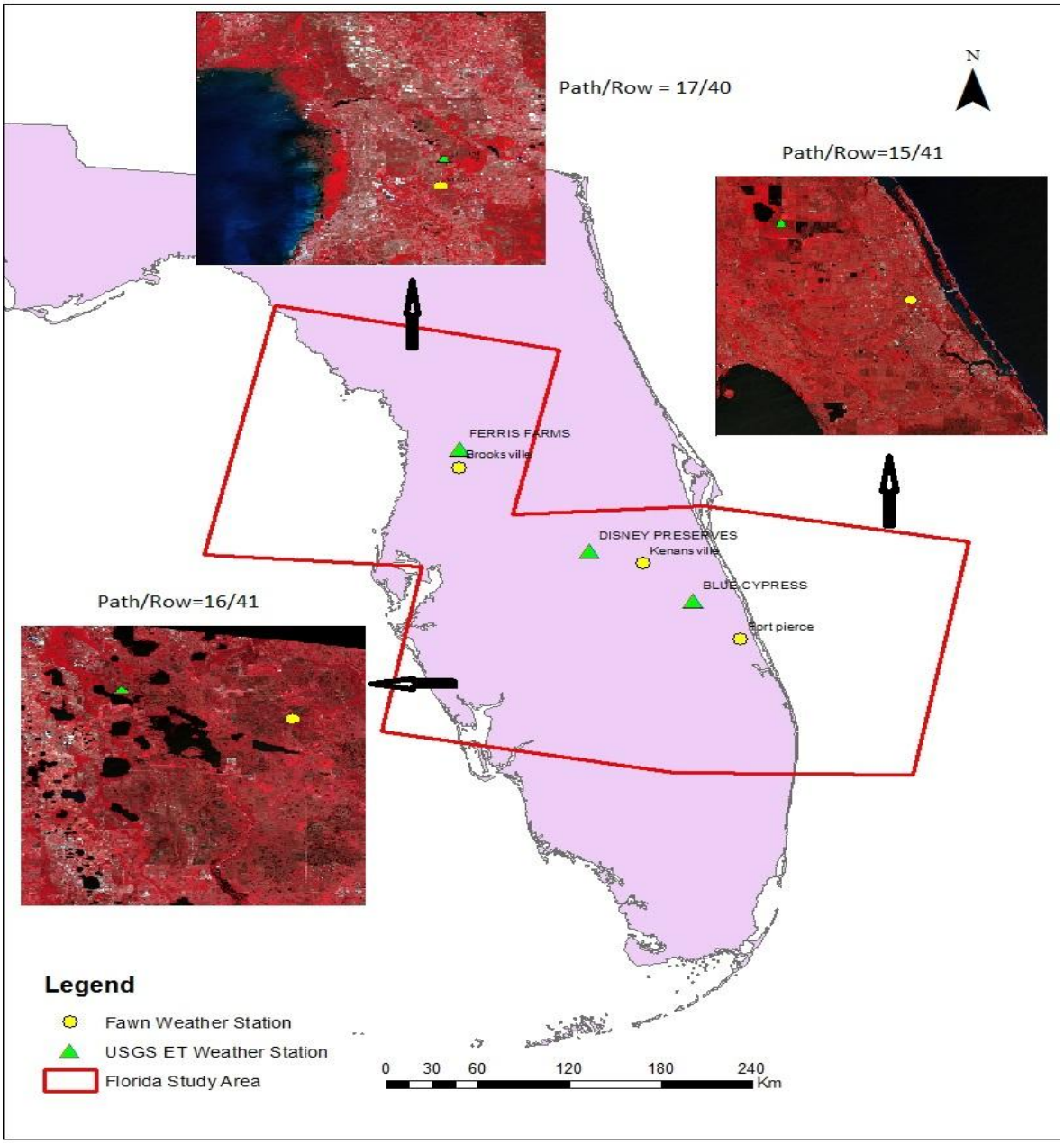

Figure 4.6: Landsat 5 TM Images and USGS and Florida Automated Weather Network (FAWN) weather stations in Florida

4.6.2.3 Estimation of ET in twenty (HUC) 12 watersheds in the Wiregrass region

The Landsat images for the study area of twenty HUC12 watersheds in the Wiregrass region of Houston County were downloaded from the USGS Glovis website (http://glovis.usgs.gov) for the path/row of 19/38. The Landsat images for the year 2005 and 2010 were processed to estimate ET and compared to analyze the trends in water usage. Since the images should have minimum cloud cover, it was only possible to download a total of four images for the year 2005 and five for the year 2010. As most of the irrigation is done during the growing season, the Landsat images were acquired only for the crop growing months from April to September. The location of the weather stations in all Landsat images should be cloud free in order to get surface observations. Only those Landsat images having cloud cover less than 10 percent were used. The pixels that have clouds in the study area does not give accurate ET values therefore these areas were be neglected in the ET maps.

The weather data for the Houston County was downloaded from the AWIS Weather Services and CHILI websites for the year 2005 and 2010. Weather conditions might not be uniform within the satellite images if the study area is very large or has variety of terrain and land uses. For the study area, weather data from Headland AWIS weather station and Ashford CHILI weather station (Figure 4.7) were used to compute the ET_{ref}. While choosing hot and cold pixels in the METRIC model, only those pixels that are within the 20 km buffer zone from the weather data are chosen (Allen et al., 2002a). Hourly weather data were used to compute daily ET while daily weather data were summed up to calculate seasonal ET. The details of the ET workflow are provided in Appendix section.

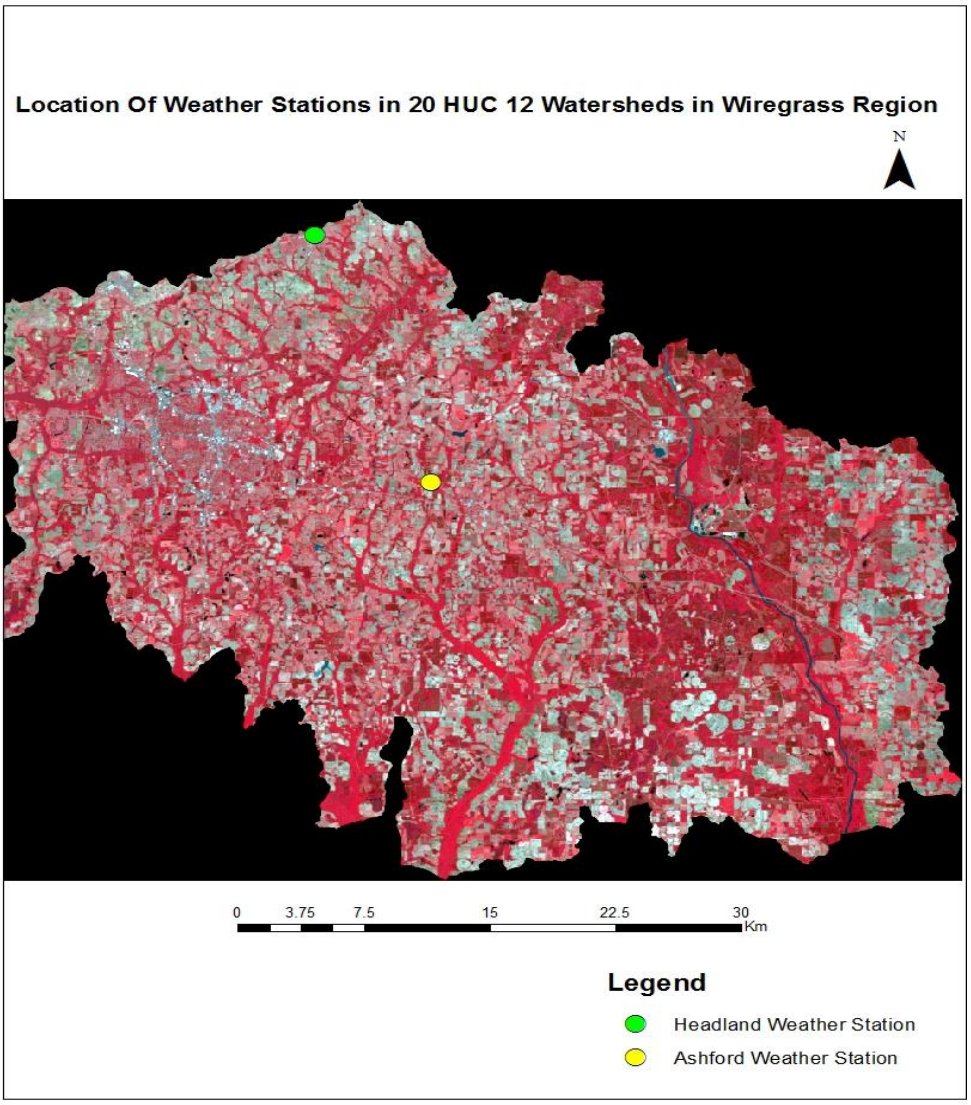

Figure 4.7: Location of weather stations used for the study

The daily ET for each pixel of the image was calculated from the model for the day the image was captured. After estimating the daily ET for each satellite image during the growing season, seasonal ET was calculated for the crop growing months. Seasonal ET was calculated by multiplying interpolated Reference ET Fraction (ET_rF) maps with daily ET_{ref} values. This gives daily ET for each day for the whole crop growing season. Once the daily ET for each day of the whole crop season was calculated, seasonal ET can be computed by summing the daily ET for

the whole season. Since this process takes a considerably long time to run in the model, a python script was coded to perform this step.

The project is primarily concerned with ET on agricultural lands and golf courses, seasonal ET was also evaluated for other land use/land cover types (section 4.7.2) to assess overall performance as an indicator of water usage. Secondary data from NLCD and crop layer data from NASS were used to mask out only agricultural lands in the GIS environment so that seasonal ET for only agricultural land and golf courses were estimated for year 2005 and 2010 in sections 4.7.4 and 4.7.5.

4.7 Results and discussion

4.7.1 Estimating and validating ET from METRIC model with ET from USGS ET station data of Florida

ET was calculated using red, NIR and thermal bands of Landsat images, and weather parameters in the METRIC model. The pixel values for ET in the Landsat images where there were USGS weather station data were compared with the USGS weather station data. Table 4.4 shows the comparison between the METRIC daily ET and USGS daily ET at the USGS ET weather station that was done for this study which added April and August to what had previously been done by Bhattarai (2010). The satellite images used were mostly during the spring season (April) so as to get images that were free of clouds. During this period, the ET values are relatively low compared to the summer season when the temperatures are very high. Much of the validation of ET from model with ET from USGS weather station in Florida was already conducted by Bhattarai (2010) for both spring and summer periods.

S.N	Date	Path/Row	METRIC daily ET (mm/day)	USGS daily ET (mm/day)
1	4/1/2003	16/41	**2.89**	**2.5**
2	4/3/2004	16/41	**2.75**	**2.6**
3	7/8/2004	16/41	**5.20**	**5.70**
4	4/28/2004	15/41	**6.01**	**5.3**
5	4/18/2001	17/40	**1.22**	**2.00**

Table 4.4: ET Data from METRIC model and USGS Evapotranspiration stations

METRIC model performed very well in estimating daily ET at USGS stations. The error in daily METRIC ET varied from -0.78 mm to 0.71 mm with root mean square error (RMSE) of 0.55 mm/day. Two Sample Paired t-test was performed in Microsoft Excel to see if there was a significant difference between the ET from model and USGS evapotranspiration station. The null hypothesis for this statistical analysis is that there is no significant difference between ET from METRIC model and ET from USGS evapotranspiration Station Data at a confidence level of 95%.

Null Hypothesis H_0: There is no significant difference between METRIC model ET and ET from USGS evapotranspiration Station Data

Alternative Hypothesis H_1: There is significant difference between METRIC model ET and ET from USGS evapotranspiration Station Data

Significance Level (a) = 0.05

	METRIC daily estimates(mm/day)	USGS daily estimates(mm/day)
Mean	3.614	3.62
Variance	3.81453	3.017
Observations	5	5
Pearson correlation	0.950254	
Hypothesized mean difference	0	
Df	4	
t Stat	-0.02164	
P(T<=t) one-tail	0.491884	
t Critical one-tail	2.131847	
P(T<=t) two-tail	0.983768	
t Critical two-tail	2.776445	

Table 4.5: Two Sample T Test results

Table 4.5 shows the value of t stat = -0.02164 and t Critical two-tail = 2.776445. The t-stat value is within the critical two tail range and lies in acceptance zone of the normal distribution curve, which accepts the null hypothesis. Similarly, p-value for two-tailed data, P (T<=t) is 0.983768 which is greater than a= 0.05. Therefore, there is no significant difference between the means of the two datasets. Similarly, Bhattarai (2010) analyzed the daily, monthly and two- month ET validation using regression analysis by plotting estimated model ET versus

observed ET values at USGS stations. The validation performed well in terms of estimating daily, monthly and two-month ET at USGS.

4.7.2 Estimation of ET at twenty HUC 12 watersheds in the wiregrass region compared by land use/land cover type

A comparison of ET by land use/land cover type was done to evaluate how well the ET dataset estimated water consumption. For instance, developed/built-up lands should experience less ET than irrigated agricultural lands. Daily ET was estimated for each Landsat images using the red, green, blue, NIR, and thermal bands and weather parameters in METRIC model. Similarly monthly or two-month ET was also calculated by multiplying interpolated Reference ET Fraction (ET_rF) maps with daily ET_{ref} values. Total seasonal ET was estimated by summing up daily ET during the growing season. ET_rF for each day of the month was calculated by linearly interpolating the ET_rF values from the two dates of images captured consecutively. The interpolated ETrF of each day was multiplied with daily ET_{ref} for that same day and daily ET for that day was computed. The daily ET for the whole crop growing season was added and a new seasonal ET map was generated using a python script. Seasonal ET maps were prepared for year 2005 and 2010. Because of the presence of cloud cover in some of the Landsat TM images, the estimation of seasonal ET for those locations were excluded as it would affect the results. The clouds in each image were digitized into a GIS layer in order to exclude those areas while computing the seasonal ET.

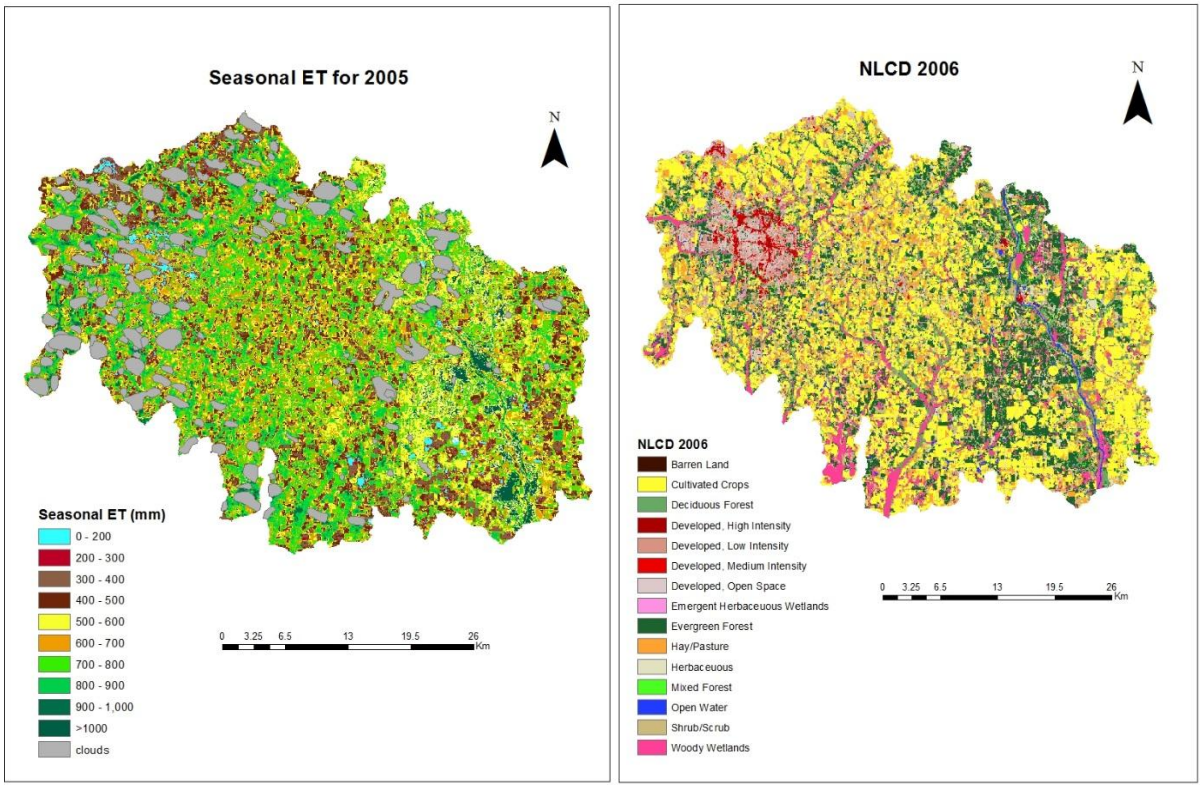

(i) (ii)

Figure 4.8: (i) Seasonal ET map for the year 2005 (ii) NLCD land-use land-cover map 2006

Figure 4.8 shows the seasonal ET map for the year of 2005 during the crop growing season from April to end of September. The area having clouds in the Landsat images were not taken into consideration for estimating ET. While comparing the ET map with the NLCD land use/land cover map for 2006, it can be seen that pixels in wetland and forests had the highest ET values. Forest areas had higher ET than agricultural lands and shrub lands. While urban areas with high density had the least values of ET.

The seasonal ET for 2005 map was distributed with 130 random points using the AlaskaPak v3.0 for ArcGIS 10.x**.** After randomly distributing the points, the pixel values for ET were extracted for each NLCD land cover type. Pixels that are covered by the clouds in the Landsat images were omitted for the study. The random points were divided according to their

class and average values for the ET was calculated for each class. Table 4.6 below shows the class, number of points in the class and the average ET for that class for year 2005.

S.N	Class	Number of points	Average seasonal ET(mm)
1	Agricultural crops	40	511.58
2	Developed/High Intensity	5	43.59
3	Developed/Low Intensity	5	396.36
4	Forest	26	717.50
5	Hay/Pasture	24	542.91
6	Open Water	4	889.65
7	Shrub land	19	702.69
8	Woody Wetlands	7	1000.15

Table 4.6: Seasonal ET values for different class from 130 randomly selected points for 2005

From the Table 4.6, it was observed that wetlands and water bodies had the highest ET values. Forest areas and shrub lands had higher ET than agricultural lands and hay/pastures. Highly developed areas had the least ET because of lack of vegetation at core urban area. However, developed areas with low intensity (suburban areas) had higher ET than main urban city areas likely because sub-urban areas have more areas covered with vegetation and lawns that are often irrigated.

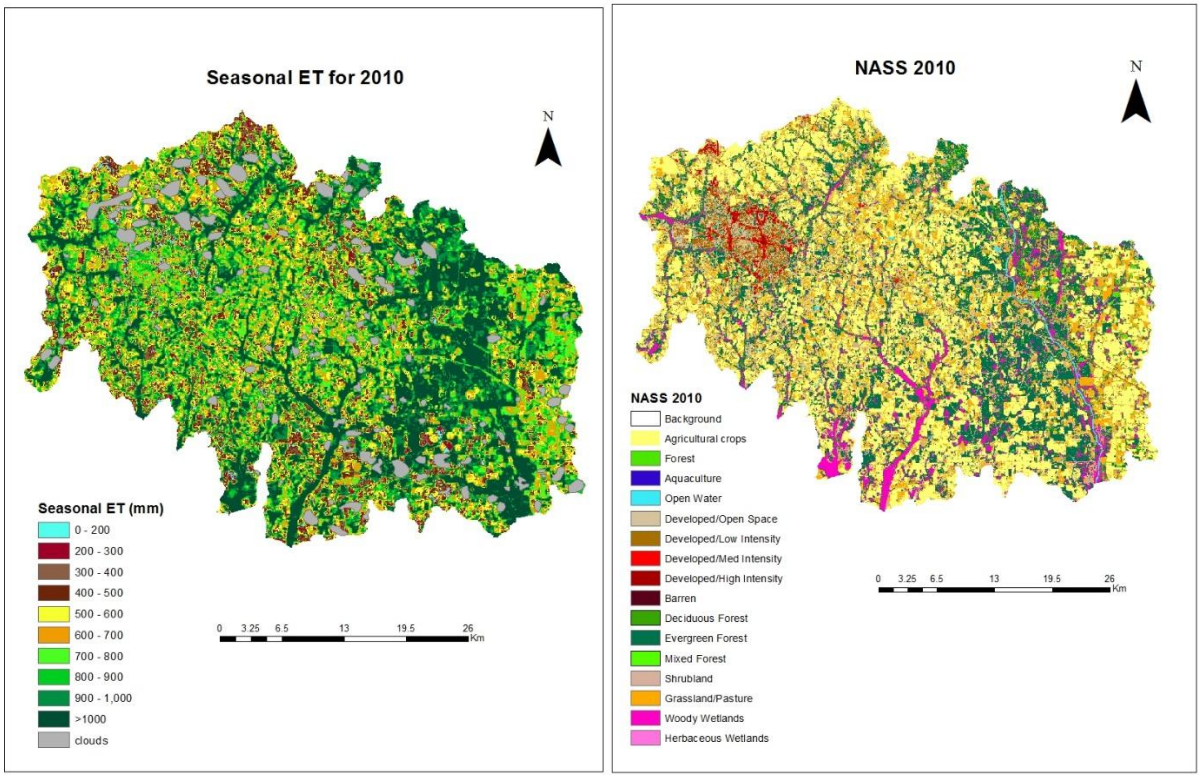

(i) (ii)

Figure 4.9: (i) Seasonal ET map for the year 2010 (ii) NASS land-use land-cover map 2010

Figure 4.9 shows the seasonal ET map for the year of 2010 during the crop growing season from April to end of September. While comparing ET map with the NASS land use/land cover map for 2010, pixels in wetland and forests had higher ET values. Forest areas had higher ET than agricultural lands and shrub lands. While urban areas with high density had the least value of ET.

Similarly, the seasonal ET map for 2010 was distributed with 130 random points using the AlaskaPak v3.0 for ArcGIS 10.x**.** Extraction of pixels values for seasonal ET and NASS land use/land cover maps to the random points was done in GIS while omitting the pixels covered with clouds. The random points were divided according to their class and average values for the

ET was calculated for each class. Table 4.7 shows the class, number of points in that class and the average ET for that class for year 2010.

S.N	Class	Number of points	Average seasonal ET (mm)
1	Agricultural crops	50	588.50
2	Developed/High Intensity	4	88.28
3	Developed/Low Intensity	3	474.38
4	Forest	36	957.24
5	Grassland/Pasture	20	723.64
6	Open Water	2	1097.43
7	Shrub land	7	867.13
8	Woody Wetlands	8	1046.11

Table 4.7: Seasonal ET values for different class from 130 randomly selected points for 2005

From the Table 4.7, it was observed that values of ET for different land use/land cover classes for 2010 were very similar to that of ET values 2005 in Table 4.6. The ET map for 2010 had wetlands with higher ET followed by water bodies. Forest areas and shrub lands had higher ET than agricultural lands and grassland/pastures. Highly developed areas had the least ET while developed areas with low intensity (sub urban areas) had higher ET than main urban city areas.

4.7.3 Comparing land surface temperature (T_s) and daily evapotranspiration (ET)

The plot for daily evapotranspiration (ET) versus land surface temperature (T_s) was done to see the trend line between the daily ET and T_s. If a strong relationship exists between T_s and ET then it could be argued that T_s can provide a quick estimate of relative water usage. The Landsat image for July 30 of 2010 was considered for this test and the study area in the image

was distributed with 130 random points using the AlaskaPak v3.0 for ArcGIS 10.x**.** After randomly distributing the points, extraction of pixels values from T_s, ET and NASS land use/land cover to those random points was done in GIS. Pixels that were covered by the clouds in the Landsat images were omitted for the study. The points having the T_s and ET values were plotted in MS-Excel. From the Figure 4.10 it can be seen that there is negative correlation between ET and T_s. Higher ET values are associated with lower T_s and vice versa. Developed and urban areas with high intensity had minimum ET and very high T_s. ET value of zero was observed for some urban areas with high density. While highest ET and low T_s was obtained for most points in open water body, wetlands and forest area. Ahmed et al. (2005) and Bhattarai (2010) also observed strong negative correlation between T_s and ET. Therefore T_s data might also be used as a quick predictor to see the relative consumption of water in the irrigated areas.

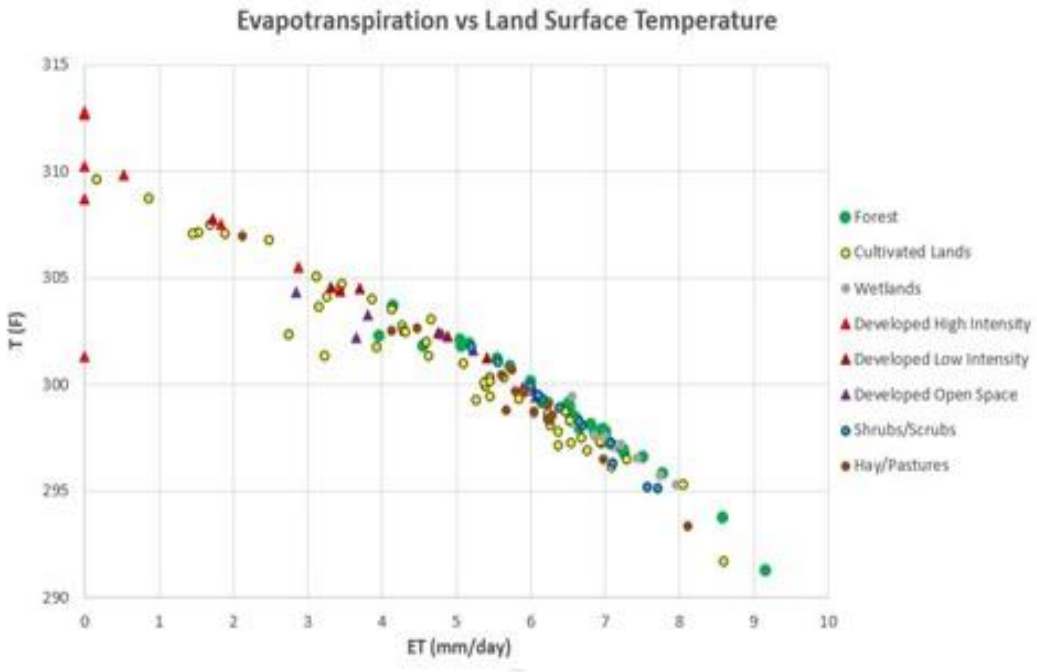

Figure 4.10: T_s vs daily ET for Landsat image of July 30, 2010.

4.7.4 Estimation of ET in irrigated agricultural areas

The main focus of this study was in agricultural land and golf courses. Secondary data from National Agricultural Statistics Service *(*NASS) crop data layer (CDL) maps and National Land Cover Data (NLCD) maps were used to identify agricultural lands in the study area. The NASS provides timely, accurate, and useful statistics in service to U.S. agriculture and National CDL provides classification maps based on different crops. The NASS data for 2005 was not available therefore NLCD LULC map for 2006 was used to compare with seasonal ET for 2005. The NLCD data does not have classification based on individual crops but agricultural lands as a whole. NASS data for agricultural land for the year 2010 were available and used to compare and clip seasonal ET for 2010. Crops that are grown from April to end of September were taken into consideration as seasonal ET was calculated only for that time. Therefore, only croplands having planting dates from April and harvesting dates until the end of September were considered. According to the USDA field crops data, crops that are commonly grown in the state of Alabama are corn, cotton, hay, oats, peanuts, soybeans and winter wheat (USDA NASS,2010). However, oats and winter wheat were not taken into consideration as they are winter crops and are highlighted in red. The Table 4.8 shows the crops planting and harvesting dates in Alabama.

Usual Planting and Harvesting dates by crops – Alabama							
	2009 Harvested Acres(1000 acres)	Usual planting dates			Usual harvesting dates		
Crops		Begin	Most Active	End	Begin	Most Active	End
Corn for grain	250	15-Mar	Mar 25 - Apr 25	18-May	2-Aug	Aug 11 - Sep 20	15-Oct
Cotton, all	248	5-Apr	Apr 24 - May 24	6-Jun	5-Sep	Sep 20 - Oct 20	1-Dec
Hay, other	800	(NA)	(NA)	(NA)	10-May	Jun 20 - Sep 1	15-Oct
Oats, fall	11	1-Sep	Sep 15 - Oct 15	1-Dec	1-May	May 25 - Jun 25	1-Jul
Peanuts	152	16-Apr	Apr 25 - May 25	15-Jun	15-Sep	Sep 22 - Oct 22	20-Nov
Soybeans	430	15-Apr	May 25 - Jun 25	3-Jul	3-Sep	Oct 28 - Nov 28	15-Dec
Wheat, winter	180	2-Oct	Oct 21 - Nov 21	12-Dec	1-May	May 25 - Jun 25	1-Jul

Table 4.8: Field Crops Usual Planting and Harvesting Dates for Alabama (Source USDA, NASS)

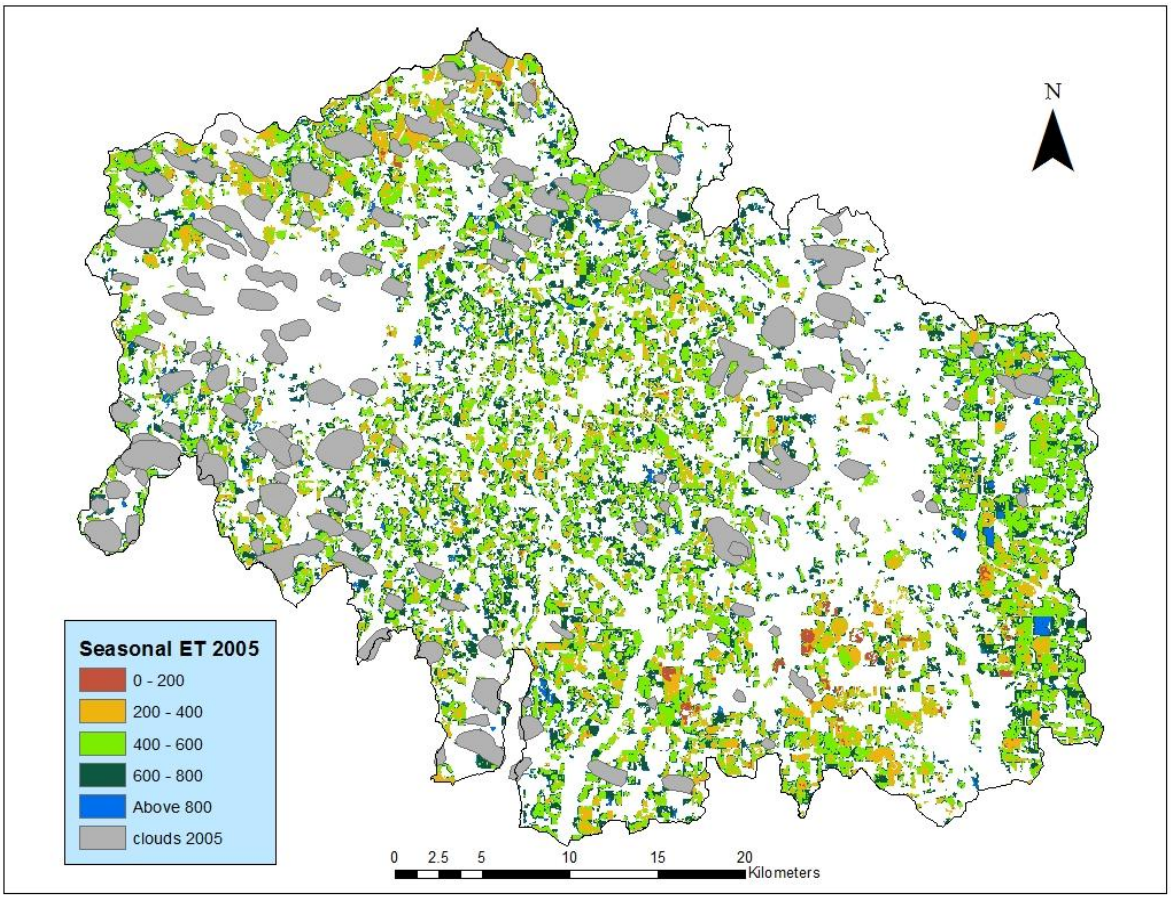

Figure 4.11: Seasonal ET Map for agricultural land for year 2005

As the crop layer data were not available for 2005, NLCD data for year 2006 were used where classification was based on all agricultural land. Therefore, both summer crops and winter crops were considered even though ET was calculated for only crop growing season from April to September. The ET maps shows that most of the agricultural lands had ET ranging from 400 to 800 mm. The total irrigated agricultural area excluding covered by clouds was 593.51 sq.km.

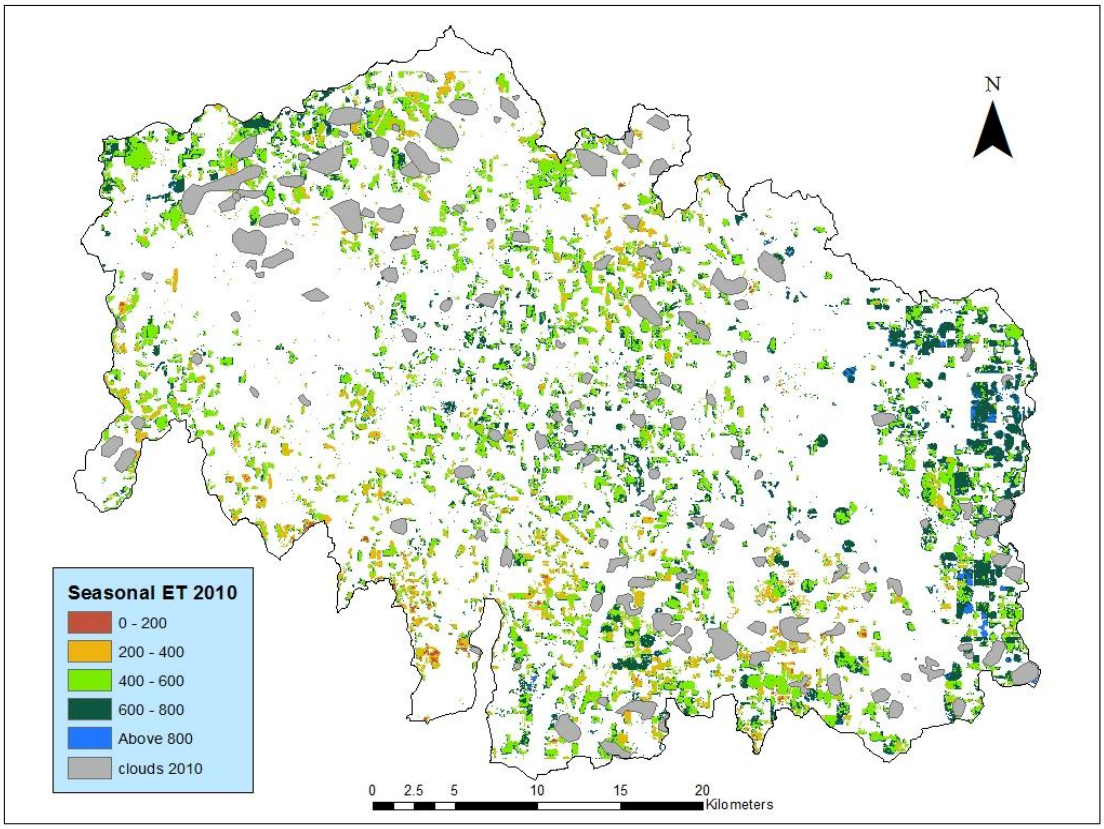

Figure 4.12: Seasonal ET Map for agricultural land for year 2010

From the map, it can be deduced that most of the agricultural area for summer crops had seasonal ET values from 400- 800 mm and provide an estimate of how much water was consumed by the plants. There were very few areas that had ET greater than 800 mm. The areas that had clouds in the Landsat images were neglected as it introduces errors in ET estimation. The total irrigated agricultural areas for summer crops excluding covered by clouds was 343.26 sq. km. In analyzing the water usage for agriculture areas, land use/land cover change had to be considered since there were approximately 250 fewer sq. km (out of a total of 1,729 square kilometers of the study area) of agricultural land in 2010 than in 2005 as indicated by the land use/land cover datasets. Overall, based on the analysis in section 4.7.2 the average ET per pixel on agricultural land increased from approximately 511mm in 2005 to 588mm in 2010.

4.7.5 Classification of golf courses using GEOBIA and estimating ET

The attributes of golf courses in the study area varied from place to place. Therefore different classification ruleset had to be built for each golf course. For example, the grasses used at different golf courses varied therefore different spectral value for NIR had to be used for different golf courses. Similarly other attribute parameters also varied for different golf courses. These different rulesets were combined into one common ruleset which was applied to all the NAIP images of study area.

There are total of four golf courses in the study area and all four were classified using GEOBIA as shown in Figure 4.13, 4.14, 4.15 and 4.16. The classified golf courses were exported into vector layers. The layers were used to clip the ET raster for both 2005 and 2010 to analyze the seasonal ET for the golf courses. Table 4.9 shows the classified golf courses and their total area for the greens that are irrigated. The areas of trees and buildings at the golf courses have been neglected since these areas are not irrigated. Figure 4.13, 4.14, 4.15 and 4.16 shows the seasonal ET at the four golf courses for 2005 and 2010 and by comparing, it can be deduced that water usages has increased in 2010.

S.N	Date	Area (m^2)
1	Highland oaks golf courses	723,678
2	Kilgores Roundabout Plantation	797,001.5
3	Dothan National golf club hotel	362,484.5
4	Dothan Country Club	313,913.5

Table 4.9: Field Crops Usual Planting and Harvesting Dates for Alabama (Source USDA, NASS)

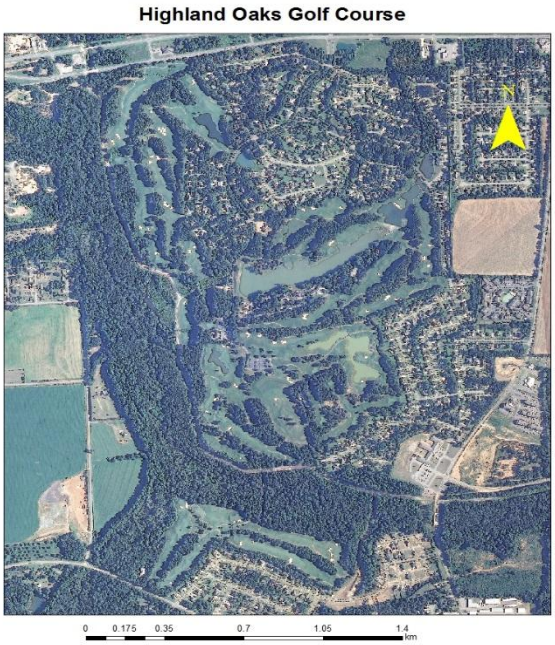

(i)

(ii)

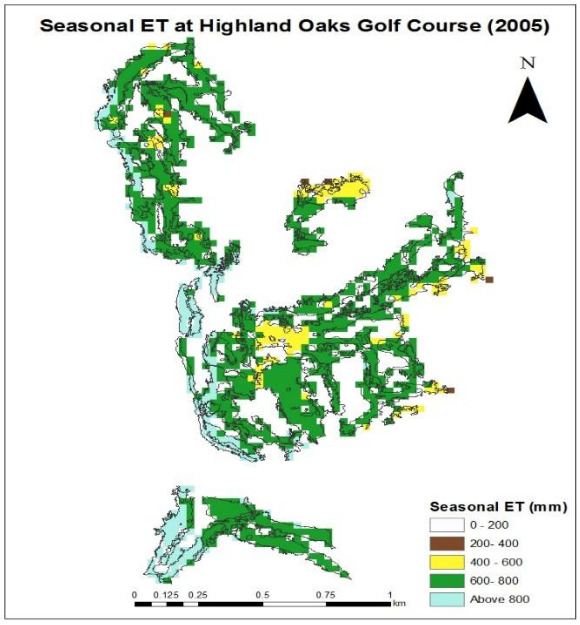

(iii)

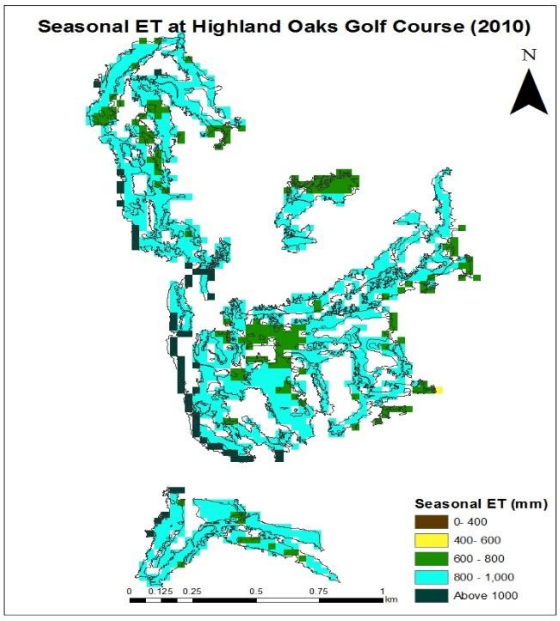

(iv)

Figure 4.13 (i) NAIP image at Highland Oaks golf course (ii) Classified images from GEOBIA (iii) Seasonal ET for 2005 at the golf course (iv) Seasonal ET for 2010 at the golf course

(i)

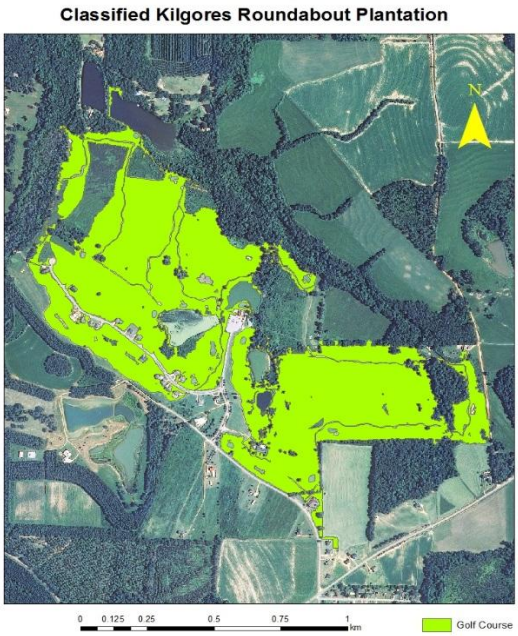

(ii)

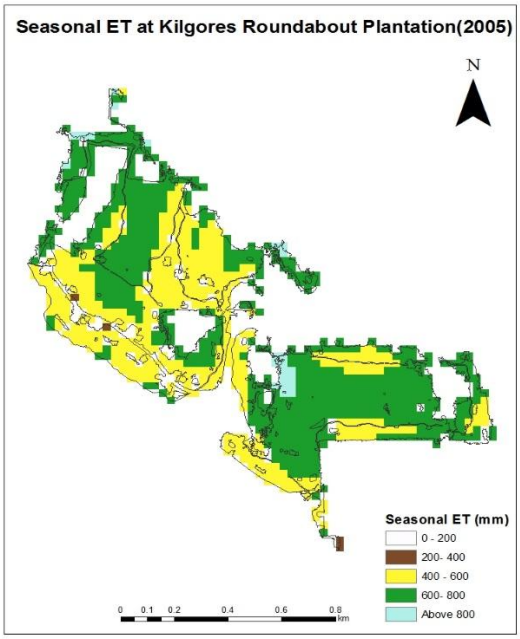

(iii)

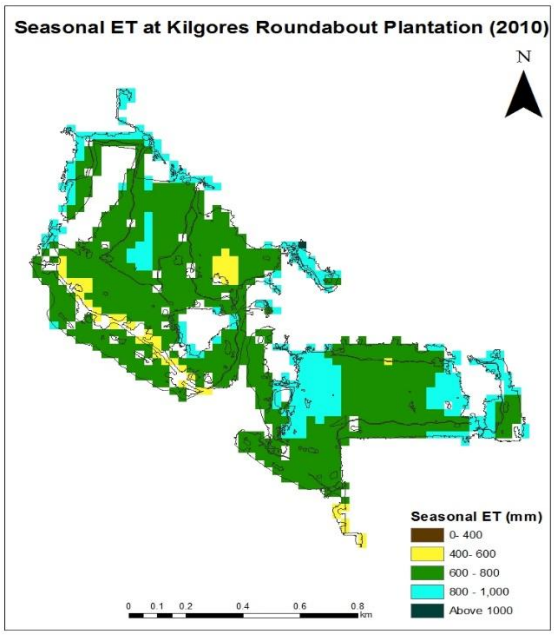

(iv)

Figure 4.14 (i) NAIP image at Kilgore Roundabout Plantation (ii) Classified images from GEOBIA

(iii) Seasonal ET for 2005 at the golf course (iv) Seasonal ET for 2010 at the golf course

(i)

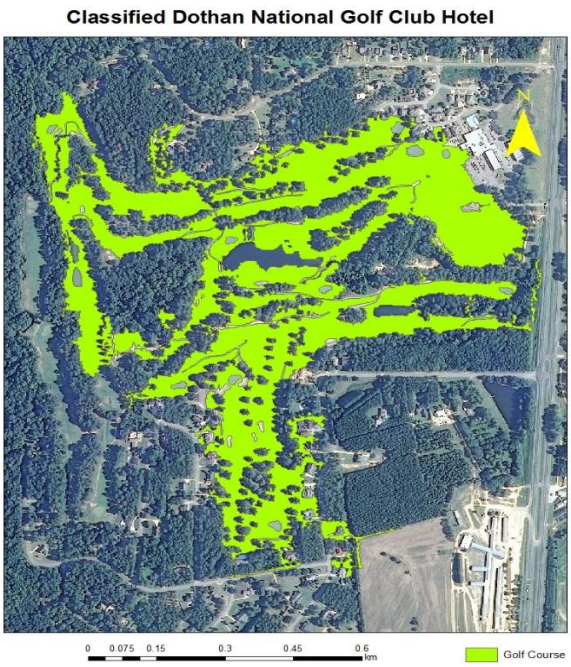

(ii)

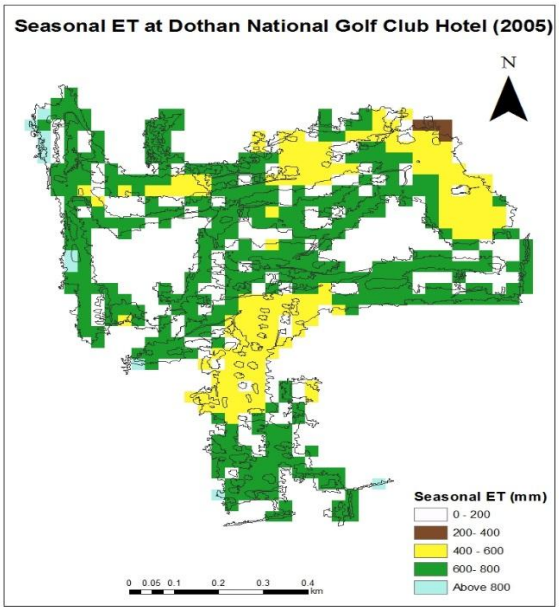

(iii)

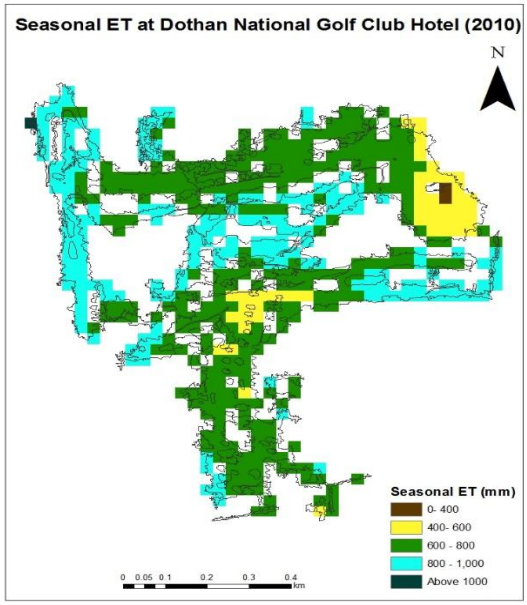

(iv)

Figure 4.15 (i) NAIP image at Dothan National Golf Club Hotel (ii) Classified images from GEOBIA

(iii) Seasonal ET for 2005 at the golf course (iv) Seasonal ET for 2010 at the golf course

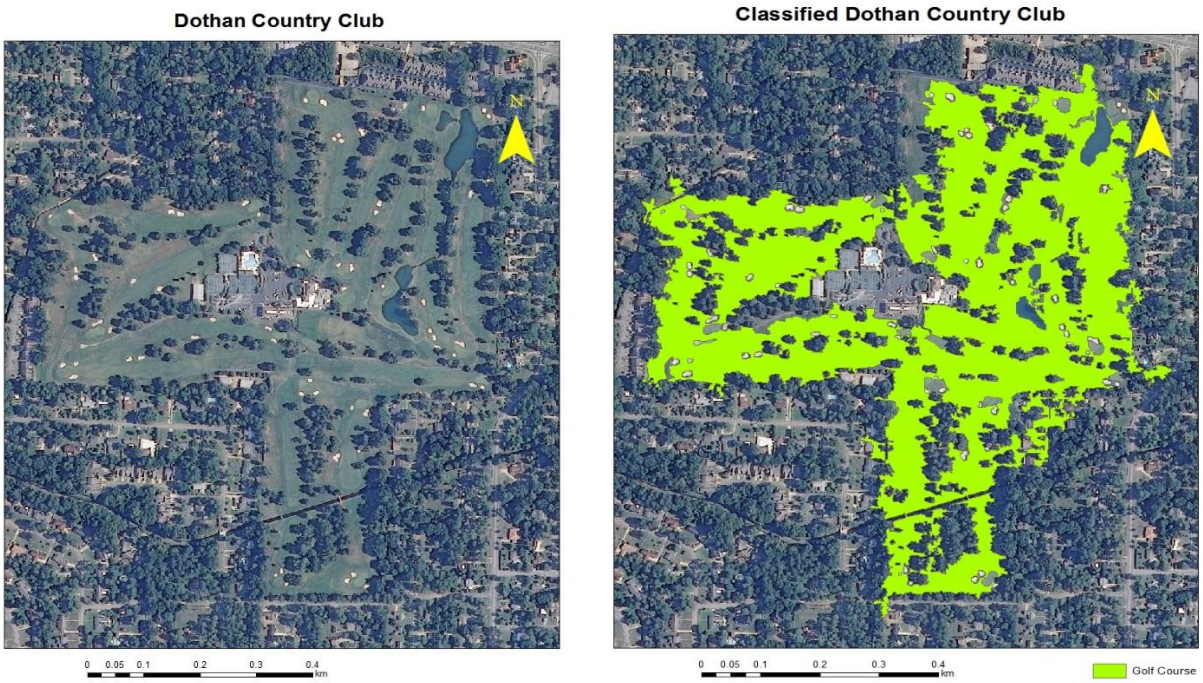

(i) (ii)

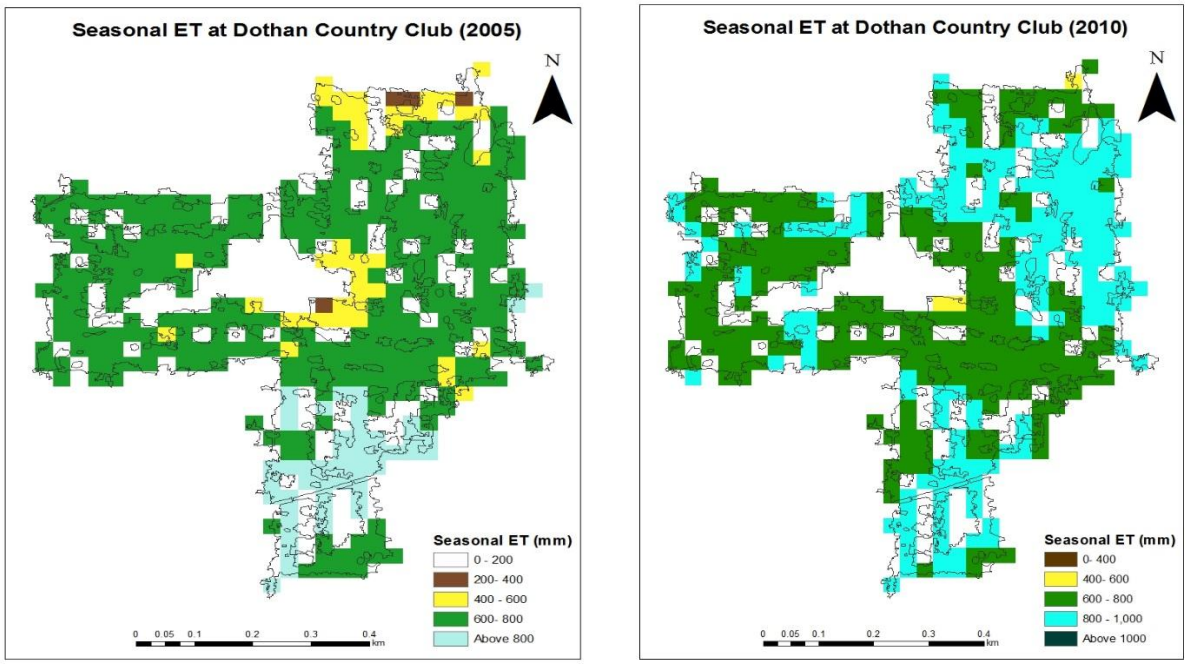

(iii) (iv)

Figure 4.16: (i) NAIP image at Dothan Country Club (ii) Classified images from GEOBIA (iii) Seasonal ET for 2005 at the golf course (iv) Seasonal ET for 2010 at the golf course

While comparing the Seasonal ET maps for golf courses from 2005 and 2010, it can be stated that the water consumption has increased by considerable amount in 2010 for all the golf courses. Analyzing the ET maps for golf courses from Figures 4.13, 4.14, 4.15 and 4.16, the map color grading has changed in most areas into darker colors indicating that there is more ET in that area and more water has been consumed from 2005 to 2010. The average value of seasonal ET for all pixels for golf courses was 679 mm in 2005 and 791 mm in 2010. Therefore, there was a substantial increase in the amount of water usage in the golf courses.

Since there was increase in the water consumption for both agricultural lands and golf courses, it was important to see if the increment had to do anything with the weather during the crop growing season for both years. The weather data from the Headland AWIS weather station was compared for the year 2005 and 2010 to find out which was a dry year during the crop growing season. Table 4.10 and 4.11 show the average minimum temperature, average maximum temperature and total precipitation from April to September for 2005 and 2010 respectively.

Month (2005)	Average maximum temperature (F)	Average minimum temperature(F)	Total precipitation (inches)
April	74.5	52.7	8.01
May	83	61.8	2.36
June	87.4	70.5	9.74
July	90	73.7	5.35
August	88.4	73	7.93
September	88.8	69.3	1.72

Table 4.10 : Temperature and precipitation data during the crop growing season for 2005 (Source: AWIS, 2015)

Month (2010)	Average maximum temperature (F)	Average minimum temperature(F)	Total precipitation (inches)
April	82.1	55.3	2.39
May	88.5	67.9	4.7
June	94.1	74	4.57
July	95.4	75.3	1.72
August	94.5	75.9	2.55
September	94.7	69.1	3.04

Table 4.11: Temperature and precipitation data during the crop growing season for 2010 (Source: AWIS, 2015)

Comparing the two tables showed that 2010 was drier year than 2005. The average maximum and minimum temperature from April to September for 2010 was higher than 2005. Similarly the total rainfall from April to September for 2005 and 2010 was 35.11 inches and 18.97 inches respectively. The comparison above provides evidence that 2010 was a drier year compared to 2005 which may have led to increase in seasonal ET values for 2010.

Similarly, comparison of the weather data of 2005 and 2010 was also done with historic average weather data for 65 years during the crop growing season. Table 4.12 below shows the historic average weather data for 65 years in Headland, Alabama.

Month	April	May	June	July	August	September
Historic monthly total rainfall (inches) for 65 years	4	3.7	4.7	5.8	4.7	4
Average Maximum Temperature for 65 years (F)	78.3	85.4	90.3	91.5	91.1	87.3
Average Maximum Temperature for 65 years (F)	53.1	61.4	67.7	69.7	69	64.8

Table 4.12 : historic averages weather data of 65 years of Headland, Al (Source: NOAA Cooperative Observer Program (COOP) network of the National Weather Service)

The historic average weather data of 65 years were compared with weather data of 2005 and 2010 to see the difference in temperature and monthly rainfall. The difference between the average maximum temperature, average minimum temperature and total rainfall was calculated in their respective months and the values are shown in the Table 4.13 and 4.14 below.

Month (2005)	Difference in Average maximum temperature (F)	Difference in Average minimum temperature(F)	Difference in Total precipitation (inches)
April	-3.8	-0.4	+4.01
May	-2.4	+0.4	-1.34
June	-2.9	+2.8	+5
July	-1.5	+4	-0.45
August	-2.7	+4	+3.23
September	+1.5	+4.5	-2.28

Table 4.13: Difference between the historic average data of 65 years and weather data of 2005

Analyzing Table 4.13 gives information that the average maximum temperature for 2005 was less than the historic average weather data. There was slight increase in the average minimum temperature. Similarly, there was more rainfall in 2005 than the historic average data

suggesting that 2005 was not a dry year and had plenty of rainfall compared to the historic average of 65 years.

Month (2010)	Difference in Average maximum temperature (F)	Difference in Average minimum temperature(F)	Difference in Total precipitation (inches)
April	+3.8	+2.2	-1.61
May	+3.1	+6.5	+1
June	+3.8	+6.3	-0.13
July	+3.9	+5.6	-4.08
August	+3.4	+6.9	-2.15
September	+7.4	+4.3	-0.96

Table 4.14 : Difference between the historic average data of 65 years and weather data of 2010

Analyzing Table 4.14 gives information that the average maximum temperature and minimum temperature for 2010 was greater than the historic average weather data for 65 years. Similarly, there was less rainfall in 2010 than the historic average data suggesting that 2010 was hot and dry year with less rainfall compared to the historic average of 65 years.

Therefore by looking and analyzing the Table 4.10, 4.11, 4.12, 4.13 and 4.14, it can be summarized that 2010 was a hot and dry year compared to 2005 and was possibly part of the reason behind the increase of seasonal ET in golf courses and agricultural lands.

4.8 Discussion and summary

Remotely sensing has been used to assess the plant water consumption at a local (golf course) and regional (county-wide agriculture) scale. The METRIC model was used to estimate the plant water use in the 20 HUC 12 watersheds in the Wiregrass region of Southern Alabama.

The visible bands, NIR band and thermal bands of Landsat 5 TM were used as inputs to the model. Similarly weather parameters such as solar radiation, temperature, relative humidity, wind speed, and precipitation were also required as inputs to Ref-ET software to compute the ASCE Penman-Monteith standardized (Allen et al.,2000b) form of reference ET (ET_{ref}) for alfalfa.

A total of 15 models were built in the ERDAS model maker to get the final daily ET map from the Landsat images. Since the State of Alabama does not have any USGS evapotranspiration (ET) stations, validation of the ET from the METRIC model with the field data in Wiregrass Region was not possible. To validate the accuracy and reliability of the model, the model was tested in the areas that cover USGS ET stations in Florida. The validation study supported that the model performed well in estimating the daily, monthly, and two-month ET.

After estimating the daily ET on the acquisition day for each satellite image for the 20 HUC 12 watersheds in the wiregrass region during the growing season, daily ET for the all the days in the growing season (April to September) was calculated by multiplying interpolated Reference ET Fraction (ET_rF) maps with daily ET_{ref} values. The daily ET for the whole growing season was summed providing seasonal ET at each pixel of the study area. The study was primarily concerned with estimating ET of agricultural lands and golf courses. Agricultural lands were identified using secondary data from NASS 2010 and NLCD 2006 while golf courses were identified using classification methods in GEOBIA using NAIP images. The seasonal ET map was clipped with agricultural lands and golf courses in GIS to give ET information only on those areas.

Comparing the seasonal ET maps for year 2005 and 2010 showed that water consumption has increased by considerable amount in 2010 for golf courses as the average ET increased from 679 mm in 2005 to 791 mm in 2010. The analysis showed that water consumption increased minimally for agricultural lands, with analysis indicating an increase in average ET from approximately 511mm in 2005 to 588mm in 2010. Since 2010 was drier year than 2005, it might have led to the increase in water consumption.

.

Chapter 5: Summary and Conclusion

5.1 Remote sensing of water resources.

Remote sensing (RS) is the art and science of obtaining information about an object or phenomenon without being in direct physical contact with the body. RS has been frequently used in many applications related with hydrology, forestry, agriculture, cartography, geology and meteorology among others. Different remote sensing techniques and methods have been studied and used to obtain quantitative and spatial measurements of important hydrologic parameters (Gregg and Casey, 2004; Karaska et al., 2004) resulting in more favorable results than the traditional way in collecting extensive field data. Extracting information from a remotely sensed dataset can be achieved by trained image analysts by implementing the knowledge about the fundamental elements of image interpretation including shape, size, tone (reflectance or emittance), shadow, pattern, texture, site, and association (Olson, 1960). This research thesis focused on two case studies using remote sensing in water related applications in the state of Alabama.

5.2 Eliminating the errors of rooftops from isolated wetlands classification of Lee County using LiDAR data

This case study was funded by an EPA project titled “Inventory, classification, and assessment of Alabama’s geographically isolated wetlands” to improve the methods for mapping isolated wetlands using a highly automated process. The National Wetland Inventory data revealed that there were many gaps in the wetland inventory of Alabama with much of the state’s

wetlands not being digitized. GIS and RS technology have played an immense role in classification and mapping of wetlands. There are many automated classification methods in remote sensing but one of the new methods for the classification of high resolution images is Geographic Object Based Image Analysis (GeOBIA) which is used to group image pixels into meaningful objects and is growing rapidly in use. Jones (2013) conducted a study using GeOBIA method to classify the wetlands of Northern Alabama as a part of his Master thesis at Auburn University. Most of the errors in his classification were due to rooftops, asphalt and shadows being mistakenly classified as wetlands all of which can have low reflectance in the visible and especially near-infrared bands of satellite or aerial imagery. This part of the thesis sought to improve wetlands mapping by testing whether the rooftop errors in wetland classification could be eliminated by classifying building rooftops from LiDAR point clouds and eliminating those rooftop errors from the initial classification. The study also attempted to improve the classification by minimizing the errors of asphalt and shadows, although LiDAR did not play a role in this aspect of correcting for errors.

Wetlands were initially classified using the GeOBIA methods solely with NAIP imagery. Multi-resolution segmentation was performed and classification of the images was done for the whole of Lee County. A ruleset for the classification was developed using information such as mean spectral reflectance of NIR, open water spectral signature, homogeneity, ratio green, standard deviation of NIR, ZABUD, and texture to classify the water bodies. The classified wetlands were exported into GIS layers and isolation for the wetlands were defined using the 40 m buffer of the National Hydrography Dataset and the Federal Emergency Management Agency DFIRM floodplain data in accordance with the Tiner Methodology (Tiner, 2003). In total 976

isolated wetlands were initially classified in Lee County with the accuracy percentage of 80.4 percent.

To deal with the errors of building rooftops mistakenly classified as wetlands, two methods were adopted to classify the rooftops in a small section of Lee County and were compared to see which one performed better. The one with better performance was used to classify all the building rooftops of Lee County and used as a mask to eliminate these errors in the initial isolated wetlands classification. The first method that was tested involved GeOBIA and was done with eCognition software. This method required National Agricultural Imagery Program (NAIP) imagery, a normalized Digital Surface Model (nDSM, representing height of features) and an intensity raster to help classify building rooftops. LiDAR data were used to generate a Digital Elevation Model (DEM) and a Digital Surface Model (DSM) raster from which nDSM (DSM - DEM) was determined which was then used to separate rooftops from the ground and forest vegetation. The second method involved the Point Cloud Tasks (PCT) tools in LP360 software, which is an extension of ArcGIS. From the comparison study, it was found that PCT method was more advantageous as it required only LiDAR point clouds to classify the building rooftops whereas GeOBIA required imagery as well as LiDAR. Moreover, the PCT method of LP360 was more accurate with 90.8 percent accuracy compared to that of GeOBIA method, which was only 81.2 percent accurate, and it also performed better in mapping the accurate shapes of the rooftops.

Therefore, the Point Cloud Tasks (PCT) tool in LP360 software was chosen to classify the rooftops in Lee County, AL. In total, 49,341 building rooftops were extracted for the Lee County with acknowledgement that this is an overestimate due to errors mostly in forest and in open space, but since these errors did not intersect any of the wetlands in the original

classification they were ignored. After producing the building rooftop GIS layer, it was used to remove rooftop errors from the initial isolated wetlands layer. Only those isolated wetlands were selected which did not intersect with the building rooftop layer and were exported into a new layer of corrected isolated wetlands in Lee County. In total there were 871 isolated wetlands after the LiDAR correction process was applied. Accuracy assessment for the wetlands was done by randomly selecting 250 polygons of isolated wetlands using the Alaska Pak v3.0 for ArcGIS 10.x and was assessed by inspecting the selected polygons with NAIP images. The errors considered for this project were of commission rather than omission, meaning it was assessed for only those isolated wetlands that were classified. The percentage accuracy for the isolated wetlands classification was 90.4% for visual inspection compared to the initial accuracy of 80.4% and Jones (2013) 83.7% accuracy from aerial image inspection which both did not use LiDAR data. Similarly by introducing the ZABUD parameter, it was able to reduce the number of errors associated with asphalt. The results of this study provide evidence that integrating LiDAR data into classification methods for isolated wetlands can help improve the accuracy of the classification process.

5.2.1Research questions

- **What is the spatial extent of the isolated wetlands in Lee County?**

  Analyzing the map of isolated wetlands showed that the wetlands were distributed throughout Lee County with a total of 871 isolated wetlands resulting in a total area of 3,458,443.15 sq. meters. The largest area of the wetland was 67,786.5 sq. meters and the smallest was 449.5 sq. meter.

- **Which method was better to classify the building rooftops, GeOBIA or Point Cloud Task method in LP360 software?**

  The Point Cloud Task method of LP360 software was better to extract building rooftops than GeOBIA methods as the accuracy assessment percentage of the PCT method was higher than that of GeOBIA. The accuracy percent for PCT was 90.8% whereas for GeOBIA it is just 81.2%. Moreover, GeOBIA extracted fewer building rooftops in comparison to PCT and PCT performed better at mapping the true shapes of the building rooftops

- **How has the introduction of the LiDAR improved the wetland classification?**

  The introduction of LiDAR data has improved the classification of isolated wetlands through the removal of those classified wetlands that were actually building rooftops. The accuracy percentage of the isolated wetlands classification was 90.4%, an improvement of 10% from the initial classification analysis where LiDAR data were not used. The initial accuracy for wetland classification without LiDAR was 80.4% and that achieved by Jones (2013) was 83.7% on visual inspection to aerial image.

5.3 Estimating evapotranspiration as a proxy for water usage in the irrigated areas and golf courses in the Wiregrass region of Alabama.

Remotely sensed imagery has been used to assess the plant water usage at a local and regional scale. The estimation of water use can be done with minimum ground data. As it is very difficult to get accurate ground truth data, this method can be very useful to estimate water usage where the ground data are limited. The METRIC model was used to estimate the plant water use in the 20 HUC 12 watersheds in the Wiregrass region of southern Alabama. The model requires mostly cloud free satellite imagery and weather station data. The visible bands, NIR band and thermal bands of Landsat 5 TM were used as inputs to the model. The thermal bands of Landsat

can be used to derive Land-Surface Temperature (T_s) and provide estimates of an evaporative flux pattern that serves as a proxy of the surface moisture over a range of different spatial scales (Hain et al., 2009; Hain et al., 2011). Similarly weather parameters such as solar radiation, temperature, relative humidity, wind speed, and precipitation were required as inputs to Ref-ET software to compute the ASCE Penman-Monteith standardized (Allen et al. 2000b) form of reference ET (ET_{ref}) for alfalfa.

A limitation to the project was getting cloud free images at short intervals. Although Landsat images are captured twice every month, it was very difficult to get cloud free images especially in the humid subtropical climate of southern Alabama. METRIC model provides a good estimate of water consumption by agricultural lands and golf courses at a local and regional scale but it does not take into consideration water application efficiencies in the irrigation system (Bhattarai, 2010). A total of 15 models were built in the ERDAS model maker to produce the final daily ET map from the Landsat images. Since the state of Alabama does not have any USGS evapotranspiration (ET) stations that measure ET data on the ground, validation of the ET from the METRIC model with the field data in Wiregrass Region was not possible. To validate the accuracy and reliability of the model, the model was tested in the areas that cover USGS ET stations in Florida. The validation study supported that the model performed well in estimating the daily, monthly, and two-month ET.

After estimating the daily ET during the crop growing season (April to September) from four satellite images for the year 2005 and five satellite images for year 2010 in the study area, seasonal ET (April to September) was calculated by multiplying interpolated Reference ET Fraction (ET_rF) pixel values with daily ET_{ref} values. This gave the daily ET values for each day for the whole growing season. By summing the daily ET for the whole growing season, the

seasonal ET at each pixel of the study area was computed for 2005 and 2010. The study was primarily concerned with estimating ET for agricultural lands and golf courses although other land use/land cover types were observed to evaluate the overall performance of model estimation of ET. Agricultural lands were identified using secondary data from NASS 2010 and NLCD 2006 while golf courses were identified using classification methods in GEOBIA through the classification of NAIP imagery. The seasonal ET map was clipped with agricultural lands and golf courses in GIS to estimate water usage for those areas. By comparing the seasonal ET maps for year 2005 and 2010, the analysis showed that water consumption increased minimally for agricultural lands and that there was a more substantial increase in water consumption for golf courses which, in part may have resulted because 2010 was a dry year compared to 2005.

To conclude, the METRIC model has been identified as a useful RS method to estimate plant water usage in the Wiregrass region of southern Alabama. The information about ET and digital land use/land cover maps can be vital for policymaker's and resource manager's decisions associated with the management of water resources.

5.3.1 Research question

- **What is the spatial extent of golf courses in the study area?**

  There were a total of 4 golf courses in the study area in Houston County covering a total area of 2,197,077.50 sq. meters. They are Highland Oaks Golf courses, Kilgores Roundabout Plantation, Dothan National Golf Club Hotel and Dothan Country Club. The largest golf course was Kilgores Roundabout Plantation with an area of 797,001 sq. meters while Dothan Country Club was the smallest with an area of 313,913 sq. meters.

- **Can the ruleset developed for the classification of golf courses be applied to other places in Alabama to identify golf courses?**

The ruleset for the golf course classification was made in such a way that all the golf courses in the study area would get classified. The golf courses varied from place to place depending on the type of grasses used and how it was maintained. This ruleset could serve as a base ruleset to detect other golf courses if they are in similar environments, however, the rule parameters may need to be experimented with on a case-by-case basis.

- **Can the METRIC model be used with remotely sensed data to provide a reliable estimate of evapotranspiration?**

Based on the analysis in this thesis, the METRIC model can be used with remotely sensed data to provide a reliable estimate of evapotranspiration. The models work best with cloud free satellite imagery and weather stations in the study area to estimate the evapotranspiration of the area of interest. The visible bands, NIR band and thermal bands of Landsat 5 TM were used as inputs to the model. Weather parameters such as solar radiation, temperature, relative humidity, wind speed, and precipitation were also required as inputs to Ref-ET software to compute the ASCE Penman-Monteith standardized (Allen et al.2000b) form of reference ET (ET_{ref}) for alfalfa. Using all of these data, a raster image was created which showed estimated ET values for each pixel. First, the daily ET was calculated in Florida to validate the accuracy and reliability of the model. The model was tested in the areas that cover USGS ET stations in Florida. The validation study supported that the model performed well in estimating the daily, monthly, and two-month ET.

- **How has the trend in water consumption changed from 2005 to 2010 in both agricultural land and golf courses?**

When comparing the Seasonal ET maps for year 2005 and 2010, it was found that that water consumption increased by considerable amount in 2010 for golf courses. Comparing the average seasonal ET values of golf courses for year 2005 and 2010, it was seen the average seasonal ET increased from 679 mm in 2005 to 791 mm in 2010. Figure 5.1 for Dothan Country Club golf course also shows that the water usage has increased from 2005 to 2010. Similarly, the average seasonal ET on agricultural land increased from approximately 511mm in 2005 to 588mm in 2010. Since 2010 was a dry year compared to 2005, it might have led in increase in water usage in both agricultural lands and golf courses.

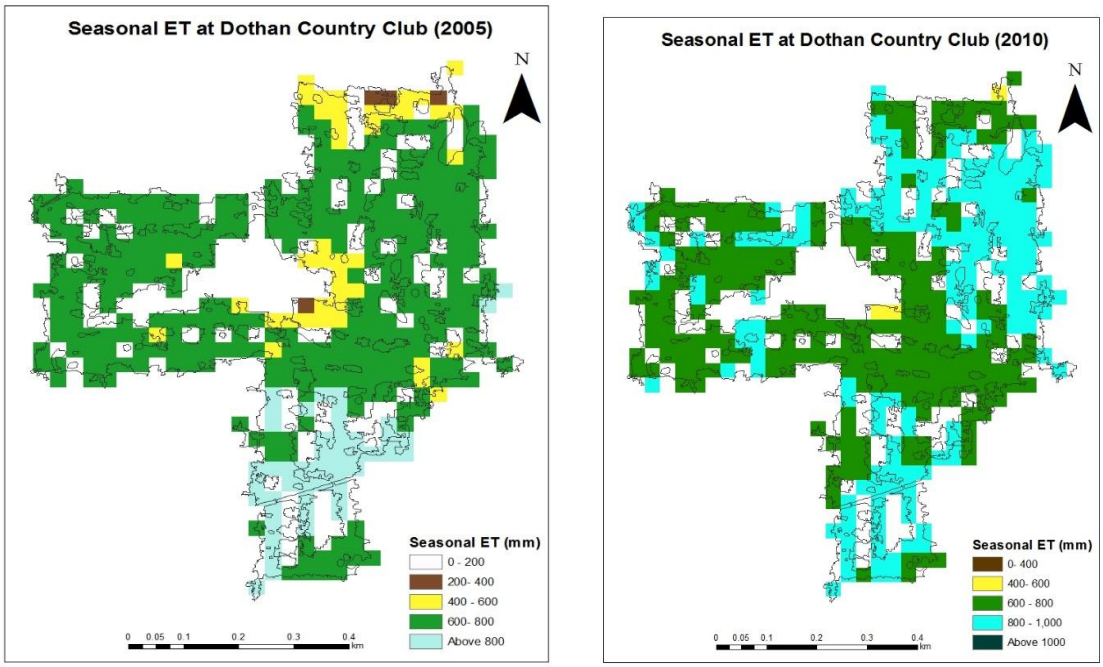

(i) (ii)

Figure 5.1: (i) Seasonal ET for 2005 (ii) Seasonal ET for 2010 at the golf course

5.4 Significance of study and future work.

Water being an indispensable element for the existence of living organisms on Earth needs to be managed wisely and sustainably (Lockaby, 2013). Managing water resources is one of the main challenges for water resource managers. This thesis looked at two remote sensing case studies that involved the monitoring of water resources. This first case study was funded by the EPA on a project titled "Inventory, classification, and assessment of Alabama's geographically isolated wetlands" with the goal to improve the methods for mapping isolated wetlands using a highly automated process. The National Wetland Inventory data revealed that there were many gaps in the wetland inventory of Alabama with most of the area's wetlands not being digitized. GIS and remote sensing technology have played an immense role in classification and mapping of wetlands. There are many classification methods in remote sensing but a newer method for the classification of high resolution images is called GeOBIA which groups pixels into meaningful objects. This research attempted to improve the classification of isolated wetland conducted by Jones (2013) using GeOBIA method and LiDAR data. Most of the errors in the initial classification were due to rooftops, asphalt and shadows. This case study emphasized improving the classification results by introducing LiDAR data. By introducing LiDAR data, the accuracy of the isolated wetland classification improved to 90.4% from the initial classification of 80.4% when Lidar was not used it. This research provides evidence that LiDAR can help in achieving higher accuracy in mapping isolated wetlands

The EPA project was conducted by for the whole state using only GeOBIA. However, this part of the thesis focused only on Lee County because of the availability of LiDAR data. In the future, as LiDAR data become available for all counties in Alabama, the methods detailed in this thesis can be extended and the classification of isolated wetlands can be improved for all

counties. This will help achieve higher accuracy and making the isolated wetland inventory more reliable. Having a good inventory of the location of the isolated wetlands can help the concerned authorities document and help protect isolated wetlands.

The second case study of the thesis was funded by the Alabama Office of Water Resources with a goal to provide state agency resource managers with a report detailing methods to estimate water usage for irrigated agricultural lands and golf courses through the RS of Evapotranspiration (ET). As both irrigated agricultural lands and golf courses consume large amounts of water, it is important that regional resource managers have an accurate inventory of agricultural lands and golf courses and also have estimates on the consumption of water in these areas. Methods for calculating ET using and the Mapping EvapoTranspiration at high Resolution with Internalized Calibration (METRIC) model can be helpful for the water resource managers to get rough estimates of water usage at local and regional scales with moderate resolution satellite imagery such as those provided by the Landsat program since 1972. The overall findings showed that agricultural irrigation has increased marginally from 2005 to 2010 while irrigation on golf courses has increased more substantially.

The state of Alabama is water rich with plenty of precipitation and it also consists of 77,000 miles (124,000 km) of perennial and intermittent streams and rivers, and has more than 560,000 acres (226,600 ha) of ponds, lakes, and reservoirs (Marcus and Kiebzak, 2008). Although the state is blessed with copious amount of water resources and precipitation, the U.S. Geological Survey (USGS) reported that in year 2000 the consumption of water for irrigation was only 28.7 million gallons (0.11 mcm) of surface water per day (mgd). The water withdrawn for agricultural use is less than 2 percent.

Estimation of evapotranspiration (ET) using remote sensing and Mapping EvapoTranspiration at high Resolution with Internalized Calibration (METRIC) model can be helpful for the water resource managers by providing a rough estimate of water usage. The thermal bands of Landsat can be used to derive the Land-Surface Temperature (T_s) and provide estimates of an evaporative flux pattern which serves as a proxy of the surface moisture over a range of different spatial scales. The use of satellite based measurements in association with energy balance models can provide information on spatial distribution of ET. Policymaker's decisions can be based on the results of the ET derived from the model and can be used to address the irrigation problems that is happening in the state of Alabama. Therefore, this research is vital for policy makers and water resource managers to help make well-informed decisions based on the information about the area occupying the irrigated lands and golf courses. This research can be extended in future by investigating methods to convert ET estimates into total volume of water consumed in the agricultural land and golf courses based on the area of the land and ET calculated. The calculated amount of water consumed can be compared with the real data of how much water was irrigated to measure the accuracy of the model.

Appendix

Mapping EvapoTranspiration at high Resolution and with Internalized Calibration (METRIC)

Mapping EvapoTranspiration at high Resolution and with Internalized Calibration (METRIC) is the modified version of SEBAL and both have similar foundation, techniques and principles of surface energy budget equation (Allen et al., 2007). METRIC is an "image-processing model which is used for measuring evapotranspiration as a residual of the surface energy balance" (Allen et al., 2005, p. 251) and is based on the theory that incoming net solar radiation drives all energy exchanges on the earth's surface including ET. The energy consumption of ET from energy balance at the surface is computed as "residual" of the surface energy equation (Allen et al., 2005) which is shown below in equation 1.

$$\lambda ET = R_n - G - H \quad (1)$$

where; λET =latent energy consumed by ET; R_n= net radiation which is the sum of all incoming and outgoing short-wave and long-wave radiation at the surface; G=sensible heat flux conducted into the ground; and H=sensible heat flux convected to the air. The parameters in equation (1) are generally expressed in Wm^{-2}.

The net surface radiation flux at the surface (R_n) is defined as the "actual radiant energy available at the surface which is computed by subtracting all outgoing radiant fluxes from all incoming radiant fluxes" (Waters et al., 2002, p.10). R_n can be expressed in surface radiation balance as shown in equation (2):

$$R_n = (1-\alpha)\, R_{S\downarrow} + R_{L\downarrow} - R_{L\uparrow} - (1-\varepsilon o)\, R_{L\downarrow} \quad (2)$$

where; $R_{S\downarrow}$ is the incoming shortwave radiation (W/m^2), α is the surface albedo which is dimensionless, $R_{L\downarrow}$ is the incoming long wave radiation (W/m^2), $R_{L\uparrow}$ is the outgoing longwave radiation (W/m^2), and εo is the surface thermal emissivity which is dimensionless (Waters et al., 2002).

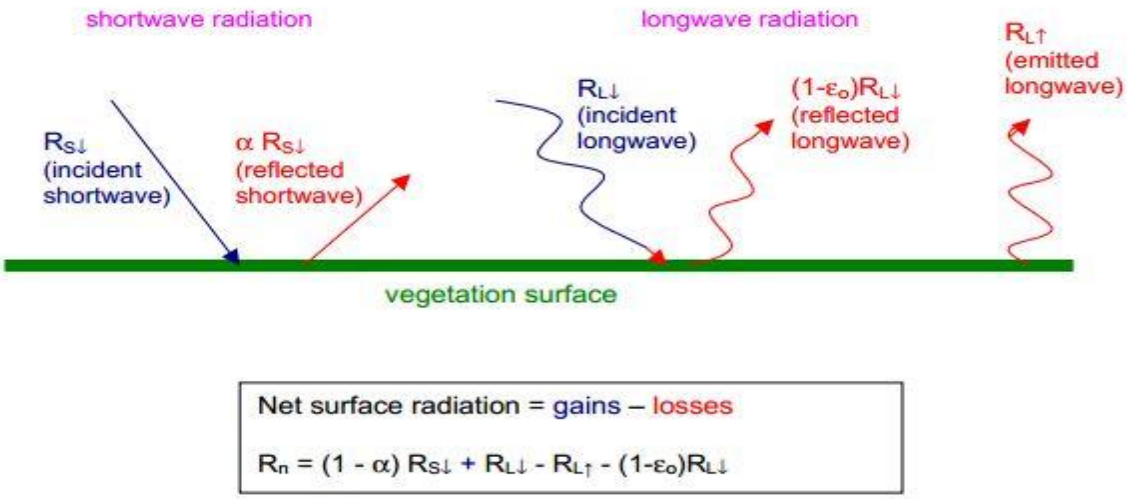

Figure A.1: Surface Radiation Balance [Source: (Waters et al., 2002)]

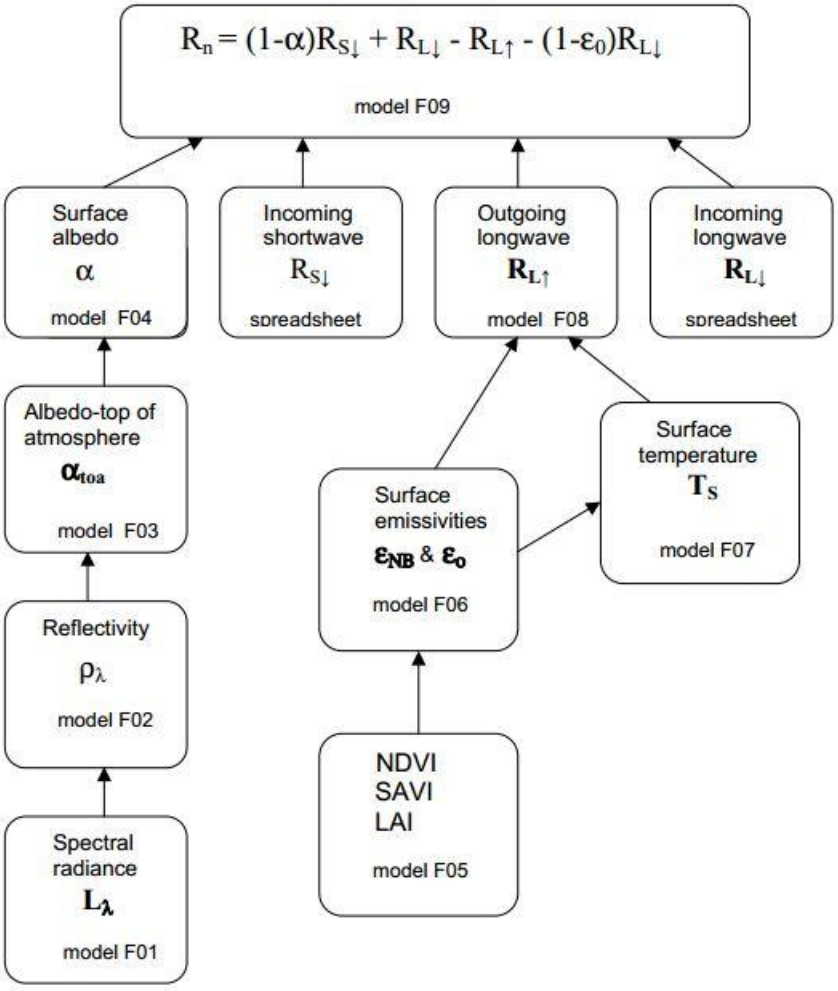

Figure A.2: Flow Chart of the Net Surface Radiation Computation [Source: (Waters et al., 2002)]

A.1 Parameters required for the METRIC model

A.1.1 Spectral radiance (L_λ)

Spectral radiance (L_λ) is the "outgoing radiation energy of the band which is observed at the top of the atmosphere by the satellite" (Waters et al., 2002, p.16). L_λ for each band can be calculated from the Digital Number (DN) of each pixel. The equation (3) shows the computation of spectral radiance for Landsat 5 satellite images:

$$L_\lambda = [DN \times (LMAX - LMIN) / 255] + LMIN \quad (3)$$

where; DN is the digital number of each pixel, LMAX and LMIN are calibration constants. The units for L_λ are $W/m^2/sr/\mu m$.

The equation 4 shows the computation of spectral radiance for Landsat 7 satellite images:

$$L\lambda = (Gain \times DN) + Bias \quad (4)$$

where; Gain and Bias values are given in the header-file of the downloaded satellite image.

A.1.2 Spectral reflectance

Waters et al. (2002) states that spectral reflectance or reflectivity (ρ_λ) of a surface is the "ratio of reflected radiation flux to the incident radiation flux" (Waters et al., 2002, p. 17). It is computed using the equation (5) for the Landsat images:

$$\rho_\lambda = \pi \times L_\lambda / (ESUN_\lambda \times \cos\theta \times d_r) \quad (5)$$

where; L_λ is the spectral radiance for each band , $ESUN_\lambda$ is the mean solar exo-atmospheric irradiance for each band ($W/m^2/\mu m$), $\cos\theta$ is the cosine of the solar incidence angle (from nadir), and d_r is the inverse squared relative earth-sun distance (Waters et al., 2002). Cosine of θ is calculated using the header file data of the satellite image on sun elevation angle (β) where $\theta = (90^0 - \beta)$. The term dr is defined as the inverse squared relative earth-sun distance in astronomical units, from the equation by Duffie and Beckham (1980). The term d_r can be expressed as shown in equation (6) below

$$d_r = 1 + 0.033 \cos (DOY \times 2\pi / 365) \quad (6)$$

where; DOY is the sequential day of the year and the angle ($DOY \times 2\pi/365$) is in radians. The values for d_r are dimensionless and can vary from 0.97 to 1.03(Waters et al., 2002).

A.1.3 Surface albedo (α)

Surface albedo (α) is a "reflection coefficient defined as the ratio of the reflected radiant flux to the incident radiant flux over the solar spectrum" (Waters et al., 2002, p. 10). It can also be described as the "ratio of the reflected radiation to the incident shortwave radiation" (Waters et al., 2002, p.16). It is computed by the following equations given below;

$$\alpha_{toa} = \sum(\omega_\lambda \times \rho_\lambda) \quad (7)$$

$$\omega_{\lambda=} \, ESUN_\lambda / \sum ESUN_\lambda \quad (8)$$

$$\tau_{sw} = 0.75 + 2 \times 10^{-5} \times z \quad (9)$$

$$\alpha = (\alpha_{toa} - \alpha_{path\_radiance})/\tau_{sw}^{2} \quad (10)$$

where; α_{toa} is the albedo at the top of the atmosphere, ρ_λ is the reflectivity , ω_λ is a weighting coefficient for each band, $ESUN_\lambda$ is the mean solar exo-atmospheric irradiance for each band ($W/m^2/\mu m$), $\alpha_{path\_radiance}$ is the average portion of the incoming solar radiation across all bands that is back-scattered to the satellite before it reaches the Earth's surface which is assumed to be 0.03 (Bastiaanssen, 2000), z is the elevation of the weather station in meters and τ_{sw} is the atmospheric transmissivity (Waters et al., 2002).

A.1.4 Incoming shortwave radiation (RS↓)

It is the "direct and diffuse solar radiation flux that actually reaches the earth's surface (W/m^2)" (Waters et al., 2002, p. 19). It is computed with an assumption of clear sky conditions, as a constant for the image time using:

$$R_{s\downarrow} = G_{sc} \times \cos\theta \times d_r \times \tau_{sw} \quad (11)$$

where; G_{sc} is the solar constant (1367 Wm^{-2}), $\cos\theta$ is the cosine of the solar incidence angle as done above, d_r is the inverse squared relative earth-sun distance, and τ_{sw} is the atmospheric

transmissivity. The values for $R_{s\downarrow}$ can vary from 200 – 1000 W/m^2 depending on the time and location of the image (Waters et al., 2002).

A.1.5 Normalized Difference Vegetation Index (NDVI)

The Normalized Difference Vegetation Index (NDVI) is derived from the red and near-infrared reflectance which can be expressed as:

$$NDVI = (\rho_4 - \rho_3) / (\rho_4 + \rho_3) \quad (12)$$

where ρ_4 and ρ_3 are the amounts of near-infrared and red light, respectively, reflected by the vegetation that are captured by the sensor of the satellite (Pettorelli et al., 2005) . The value of NDVI ranges from to +1. The values closer to +1 indicates rich and productive vegetation whereas closer to 0 or below indicates no vegetation, and anything less than 0 is most likely sediment laden water.

A.1.6 Surface emissivity (εo)

Surface emissivity (ε_o) is the "ratio of the thermal energy radiated by the surface to the thermal energy radiated by a blackbody at the same temperature" (Waters et al., 2002, p. 20). It is computed by the following equation:

$$\varepsilon_o = 1.009 + 0.047 \times \ln(NDVI) \quad (13)$$

where NDVI is Normalized Difference Vegetation Index.

A.1.7 Land surface temperature (Ts)

Land surface temperature is the measure of the temperature of the Earth's surface in a particular location from a satellite's point of view (NASA, 2000). T_s differs from the air temperature that is included in the daily weather report. The land surface temperature is calculated from the thermal band (band 6) of the Landsat TM image expressed in the following equations (Chander et al., 2009)

$$T_{bb} = K_2 / \ln (K_1/L_6 + 1) \quad (14)$$

$$T_s = T_{bb} / \varepsilon_o^{0.25} \quad (15)$$

where; L_6 is the spectral radiance of the thermal band (band 6) of the Landsat 5 TM image; T_{bb} is effective at-satellite temperature; and K_1(607.76 $Wm^{-2}sr^{-1}\mu m^{-1}$) and K_2(1260.56 $Wm^{-2}sr^{-1}\mu m^{-1}$) are constants for Landsat 5 TM (Chander et al., 2009).

A.1.8 "Hot" and "Cold" Pixels

The most important step in the METRIC model is the identification of "hot" and "cold" Pixels. The model uses two "anchor" pixels to fix boundary settings for the energy balance in the study area (Waters et al., 2002). The "cold" pixel is a pixel in the image which is chosen as a very well-irrigated crop surface. The pixel must have total amount of ground surface covered by vegetation with an assumption that the surface temperature and near-surface air temperature are similar. A "hot" pixel is a pixel which is a dry, bare agricultural field where ET is assumed to be 0 (Waters et al., 2002). Both "hot" and "cold" pixels should be located in large and homogeneous areas. They are identified manually using LST map, NDVI map, land use/land cover map and Landsat 5 TM images as described in detail by Waters et al. (2002). The temperature and x and y coordinates for both "hot" and "cold" pixels are identified and noted. This information is implemented for the calculation of sensible heat flux (H) described later in this appendix.

A.1.9 Incoming longwave radiation (RL↓)

The incoming long wave radiation can be described as "downward thermal radiation flux from the atmosphere (W/m2)" (Waters et al., 2002, p.23). It is computed using the Stefan-Boltzmann equation as shown in equation (16):

$$R_{L\downarrow} = \varepsilon_a \times \sigma \times T_a^4 \quad (16)$$

where; T_a is the near surface temperature from "cold" pixel temperature; ε_a is the atmospheric emissivity and is calculated from one-way atmospheric transmissivity (τ_{sw}) using the equation 17 derived by Bastiaanssen (1995):

$$\varepsilon_a = 1.08 \times (-\ln \tau_{sw})^{-265} \quad (17)$$

A.1.10 Outgoing longwave radiation (RL↑)

The outgoing long wave radiation is the "thermal radiation flux emitted from the earth's surface to the atmosphere (W/m^2)" (Waters et al., 2002, p. 19). The outgoing longwave radiation ($R_{L\uparrow}$) at each pixel is computed from surface emissivity (ε_o) and surface temperature (T_s) images using the Stefan-Boltzmann equation as shown in equation (18):

$$R_{L\uparrow} = \varepsilon_o \times \sigma \times T_s^4 \quad (18)$$

where; ε_o is surface emissivity (dimensionless), σ is the Stefan-Boltzmann constant (5.67×10^{-8} $Wm^{-2}K^{-4}$); and T_s is the surface temperature in Kelvin.

A.1.11 Soil heat flux (G)

Soil heat flux is the "rate of heat storage into the soil and vegetation due to conduction" (Waters et al., 2002, p.24). The ratio G/R_n is first calculated by METRIC using the empirical equation 19 developed by Bastiaanssen (2000) representing values near midday:

$$G/R_n = T_s/\alpha\,(0.0038\alpha + 0.0074\alpha^2)\,(1 - 0.98NDVI^4) \quad (19)$$

where; T_s is the surface temperature (^oC), α is the surface albedo, and NDVI is the Normalized Difference Vegetation Index.

Soil heat flux is calculated by multiplying the ratio G/R_n with net surface radiation flux.

$$G = (G/R_n) \times R_n \quad (20)$$

where R_n is net surface radiation flux.

A.1.12 Sensible heat flux (H)

Sensible heat flux can be defined as "the rate of heat loss to the air by convection and conduction, due to a temperature difference" (Waters et al., 2002, p.25). It is the function of temperature gradient, surface roughness and wind speed and is calculated by the following equation (21) for the heat transport:

$$H = (\rho \times cp \times dT) / r_{ah} \quad (21)$$

where; ρ is air density (kg/m^3),c_p is air specific heat (1004 J/kg/K), dT (K) is the temperature difference ($T_1 - T_2$) between two heights ($z_1$and z_2), and r_{ah} is the aerodynamic resistance to heat transport (s/m). Since there are two unknown parameters r_{ah} and dT in the equation (21), analyst must utilize the two anchor pixels to predict the reliable value of H, dT and wind speed at the given height.

The aerodynamic resistance to heat transport (r_{ah}) is calculated by the following equations:

$$u^* = k \times u_x / \ln(Z_x/Z_{om}) \quad (22)$$

$$r_{ah} = \ln (Z_2/Z_1)/(u^* \times k) \quad (23)$$

where; u* is friction velocity at each 30 m pixel computed using the logarithmic wind law for neutral atmospheric conditions. The term k is the Von Karman's constant and its value is 0.41. Z_1 which is 0.1 m is the height above zero-plane displacement height of crop canopy and Z_2 which is 2m is the below height of surface boundary layer. The term u_x is the wind speed (m s-1) at the height Z_x (height of the anemometer is10 m for FAWN stations and weather station in Houston County in the study area). The term Z_{om} is the momentum roughness length for each pixel as is defined as the form drag and skin friction for the layer of air that interacts with the surface (Waters et al., 2002).

The term Z_{om} for the vegetation around the weather station is empirically estimated from average vegetation height using the equation of Brutsaert (1982):

$$Z_{om}= 0.12h \quad (24)$$

The height of canopy grass is assumed to be 0.1 m for the FAWN weather stations and weather stations of the Houston County for this study. The value of 0.1 has also been used as height of grasses in USGS station in other studies (Snyder et al., 2008; Druce et al., 1997; Douglas et al., 2009; Mengistu and MJ Savage, 2010).

The term Z_{om} for weather stations which is calculated from equation (24) is used to calculate friction velocity (u*) for each weather station by using average wind velocity at the anemometer height (10m) at the image capture time using equation (22). The assumption is made that computed u* at the weather station and wind speed at 200 m is constant for all pixels.

Using the NDVI and surface albedo, Z_{om} is computed for each pixel from the equation below by Bastiaanssen (Bastiaanssen et. al., 2000) and modified by Allen (Allen et al., 2002a; Allen, 2007; Teixeira et al., 2009)

$$Z_{om}= \exp (a \times NDVI/\alpha+ b) \quad (25)$$

From the plot of ln (Z_{om}) against NDVI/ α, correlation constants "a" and "b" are derived for pixels representing vegetation with assigned Z_{om} for each pixel (Z_{om}= 0.12 h, where h is the known vegetation height). The tall and short vegetation can be distinguished from surface albedo (α) if they have similar NDVI (Bhattarai, 2010). Z_{om} for typical forests is used as 0.5 m (Allen et al., 2002a; Waters et al., 2002).

The blending height is height above the weather station where there is no effect from the surface roughness and the value of 200m is used for this. The wind speed at blending height is calculated and is expressed in the term (u_{200}) which is calculated by:

$$U_{200} = u\,[\ln(200/z_{om})] / k \quad (26)$$

where; u is the friction velocity at the weather station at the time of image captured..

The friction velocity (u*) for each pixel is calculated from Z_{om} from the equation (27). The term u_{200} is assumed constant for all pixels.

$$u^* = k \times u_{200} / \ln(200 / Z_{om}) \quad (27)$$

Using the linear equation between dT and DEM corrected surface (T_{s_dem}), the near surface temperature difference (dT) for each pixel is derived

$$dT = b + a \times T_{s\_dem} \quad (28)$$

The "hot" and "cold" pixels that were chosen earlier are used to derive correlation "a" and "b" coefficients. The soil heat flux (G), net surface radiation (R_n), surface temperature (T_s), and momentum roughness length (z_{om}) for both anchor pixels are noted and inputted from the derived images.

ET at the "hot" pixel is assumed to be zero; sensible heat flux at the "hot" pixel (H_{hot}) is calculated as

$$H_{hot} = R_n - G. \quad (29)$$

ET at the "cold" pixel is assumed to be 5% more than the reference ET (ET_{ref}) (Allan et. al, 2002a; Gowda et al., 2007; Gowda et al., 2008a; Trezza, 2006b; Conard et al., 2007) in METRIC model. Therefore, H for the "cold" pixel (H_{cold}) is calculated as:

$$H_{cold} = R_n - G - 1.05 \times \lambda ET_{ref}. \quad (30)$$

Air densities (ρ_{air}) for "hot" and "cold" pixels are calculated using DEM corrected land surface temperature image (T_{s_dem}) as:

$$\rho_{air} = P/(R \times T_{s\_dem}) \quad (31)$$

where; R is the Gas constant = 287.05 $J/kg^{-1}K^{-1}$, T is temperature in K, P is standard pressure and $P = 101325 \times (1.0 - Z \times 0.0000225577) \times 5.2559$; Z = elevation above sea level (m).

Aerodynamic resistance to heat transport (r_{ah}) for both anchor pixels (r_{ah_hot} and r_{ah_cold}) is obtained from equation (23) and are used to derive dT for the "hot" and "cold" pixels (dT_{hot} and dT_{cold}) as:

$$dT_{hot} = H_{hot} \times r_{ah\_hot} / (\rho_{hot} \times c_p) \quad (32)$$

$$dT_{cold} = H_{hot} \times r_{ah\_cold} / (\rho_{cold} \times c_p) \quad (33)$$

The correlation coefficients "a" and "b", in the Equation (28) were computed by plotting dT_{hot} versus T_{S_hot} and dT_{cold} versus T_{s_cold}.

Air temperature (T_a) for each pixel is calculated from

$$T_a = T_s - dT \quad (34)$$

with air density for each pixel derived from the T_a image. H for each pixel is computed using the derived dT, air density, and r_{ah} images.

Monin-Obukhov theory is applied iteratively to correct for buoyancy effects generated by surface heating processes. The Monin-Obukhov length (L) is computed to define atmospheric stability conditions using the equation below:

$$L = -(\rho \times c_p \times u^{*3} \times T_s) / (k \times g \times H) \quad (35)$$

where; ρ is the density of air (kgm^{-2}), c_p is the air specific heat (1004 $Jkg^{-1}k^{-1}$), u* is the friction velocity (ms^{-1}), T_s is the temperature (K), g is the gravitational constant (9.81 ms^{-2}), k is the Von Karman's constant (0.41), and H is the sensible heat flux (Wm^{-2}) (Waters et al., 2002).The Monin-Obukhov theory states that the atmosphere is considered neutral if L= 0. If L< 0, the atmosphere is considered unstable (heat flow is away from the surface); and if L>0, the atmosphere is considered stable for buoyancy effects. Stability corrections for momentum and

heat transport (Ψ_m and Ψ_h) are computed using the formulas designed by Paulson (1970) and Webb (1970).

Stability corrected value of the friction velocity (u*) and aerodynamic resistance (rah) are calculated for each successive repetition using equations below:

$$u^* = [(u_{200} \times k)/\{\ln(200/z_{om}) - \Psi_{m(200m)}\}] \quad (36)$$

$$r_{ah} = \{\ln (Z_2/Z_1) - \Psi_{h(2m)} + \Psi_{h(0.1m)}\}/(u^* \times k) \quad (37)$$

where; $\Psi_{m(200m)}$is the stability correction for momentum transport at 200 m (for L<0 or L>0 conditions, $\Psi_{h(2m)}$and $\Psi_{h(0.1m)}$are the stability corrections for heat transport at 2 m and 1 m, Z_1= 0.1m and Z_2 = 2m, and k is the Von Karman's constant (Waters et al., 2002).

The stability corrected r_{ah} is used to compute new dT values for "hot" and "cold" pixels, and new values for correlation coefficients, "a" and "b". These values were then used to compute a new corrected H at each pixel level. A new stability correction is done using the corrected H image. Until successive values for dT_{hot} and r_{ah} at "hot" pixel (r_{ah_hot}) are stabilized, these processes are repeated. When the change in r_{ah} at the "hot" pixel is less than 5%, the process is stopped and the corrected value of H is determined (Allen et al., 2002a). The corrected value of H at each pixel is derived by using the corrected final dT and stability corrected r_{ah} image in equation 21.

A.1.13 Latent heat flux (λET)

Latent heat flux (λET) can be defined as "the rate of latent heat loss from the surface due to evapotranspiration" (Waters et al., 2002, p.34). Latent heat flux for the instantaneous time of the satellite overpass is computed at each pixel using equation (38) below:

$$\lambda ET = Rn - G - H \quad (38)$$

where; λET is an instantaneous value for the time of the satellite overpass (W/m2) (Waters et al., 2002).

A.1.14 Instantaneous ET

The instantaneous ET (ET_{inst}) is defined as the ET at the time of the satellite overpass time and is computed as:

$$ET_{inst} = 3600 \times \lambda ET / \lambda \quad (39)$$

where; ET_{inst} is the instantaneous ET (mm/hr) ,λ is the latent heat of vaporization or the heat absorbed when a kilogram of water evaporates (J/kg) . It is calculated from the surface temperature image by

$$\lambda = [[2.501 - (0.002361 \times T_o)] \times 10^6] \quad (40)$$

where; T_o is surface temperature in degree Celsius (Waters et al., 2002).

A.1.15 Reference ET Fraction (ETrF)

Reference ET Fraction (ET_rF) or Evaporative fraction is defined as "the ratio of the computed instantaneous ET (ET_{inst}) for each pixel to the reference ET (ET_r) computed from weather data" (Waters et al., 2002, p.35). ET_rF at each pixel level is computed using reference ET at the image time as:

$$ET_rF = ET_{inst} / ET_{ref} \quad (41)$$

where; ET_{ref} is the ASCE Penman-Monteith standardized form of reference ET (mm hr^{-1}) at the image time derived from REF-ET software (Allen et al., 2000b; Waters et al., 2002).

A.1.16 Daily ET

A Daily ET (ET_{24}) map is derived using the evaporative fraction (ET_rF) and cumulative 24-hour ET for the day of the image. It is more important and useful than the instantaneous ET.

It is calculated assuming that the ET_rF computed in equation (41) is constant for 24 hour average. It can be expressed as:

$$ET_{24} = ET_rF \times ET_{ref\_24} \quad (42)$$

ET for a period (monthly or two-month) is calculated by computing cumulative reference ET for the period represented by the image processed as:

$$ET_{period} = ET_rF \times \sum_{i=1}^{n} ET_{ref\_24i} \quad (43)$$

where; ET_{ref_24i} is the cumulative reference ET for the time period from REF-ET software, and n is the number of days used for ET extrapolation (Waters et al., 2002).

A.1.17 Seasonal ET

While computing the seasonal ET, an assumption is made that ET_rF computed for the time of image is constant for the entire period represented by the image, and ET for the entire area of interest changes in proportion to the change in ET_{ref} at the weather station. The ET calculated for the Houston County was during the crop growing season from April to September. An image is used to extrapolate either one month or two months ET depending on availability of image.

Chapter 6: Reference

Addink, Elisabeth A., Frieke MB Van Coillie, and Steven M. De Jong. "Introduction to the GEOBIA 2010 special issue: From pixels to geographic objects in remote sensing image analysis." *International Journal of Applied Earth Observation and Geoinformation* 15 (2012): 1-6.

Alabama Cooperative Extension Service (ACES), Water harvesting for irrigation: developing an adequate water supply.ANR-827, Alabama Cooperative Extension Service, Auburn, AL. 1994, http://www.aces.edu/pubs/docs/A/ANR-0827/ANR-0827.html. (Accessed February 27, 2015)

Alcamo, Joseph, Petra Döll, Frank Kaspar, and Stefan Siebert. "Global change and global scenarios of water use and availability: an application of WaterGAP 1.0." *Center for Environmental Systems Research (CESR), University of Kassel, Germany* (1997): 17-20.

Alcamo, J., T. Henrichs, and T. Rosch. "World water in 2025: Global modeling and scenario analysis." *World water scenarios analyses* (2000).

Allen, R.G., "REF-ET: Reference Evapotranspiration Calculation Software for FAO and ASCE standardized Equations, University of Idaho", (2000a) www.kimberly.uidaho.edu/ref-et/ (last accessed on Feb 20, 2015).

Allen, Richard G., Luis S. Pereira, Dirk Raes, and Martin Smith. "Crop evapotranspiration-Guidelines for computing crop water requirements-FAO Irrigation and drainage paper 56." *FAO, Rome* 300, no.9 (1998).

Allen, Richard G., M. Tasumi, Anthony Morse, and Ricardo Trezza. "A Landsat-based energy balance and evapotranspiration model in Western US water rights regulation and planning." *Irrigation and Drainage Systems* 19, no. 3-4 (2005): 251-268.

Allen, Richard G. Masahiro Tasumi and Ricardo Trezza, "Satellite-Based Energy Balance for Mapping EvapoTranspiration with Internalized Calibration METRIC -Model" *J. Irrig. Drain Eng.*133, (2007): 380-394

Allen, R.G., R. Waters, and , W.G.M. Bastiaanseen, "SEBAL Expert Training", The University of Idaho and the Idaho Department of Water Resources, Idaho State University, August 19-23, 2002.

Allen, R. G., W. O. Pruitt, J. A. Businger, L. J. Fritschen, M. E. Jensen, and F. H. Quinn. "Chapter 4 “Evaporation and Transpiration” in ASCE Handbook of Hydrology." *New York, NY*, 1996: 125- 252.

Anderson, Martha C., Richard G. Allen, Anthony Morse, and William P. Kustas. "Use of Landsat thermal imagery in monitoring evapotranspiration and managing water resources." *Remote Sensing of Environment* 122 (2012): 50-65.

Anderson, Martha C., William P. Kustas, Joseph G. Alfieri, Feng Gao, Christopher Hain, John H. Prueger, Steven Evett, Paul Colaizzi, Terry Howell, and José L. Chávez. "Mapping daily evapotranspiration at Landsat spatial scales during the BEAREX’08 field campaign." *Advances in Water Resources* 50 (2012): 162-177.

Antonarakis, A. S., Keith S. Richards, and James Brasington. "Object-based land cover classification using airborne LiDAR." *Remote Sensing of Environment* 112, no. 6 (2008): 2988-2998.

ASCE–EWRI, “The ASCE Standardized Reference Evapotranspiration Equation.” ASCE–EWRI Standardization of Reference Evapotranspiration Task Committee Rep., ASCE Reston, VA, 2005

AWIS, “Alabama Mesonet Weather Data” 2015, http://www.awis.com/mesonet/index.html (accessed April 15, 2015)

Baatz, Martin, and Arno Schäpe. "Multiresolution segmentation: an optimization approach for high quality multi-scale image segmentation." *Angewandte Geographische Informationsverarbeitung XII* (2000): 12-23.

Baker, Corey, Rick Lawrence, Clifford Montagne, and Duncan Patten. "Mapping wetlands and riparian areas using Landsat ETM+ imagery and decision-tree-based models. “Wetlands 26, no. 2 (2006): 465-474.

Bastiaanssen, Wilhelmus Gerardus Maria. *Regionalization of surface flux desities and moisture indicators in composite terrain: a remote sensing approach under clear skies in Mediterranean climates*. Landbouwuniversiteit te Wageningen, 1995.

Bastiaanssen, W. G. M. "SEBAL-based sensible and latent heat fluxes in the irrigated Gediz Basin, Turkey." *Journal of hydrology* 229, no. 1 (2000): 87-100.

Bastiaanssen, W. G. M., E. J. M. Noordman, H. Pelgrum, G. Davids, B. P. Thoreson, and R. G. Allen. "SEBAL model with remotely sensed data to improve water-resources management under actual field conditions.” *Journal of irrigation and drainage engineering* 131, no. 1 (2005): 85-93.

Bastiaanssen, W. G. M., and M. G. Bos. "Irrigation performance indicators based on remotely sensed data: a review of literature." *Irrigation and drainage systems* 13, no. 4 (1999): 291-311.

Bastiaanssen, Wim GM, David J. Molden, and Ian W. Makin. "Remote sensing for irrigated agriculture: examples from research and possible applications."*Agricultural water management* 46, no. 2 (2000): 137-155.

Bastiaanssen, W. G. M., M. Menenti, R. A. Feddes, and A. A. M. Holtslag. "A remote sensing surface energy balance algorithm for land (SEBAL). 1. Formulation." *Journal of hydrology* 212 (1998a): 198-212.

Bastiaanssen, W. G. M., H. Pelgrum, J. Wang, Y. Ma, J. F. Moreno, G. J. Roerink, and T. Van der Wal. "A remote sensing surface energy balance algorithm for land (SEBAL): Part 2: Validation." *Journal of hydrology* 212 (1998b): 213-229.

Benz, Ursula C., Peter Hofmann, Gregor Willhauck, Iris Lingenfelder, and Markus Heynen. "Multi-resolution, object-oriented fuzzy analysis of remote sensing data for GIS-ready information." *ISPRS Journal of photogrammetry and remote sensing* 58, no. 3 (2004): 239-258.

Berger, Christian, Michael Voltersen, Robert Eckardt, Jonas Eberle, Thomas Heyer, Nesrin Salepci, Sören Hese et al. "Multi-modal and multi-temporal data fusion: Outcome of the 2012 GRSS data fusion contest." *Selected Topics in Applied Earth Observations and Remote Sensing, IEEE Journal of* 6, no. 3 (2013): 1324-1340.

Bhattarai, N. "Use of Remotely Sensed Data to Quantify Plant Water Use from Irrigated Lands in Wolf Bay Watershed Area" MS diss. Auburn University, Alabama, 2010

Blaschke, Thomas, Stefan Lang, Eric Lorup, Josef Strobl, and Peter Zeil. "Object-oriented image processing in an integrated GIS/remote sensing environment and perspectives for environmental applications." *Environmental information for planning, politics and the public* 2 (2000): 555-570.

Blaschke, Thomas, Stefan Lang and Geoffrey Hay, "Object-Based image analysis for remote sensing applications: modeling reality dealing with complexity." In *Object-Based Image Analysis: Spatial Concepts for Knowledge-Driven Remote Sensing Applications*, 1 -27, Berlin Heidelberg: Springer, 2008

Blaschke, Thomas. "Object based image analysis for remote sensing." *ISPRS journal of photogrammetry and remote sensing* 65, no. 1 (2010): 2-16.

Bliesner, Ron D. and Dan Spare, "Center Pivot Irrigation", *Four Corners Irrigation Workshop* pp 25-32, 2001, http://aces.nmsu.edu/aes/farmington/progress_reports/irri_wkshp_2001.pdf#page=34 (accessed on February 16, 2014)

Brown, Lester R. and others, "State of the World 2001", 2001, http://www.worldwatch.org/system/files/ESW01A.pdf (accessed February 19, 2014)

Brutsaert, Wilfried. *Evaporation into the atmosphere: theory, history, and applications*. Dordrecht: Reidel, 1982.

Chan, Jonathan Cheung-Wai, Rik Bellens, Frank Canters, and Sidharta Gautama. "An assessment of geometric activity features for per-pixel classification of urban man-made objects using very high resolution satellite imagery." *Photogrammetric Engineering & Remote Sensing* 75, no. 4 (2009): 397-411.

Chander, Gyanesh, and Brian Markham. "Revised Landsat-5 TM radiometric calibration procedures and postcalibration dynamic ranges." *Geoscience and Remote Sensing, IEEE Transactions on* 41, no.11 (2003): 2674-2677.

Chander, Gyanesh, Brian L. Markham, and Dennis L. Helder. "Summary of current radiometric calibration coefficients for Landsat MSS, TM, ETM+, and EO-1 ALI sensors." *Remote sensing of environment* 113, no. 5 (2009): 893-903.

Chen, Zi-Tan, and J. Armando Guevara. "Systematic selection of very important points (VIP) from digital terrain model for constructing triangular irregular networks." *Auto-carto*, vol. 8,(1987): 50-56.

City of Durham Public Works Department, "Stormwater utility fee," 2015, http://www.durhamnc.gov/departments/works/stormwater_fees.cfm, (accessed on February 16, 2015)

Cleve, Casey, Maggi Kelly, Faith R. Kearns, and Max Moritz. "Classification of the wildland–urban interface: A comparison of pixel-and object-based classifications using high-resolution aerial photography." *Computers, Environment and Urban Systems* 32, no. 4 (2008): 317-326.

Cohen, Stuart, Amelia Svrjcek, Tom Durborow, and N. LaJan Barnes. "Water quality impacts by golf courses." *Journal of environmental quality* 28, no. 3 (1999): 798-809.

NOAA, "NOAA National Weather Service Cooperative Observer Program (COOP)", 2015 http://www.nws.noaa.gov/om/coop/ (accessed on April 16, 2015)

Conrad, Christopher, Stefan W. Dech, Mohsin Hafeez, John Lamers, Christopher Martius, and Günter Strunz. "Mapping and assessing water use in a Central Asian irrigation system by utilizing MODIS remote sensing products." *Irrigation and Drainage Systems* 21, no. 3-4 (2007): 197-218.

Cowardin, Lewis M., Virginia Carter, Francis C. Golet, and Edward T. LaRoe. *Classification of wetlands and deepwater habitats of the United States*. Washington, DC, USA: Fish and Wildlife Service, US Department of the Interior, 1979.

Courault, Dominique, Bernard Seguin, and Albert Olioso. "Review on estimation of evapotranspiration from remote sensing data: From empirical to numerical modeling approaches." *Irrigation and Drainage systems* 19, no. 3-4 (2005): 223-249.

de Winter, Joost CF. "Using the Student's t-test with extremely small sample sizes." *Practical Assessment, Research & Evaluation* 18, no. 10 (2013): 2.

Definiens, A. G. "Definiens Developer 7 User Guide." *München: Definiens AG* (2008). (Part of eCognition software)

Diaz, J. A., J. W. Knox, and E. K. Weatherhead. "Competing demands for irrigation water: golf and agriculture in Spain." *Irrigation and Drainage* 56, no. 5 (2007): 541-549.

Doorenbos, J. and W. O Pruitt, "Crop Water Requirements" *Irrigation and Drainage* Paper No. 24, FAO, Rome, (1977).

Douglas, Ellen M., Jennifer M. Jacobs, David M. Sumner, and Ram L. Ray. "A comparison of models for estimating potential evapotranspiration for Florida land cover types." *Journal of Hydrology* 373, no. 3 (2009): 366-376.

Dougherty, Mark, David Bayne, Larry Curtis, Eric Reutebuch, and Wendy Seesock. "Water quality in a non-traditional off-stream polyethylene-lined reservoir." *Journal of environmental management* 85, no. 4 (2007): 1015-1023.

Duce, P., D. Spano, R. L. Snyder, and K. T. Paw U. "Surface renewal estimates of evapotranspiration. Short canopies." In *II International Symposium on Irrigation of Horticultural Crops 449*, pp. 57-62. 1996.

Elsevier, B.V. "Introduction to the GEOBIA 2010 special issue: From pixels to geographic objects in remote sensing image analysis" *International Journal of Applied Earth Observation and Geo-information* 15, (2012): 1–6

Falkenmark, Malin, Jan Lundqvist, and Carl Widstrand. "Macro-scale water scarcity requires micro-scale approaches." In *Natural resources forum*, vol. 13, no. 4, pp. 258-267. Blackwell Publishing Ltd, 1989.

Frohn, Robert C., Molly Reif, Charles Lane, and Brad Autrey. "Satellite remote sensing of isolated wetlands using object-oriented classification of Landsat-7 data." *Wetlands* 29, no. 3 (2009): 931-941.

Gonzalez, R. C. "Wintz P (1987) Digital Image Processing." *Reading, MA, Addison-Waley* (1987).

Gowda, P. H., J. L. Chavez, P. D. Colaizzi, S. R. Evett, Terry Howell, and J. A. Tolk. "Remote sensing based energy balance algorithms for mapping ET: Current status and future challenges." *Transactions of the ASABE* 50, no. 5 (2007): 1639-1644.

Gowda, Prasanna H., José L. Chávez, Terry A. Howell, Thomas H. Marek, and Leon L. New. "Surface energy balance based evapotranspiration mapping in the Texas high plains." *Sensors* 8, no. 8 (2008): 5186-5201.

Gregg, Watson W., and Nancy W. Casey. "Global and regional evaluation of the SeaWiFS chlorophyll data set." *Remote Sensing of Environment* 93, no. 4 (2004): 463-479.

Ground Water Foundation, The Basics Center Pivots, 2014,. http://www.groundwater.org/get-informed/basics/pivots.html (accessed on February 16, 2014)

Hain, Christopher R., John R. Mecikalski, and Martha C. Anderson. "Retrieval of an available water-based soil moisture proxy from thermal infrared remote sensing. Part I: Methodology and validation." *Journal of Hydrometeorology* 10, no. 3 (2009): 665-683.

Hain, Christopher R., Wade T. Crow, John R. Mecikalski, Martha C. Anderson, and Thomas Holmes. "An intercomparison of available soil moisture estimates from thermal infrared and passive microwave remote sensing and land surface modeling." *Journal of Geophysical Research: Atmospheres (1984–2012)* 116, no. D15 (2011).

Haralick, R.M. and L.G. Shapiro. "Image segmentation techniques." *Computer Vision, Graphics and Image Processing* 29, (1985): 100–132

Hay, G. J., and G. Castilla. "Object-based image analysis: strengths, weaknesses, opportunities and threats (SWOT)." *International Archives of Photogrammetry, Remote Sensing and Spatial Information Sciences* 36, no. 4 (2006).

Hippenstiel, Ryan, and J. R. Brownson. "Computing solar energy potential of urban areas using airborne LiDAR and orthoimagery." In *Proceedings of the National Solar Conference and World Renewable Energy Forum*, vol. 3, pp. 2004-2008. 2012.

Hofmann, Alexandra D., Hans-Gerd Maas, and André Streilein. "Knowledge-based building detection based on laser scanner data and topographic map information." *International Archives of Photogrammetry Remote Sensing and Spatial Information Sciences* 34, no. 3/A (2002): 169- 174.

Hutson, Susan S. *Estimated use of water in the United States in 2000*. Vol. 1268. Geological Survey (USGS), 2004, https://play.google.com/books/reader?id=c8PiAAAAMAAJ&printsec=frontcover&output=reader&hl=en&pg=GBS.PP1 (Accessed February 20, 2015)

Im, Jungho, John R. Jensen, and Michael E. Hodgson. "Object-based land cover classification using high-posting-density LiDAR data." *GIScience & Remote Sensing* 45, no. 2 (2008): 209-228.

Irish, Jennifer L., and W. Jeff Lillycrop. "Scanning laser mapping of the coastal zone: the SHOALS system." *ISPRS Journal of Photogrammetry and Remote Sensing* 54, no. 2 (1999): 123-129.

Jawak, S. D., S. N. Panditraob, and A. J. Luisa. "Airborne LIDAR and high resolution satellite data for rapid 3D feature extraction." *ISPRS-International Archives of the Photogrammetry, Remote Sensing and Spatial Information Sciences* 1 (2014): 573-580.

Jensen, John R. *Remote Sensing of the Environment: An Earth Resource Perspective. Second Edition*. Prentice Hall, 2006

Jensen, M.E., "*Plant and irrigation water requirements*". USDA-ARS-SWC, Snake River Conservation Research Center, Kimberly, Idaho. (1969)

Jensen, M. E., R. D. Burman and R. G. Allen, "*Evapotranspiration and Irrigation Water Requirements, ASCE Manuals and Reports on Engineering Practice*," No. 70, ASCE, New York, 1990.

Jones, Tyler W. "Identification and Classification of Geographically Isolated Wetlands in North Alabama using Geographic Object Based Image Analysis (GeOBIA)."MS diss. Auburn University, Alabama, 2013

Karaska, Mark A., Robert L. Huguenin, Jeff L. Beacham, Mo-Hwa Wang, John R. Jensen, and Ronald S.Kaufmann. "AVIRIS measurements of chlorophyll, suspended minerals, dissolved organic carbon, and turbidity in the Neuse River, North Carolina." *Photogrammetric Engineering &Remote Sensing* 70, no. 1 (2004): 125-133.

Kenna, Michael P. "What happens to pesticides applied to golf courses." *USGA Green Section Record* 33, no. 1 (1995): 1-9.

Kenny, J. F., Barber, Nancy L., Susan S. Hutson, Kristin S. Linsey, John K. Lovelace, and Molly A. Maupin. *Estimated use of water in the United States in 2005*. Reston, VA: US Geological Survey, 2009. http://pubs.usgs.gov/circ/1344/pdf/c1344.pdf (Accessed January 20, 2015)

Kokje, Amit A., and Jay Gao. "A Simplified Approach for Classifying Urban Land Cover using Data Fusion." In *Proceedings of the SIRC NZ Conference*. 2013.

Kovač, Boštjan, and Borut Žalik. "Visualization of LIDAR datasets using point-based rendering technique." *Computers & Geosciences* 36, no. 11 (2010): 1443-1450.

Kramber, William J., Anthony Morse, Richard G. Allen, and Ricardo Trezza. "Landsat thermal data for water resources management in Idaho." In *ASPRS 2008 Annual Conference Portland, Oregon*. 2008.

Lee, Mark. "Benthic mapping of coastal waters using data fusion of hyperspectral imagery and airborne laser bathymetry" PhD. diss. University of Florida, Gainesville, Florida, 2003

Lee, D. Scott, and Jie Shan. "Combining lidar elevation data and IKONOS multispectral imagery for coastal classification mapping." *Marine Geodesy* 26, no. 1-2 (2003): 117-127.

Leibowitz, Scott G. "Isolated wetlands and their functions: an ecological perspective." *Wetlands* 23, no. 3 (2003): 517-531.

Lewinski, S. "Applying fused multispectral and panchromatic data of Landsat ETM+ to object oriented classification." (2007).

Li, Junhua, and Wenjun Chen. "A rule-based method for mapping Canada's wetlands using optical, radar and DEM data." *International Journal of Remote Sensing* 26, no. 22 (2005): 5051-5069.

Lillesand, Thomas and Ralph W. Kiefer. Remote *sensing and image interpretation. 4th Edition*. Toronto: John Wiley & Sons, Inc, 2000

Lockaby, Graeme B., "Auburn Speaks on Water", 2014, http://www.auburnspeaks.org/on-water/nai (Accessed March 26, 2014)

Lyon, J. G. *Practical Handbook for Wetland Identification and Delineation*. CRC Press, Boca Raton, FL, USA. 1993.

Maas, Hans-Gerd, and George Vosselman. "Two algorithms for extracting building models from raw laser altimetry data." *ISPRS Journal of photogrammetry and remote sensing* 54, no. 2 (1999): 153-163.

Marcus, Richard R., and Stephen Kiebzak. "The Role of Water Doctrines in Enhancing Opportunities for Sustainable Agriculture in Alabama1." (2008): 1578-1590.

Maryland Department of Natural Resources, “Baltimore City commits to urban tree canopy goal,” URL:http://www.dnr.state.md.us/dnrnews/pressrelease2005/100605.html, (Accessed January 26, 2015)

Matthews, Geoffrey Vernon Townsend. "The Ramsar Convention on Wetlands: its history and development." Gland: Ramsar convention bureau, 1993.

Maxa, Melissa, and Paul Bolstad. "Mapping northern wetlands with high resolution satellite images and LiDAR." *Wetlands* 29, no. 1 (2009): 248-260.

Mayer, Helmut. "Automatic object extraction from aerial imagery - a survey focusing on buildings." *Computer vision and image understanding* 74, no. 2 (1999): 138-149.

McCauley, Lisa A., and David G. Jenkins. "GIS-based estimates of former and current depressional wetlands in an agricultural landscape." *Ecological Applications* 15, no. 4 (2005): 1199-1208.

MacFaden, S. W. , J. P. M. O’Neil-Dunne, A. R. Royar, J. W. T. Lu, and A. G. Rundle, “High-Resolution Tree Canopy Mapping for New York City using LIDAR and Object-based Image Analysis,” *Journal of Applied Remote Sensing* 6.,no. 1(2012) : 1–23.

McNider, R., J. Christy, J. Cruise, R. Marcus, A. Limaye, J. Hairston, and U. Hatch, Agricultural Water Issues. Presentation prepared for Annual Meeting of the Alabama Water Resource Association, Orange Beach, September 3-5, 2005.

Menenti, Massimo. "Irrigation and drainage." In *Remote Sensing in Hydrology and Water Management*, pp. 377-400. Springer Berlin Heidelberg, 2000.

Mengistu, M. G., and M. J. Savage. "Surface renewal method for estimating sensible heat flux." *Water SA* 36, no. 1 (2010): 9-18.

Mumtaz, S. A., and K. Mooney. "Extraction of spatial information in the environment of Irish roads using airborne laser scanning." *The International Archives of the Photogrammetry, Remote Sensing and Spatial Information Sciences.* Vol.37. Part B3b. Beijing 2008

Myint, Soe W., Patricia Gober, Anthony Brazel, Susanne Grossman-Clarke, and Qihao Weng. "Per-pixel vs. object-based classification of urban land cover extraction using high spatial resolution imagery." *Remote sensing of environment* 115, no. 5 (2011): 1145-1161.

National Aeronautics and Space Administration (NASA), 2000, http://earthobservatory.nasa.gov/GlobalMaps/view.php?d1=MOD11C1_M_LSTDA (last accessed on February 23, 2015).

National Golf Foundation (NGF), “NGF post 2012 golf facilities data”, Golf Course Industry,2014, http://www.golfcourseindustry.com/gci-030513-NGF-2012-Data.aspx (accessed on February 19, 2014)

Navulur, Kumar. *Multispectral Image Analysis Using the Object-oriented Paradigm*. CRC Press, Boca Raton, 2007

Neely, Robert K., James L. Baker, and A. Valk. "Nitrogen and phosphorus dynamics and the fate of agricultural runoff." *Northern prairie wetlands.* (1989): 92-131.

Olson, C.E., “Elements of photographic interpretation common to several sensors”, *Photogrammetric Engineering*, vol. 26, no. 4, (1960):651- 656

O’Neil-Dunne, J. P. M. , S. W. MacFaden, A. R. Royar, and K. C. Pelletier, “An object-based system for LiDAR data fusion and feature extraction,”*Geocarto Int.*, (2012) :1–16

O'Neil-Dunne, J., K. Pelletier, S. MacFaden, A. Troy, and J. M. Grove. "Object-based high-resolution land-cover mapping." In *Geoinformatics, 2009 17th International Conference on*, pp. 1-6. IEEE, 2009.

Ozesmi, Stacy L., and Marvin E. Bauer. "Satellite remote sensing of wetlands" *Wetlands ecology and management* 10, no. 5 (2002): 381-402.

Paine, Jeffrey G., William A. White, Rebecca C. Smyth, John R. Andrews, and James C. Gibeaut."Mapping coastal environments with lidar and EM on Mustang Island, Texas, US." *The Leading Edge* 23, no. 9 (2004): 894-898.

Paulson, Ca A. "The mathematical representation of wind speed and temperature profiles in the unstable atmospheric surface layer." *Journal of Applied Meteorology* 9, no. 6 (1970): 857-861.

Pettorelli, Nathalie, Jon Olav Vik, Atle Mysterud, Jean-Michel Gaillard, Compton J. Tucker, and Nils Chr Stenseth. "Using the satellite-derived NDVI to assess ecological responses to environmental change." *Trends in ecology & evolution* 20, no. 9 (2005): 503-510.

Phocaides, A. “The center pivot irrigation systems” in *Handbook on Pressurized Irrigation Techniques Second Edition*, 2007, ftp://ftp.fao.org/docrep/fao/010/a1336e/a1336e.pdf (accessed on February 16, 2014)

Pidwirny, Michael and Scott Jones, “Actual and Potential ET” 2009 http://www.physicalgeography.net/fundamentals/8j.html (accessed on April 7, 2014)

Porwal, Mahesh Kumar, and Nakul Udeechya. "LIDAR Technology and Applications. “International *Journal of Research in Computer Engineering & Electronics* 2, no. 3 (2013).

QCoherent, “Getting Started with LP360” 2012, http://qcoherent.com/products/docs/lp360_gettingstarted.pdf nai (Accessed December 5, 2014)

QCoherent , “Training Exercise” QCoherent Student Exercises Handout Sheets, Annual LP360 Training Event, Huntsville, AL, 23rd– 25th September 2014

Raskin, P., and others, “Water Futures: Assessment of Long-range Patterns and Prospects.” Stockholm Environment Institute, Stockholm, Sweden (1997)

Rijsberman, Frank R. "Water scarcity: Fact or fiction?" *Agricultural water management* 80, no. 1 (2006): 5-22.

Rottensteiner, F., Summer, G., Trinder, J., Clode, S. and K. Kubik “Evaluation of a Method for fusing LIDAR data and mulitspectral images for building detection”, *IAPRS* 36 (Part 3/W24), pp.15-20. (2005)

Rutzinger, M. A. R. T. I. N., Bernhard Höfle, Thomas Geist, and Johann Stötter. "Object-based building detection based on airborne laser scanning data within GRASS GIS environment." In *Proceedings of UDMS*, vol. 2006, p. 25th. 2006.

Schultz, Gert A. "Remote sensing in hydrology." *Journal of Hydrology* 100, no. 1 (1988): 239-265.

Schmugge, Thomas J., William P. Kustas, Jerry C. Ritchie, Thomas J. Jackson, and Al Rango. "Remote sensing in hydrology." *Advances in water resources* 25, no. 8 (2002): 1367-1385.

Seckler, David, David Molden, and R. Sakthivadivel. "The concept of efficiency in water resources management and policy." *Water productivity in agriculture: Limits and opportunities for improvement* (2003): 37-51.

Shaker, Ahmed, and N. El-Ashmawy. "Land cover information extraction using lidar data." *International Archives of the Photogrammetry, Remote Sensing and Spatial Information Sciences (ISPRS)(ISPRS, 2012)* 39 (2012): 167-172.

Shiklomanov, I. A. "The world’s water resources." In *Proceedings of the international symposium to commemorate*, vol. 25, pp. 93-126. 1991.

Srivastava, Puneet, Anand K. Gupta, and Latif Kalin. "An ecologically-sustainable surface water withdrawal framework for cropland irrigation: A case study in Alabama." *Environmental management* 46, no. 2 (2010): 302-313.

Snodgrass, Joel W., A. Lawrence Bryan, Jr, Robert F. Lide, and Gordon M. Smith. "Factors affecting the occurrence and structure of fish assemblages in isolated wetlands of the

upper coastal plain, USA." *Canadian Journal of Fisheries and Aquatic Sciences* 53, no. 2 (1996): 443-454.

Snyder, R. L., D. Spano, and K. T. Pawu. "Surface renewal analysis for sensible and latent heat flux density." *Boundary-Layer Meteorology* 77, no. 3-4 (1996): 249-266.

Sutter, Robert D., and Robert Kral. "The ecology, status, and conservation of two non-alluvial wetland communities in the south Atlantic and eastern Gulf coastal plain, USA." *Biological Conservation* 68, no. 3 (1994): 235-243.

Tang, Qiuhong, Shannon Peterson, Richard H. Cuenca, Yutaka Hagimoto, and Dennis P. Lettenmaier. "Satellite-based near-real-time estimation of irrigated crop water consumption." *Journal of Geophysical Research: Atmospheres (1984–2012)* 114, no. D5 (2009a).

Tang, Q., E. A. Rosenberg, and D. P. Lettenmaier. "Use of satellite data to assess the impacts of irrigation withdrawals on Upper Klamath Lake, Oregon."*Hydrology and Earth System Sciences* 13, no. 5 (2009b): 617-627.

Tasumi, Masahiro, Ricardo Trezza, Richard G. Allen, and James L. Wright. "Operational aspects of satellite-based energy balance models for irrigated crops in the semi-arid US." *Irrigation and Drainage Systems* 19, no. 3-4 (2005): 355-376.

Teixeira, AH de C., W. G. M. Bastiaanssen, and L. H. Bassoi. "Crop water parameters of irrigated wine and table grapes to support water productivity analysis in the Sao Francisco river basin, Brazil." *Agricultural water management* 94, no. 1 (2007): 31-42.

Tiner, Ralph W. "Estimated extent of geographically isolated wetlands in selected areas of the United States." *Wetlands* 23, no. 3 (2003): 636-652.

Tiner, R. W. *Wetland Indicators: A Guide to Wetland Identification, Delineation, Classification, and Mapping*. Lewis Publishers, CRC Press, Boca Raton, FL, USA 1999.

T.L. Irrigation, "History of the Pivot" 2015, http://tlirr.com/news-story/history-pivot/ (Accessed February 26, 2015)

Töyrä, Jessika, and Alain Pietroniro. "Towards operational monitoring of a northern wetland using geomatics-based techniques." *Remote Sensing of Environment* 97, no. 2 (2005): 174-191.

Tóvári, D., and T. Vögtle. "Classification methods for 3D objects in laserscanning data." *International Archives of Photogrammetry and Remote Sensing* 35, no. B3 (2004): 1682-1750.

Trezza, Ricardo. "Evapotranspiration from a remote sensing model for water management in an irrigation system in Venezuela." *INTERCIENCIA-CARACAS*- 31, no. 6 (2006): 417.

Twine, Tracy E., W. P. Kustas, J. M. Norman, D. R. Cook, PRea Houser, T. P. Meyers, J. H. Prueger, P. J. Starks, and M. L. Wesely. "Correcting eddy-covariance flux underestimates over a grassland." *Agricultural and Forest Meteorology* 103, no. 3 (2000): 279-300.

U.S. Census Bureau, "State and County QuickFacts", 2015, http://quickfacts.census.gov/qfd/states/01/01081.html (Accessed February 26, 2013)

U.S. Department of Agriculture (USDA) National Agricultural Statistics Service, "Census of Agriculture – State Data. USDA (U.S. Department of Agriculture)", Washington, D.C., 2010

U.S. Department of Agriculture (USDA). "National Agriculture Imagery Program (NAIP). 2013,"http://www.fsa.usda.gov/FSA/apfoapp?area=home&subject=pro &topic=nai (Accessed November 16, 2013)

U.S. Department of Agriculture (USDA). "Cropland Data Layer Metadata.", 2014, http://www.nass.usda.gov/research/Cropland/metadata/metadata_al10.htm (Accessed January 16, 2015)

U.S. Fish and Wildlife Service [USFWS]." National Wetlands Inventory Overview.", 2013, http://www.fws.gov/wetlands/NWI/Overview.html (Accessed November 13, 2013).

U. S. Geological Society (USGS), 2005, "Irrigation Water Use" http://ga.water.usgs.gov/edu/wuir.html (accessed February 19, 2014)

U. S. Geological Society (USGS), "Groundwater Depletion", 2014a, http://water.usgs.gov/edu/gwdepletion.html (accessed March 9, 2014)

U. S. Geological Society (USGS), "Groundwater Depletion", 2014b, http://water.usgs.gov/edu/gwdepletion.html (accessed March 9, 2014)

U.S. Geological Survey [USGS]. "National Hydrography Dataset (NHD)", 2013, http://nhd.usgs.gov. (Accessed November 16, 2013)

U.S. Geological Survey (USGS), "LandSat 5 History", 2015, http://landsat.usgs.gov/about_landsat5.php (Accessed January 16, 2015)

U.S. Geological Survey (USGS). "National Land Cover data 1992", 2012, http://landcover.usgs.gov/prodescription.php (Accessed January 16, 2015)

UserGuide eCognition, 2014. Website: www.definiens_imaging.com (accessed September 01, 2014).

Vörösmarty, Charles J., Pamela Green, Joseph Salisbury, and Richard B. Lammers. "Global water resources: vulnerability from climate change and population growth." *Science* 289, no. 5477 (2000): 284-288.

Vozikis, G. "Automated generation and updating of digital city models using high resolution line scanning systems", *IAPRS* 35 (Part B/7), (2004):1033–1038.

Wallace, J. S. "Increasing agricultural water use efficiency to meet future food production." *Agriculture, Ecosystems & Environment* 82, no. 1 (2000): 105-119.

Wallace, Jim S., and Peter J. Gregory. "Water resources and their use in food production systems." *Aquatic Sciences* 64, no. 4 (2002): 363-375.

Ward, A.D. and W. J. Elliot. *Environmental Hydrology. CRC Lewis Publishers, Boca Raton, FL, USA* (1995)

Waters, R., R. Allen, W. Bastiaanssen, M. Tasumi, and R. Trezza. "Surface energy balance algorithms for land, Idaho implementation, advanced training and user's manual." *NASA, USA* (2002).

Webb, Eric K. "Profile relationships: The log-linear range, and extension to strong stability." Quarterly *Journal of the Royal Meteorological Society* 96, no. 407 (1970): 67-90.

Weatherhead, E.K. and others "Sustainable water resources: a framework for assessing adaptation options in the rural sector." *Tyndall Centre Technical Report* 44, Tyndall Centre for Climate Change Research, UEA, Norwich. 2006

Welterlen, M.S., and others. "Surface Runoff from Turf" in *A.R. Leslie and R.L. Metcalf (ed.) Integrated Pest Management for Turf-grass and Ornamentals*, 153-160. Office of Pesticide Programs, USEPA, Washington, DC, 1989

Wheeler, Kit, and John Nauright. "A global perspective on the environmental impact of golf." *Sport in Society* 9, no. 3 (2006): 427-443.

Wickware, Gregory. M. "Wetland Mapping and Environmental Monitoring Using Landsat Data" in *Proceedings of the 5th Canadian Symposium on Remote Sensing*. Victoria, British Columbia, August 1978, P 150 – 157

Wiebe, Keith and Noel Gollehon, 2006, *Agricultural Resources and Environmental Indicators, 2006 Edition*, USDA Economic Bulletin (EIB-16), *US Department of Agriculture, Economic Research Service. Washington, DC*. 2006

Wigmosta, Mark S., Lance W. Vail, and Dennis P. Lettenmaier. "A distributed hydrology-vegetation model for complex terrain." *Water resources research* 30, no. 6 (1994): 1665-1679.

Winter, Thomas C., and James W. LaBaugh. "Hydrologic considerations in defining isolated wetlands." *Wetlands* 23, no. 3 (2003): 532-540.

Wright, James L., and Marvin E. Jensen. "Peak water requirements of crops in southern Idaho." *Proceedings of the American Society of Civil Engineers, Journal of the Irrigation and Drainage Division* 98, no. IR2 (1972): 193-201.

Wright, James L. "New evapotranspiration crop coefficients." *Proceedings of the American Society of Civil Engineers, Journal of the Irrigation and Drainage Division* 108, no. IR2 (1982): 57-74.

World Health Organization and UNICEF, "Progress on Sanitation and Drinking Water- 2013 Update", 2013, http://www.wssinfo.org/fileadmin/user_upload/resources/JMPreport2013.pdf (Accessed March 7, 2014)

Zhou, Weiqi. "An object-based approach for urban land cover classification: integrating LiDAR height and intensity data." *Geoscience and Remote Sensing Letters, IEEE* 10, no. 4 (2013): 928-931.

Zhou, W., and A. Troy. "An object-oriented approach for analyzing and characterizing urban landscape at the parcel level." *International Journal of Remote Sensing* 29, no. 11 (2008): 3119-3135.

Zhou, Weiqi, Ganlin Huang, Austin Troy, and M. L. Cadenasso. "Object-based land cover classification of shaded areas in high spatial resolution imagery of urban areas: A comparison study." *Remote Sensing of Environment* 113, no. 8 (2009): 1769-1777

Zhang, Keqi, Jianhua Yan, and Shu-Ching Chen. "Automatic construction of building footprints from airborne LIDAR data." *Geoscience and Remote Sensing, IEEE Transactions on* 44, no. 9 (2006): 2523-2533.